NUMO
原子力発電環境整備機構

TOPAZ Project

Long-term Tectonic Hazard to Geological Repositories

Toward practical application of the ITM-TOPAZ methodology

February 2017

Nuclear Waste Management Organization of Japan (NUMO)

TOPAZ Project
Long-term Tectonic Hazard to Geological Repositories

Toward practical application of the ITM-TOPAZ methodology

February 2017

Nuclear Waste Management Organization of Japan (NUMO)

各章の和文要約

1 序論

　本報告書は，国際プロジェクトメンバーが作成した原稿を NUMO が編集したものである。NUMO は，地層処分システムに著しい影響を及ぼす火山活動や断層活動などの自然現象の発生可能性を確率論的に評価するための手法として，ITM 手法[1]を開発した。続いて，プレート運動の安定性を必ずしも前提にできない超長期の評価に向けて，ITM-TOPAZ 手法[2]の開発を進めた。東北地方および中国地方を対象としたケーススタディを通じて，ITM-TOPAZ 手法の日本の地質環境への基本的な適用性を確認してきた。今回，ITM-TOPAZ 手法の適用性のさらなる向上を目指し，再び東北地方を対象に，火山活動・断層活動に加えて隆起・侵食の変遷に関するシナリオの拡充，それらの影響の評価方法の高度化などを行った。

2 広域変遷シナリオ（RES: Regional Evolution Senarios）の拡充

　これまでに例示した将来 100 万年までのプレート運動の変遷に関する四つのシナリオ（RES1: 現在の傾向が継続，RES2: プレート収束速度が増加，RES3: プレート運動の方向が変化，RES4: プレート収束速度が減少）における，東北地方の背弧域（日本海側），脊梁山地，前弧域（太平洋側）での広域的な火山活動，断層活動，隆起・侵食の傾向について，追加情報に基づき記述を補強した。さらに，最近の科学的知見の進展を踏まえたシナリオの拡充の可能性について述べた。

3 サイト変遷シナリオ（SES: Site Evolution Senarios）の設定

　背弧域（日本海側），脊梁山地，前弧域（太平洋側）を代表する数十 km^2 程度の検討用サイトとして，WCB（West Coast Backarc），IB（Inland Basin），ECF（East Coast Forearc）の三地点を設定した。文献情報を基に，各サイトの隆起・侵食速度などを推定し，上記四つの RES の下での火山活動，断層活動，隆起・侵食の変遷を，ストーリボードを用いて概念的に示した。

4 影響シナリオ（IS: Impact Scenarios）の設定

　これまで未実施であった隆起・侵食による地層処分システムへの影響の変遷について検討を行った。廃棄体および人工バリアの状態変遷，ならびに上記 SES の情報に基づき，各サイトで仮に地下 300m に処分場を設置した場合の隆起・侵食に伴う影響（地表との距離の減少，酸化性雰囲気への移行，地表への露出など）の変遷について，ストーリボードを用いて概念的に示した。

5 火山活動および隆起・侵食のハザードマップ作成方法の検討

　将来の自然現象の発生可能性の評価結果がサイト選定プロセスに悪影響を及ぼす可能性（プロジェクト・リスク）について，判断指標のしきい値（確率）を設定し，ハザードマップを作成して評価する方法を示した。火山活動については，まず上記

---

[1] International Tectonics Meeting（日本のテクトニクス関連事象の調査・評価に関する国内外の専門家の認識共有・情報発信の場として NUMO 主催の会議体）の海外専門家とともに開発した手法で，数十万 km^2 規模のハザードマップにより，数十 km^2 程度の領域における事象の発生確率を提示する (Chapman et al., 2009a)。

[2] TOPAZ(Tectonics Of Potential Assessment Zones)手法は，将来のプレート運動の変化およびそれに伴い生じる事象の変遷，ならびに地層処分システムへの影響の変遷にかかわるシナリオを設定し，それに対する専門家の確信度と ITM 手法の発生確率を統合した評価を行う (Chapman et al., 2012)。

RESにおける火山活動場の移動を考慮できるように，コックスプロセス法[3]を高度化した。海外の事例を参考にしきい値を仮設定して，プロジェクト・リスクを区分し，上記のコックスプロセス法と既存のカーネル法[4]のモデルに基づくハザードマップを作成した。隆起・侵食については，広域的な隆起速度と，アイソスタシーに伴う隆起・沈降を仮定した重力異常を指標にしきい値を設定し，ハザードマップを作成した。さらに，総合評価に向けた火山活動と隆起・侵食を併せたハザードマップの作成例を示した。

6　断層活動のハザードマップ作成方法の検討

　ある場所における断層活動の影響シナリオの発生確率を算出し，ハザードマップあるいはリスクに基づく安全評価への数値情報として利用する方法を例示した。処分場を含む 5km x 5km x 20km の領域において，マグニチュード 6.5〜7.5 の地震を伴う断層の変位が処分場に到達するシナリオを想定し，地表変形，GPS，地震の情報に基づき，年間発生確率を求めた。年間発生確率の逆数から地震の再来期間を算出し，上記同様にしきい値を仮設定することによりハザードマップを作成する方法を示した。

7　ロジックツリーを用いた評価方法の検討

　統計解析ソフトウェアを用いた隆起・侵食の影響の確率論的な評価の事例を示した。ストーリボードに整理したシナリオ（RES, SES）や隆起・侵食速度のパラメータ[5]に基づき，地表への接近速度を評価するロジックツリーを構築した。これを基にモンテカルロ・シミュレーションを実施し，100万年後までの複数の時間枠における処分場の地表への接近量（例えば 300m）の超過確率を算出した。さらに， 異なる RES と SES の組合せに伴う地表への接近量の確率分布密度の違いや，異なる深度に設置した処分場の地表に露出する確率の時間変化などを提示できることを示した。

8　手法の適用に向けた議論

　ITM-TOPAZ 手法を，サイト選定の各段階において適用するにあたっての留意事項などを取りまとめた。その適用方法として，大きくは次の二つが考えられる。①火山活動，断層活動，隆起・侵食などによる著しい影響に関するハザードマップを示し，対象とする領域やサイトの評価（プロジェクト・リスク評価）に資する。②対象サイトで生じる事象の地層処分システムへの影響に関するシナリオの起こりやすさを定量的に示し，リスク論的な安全評価に資する。ハザードマップは，基本的には複数の領域あるいはサイトの相対比較に適しており，適用に際しては，対象とする領域やサイトの最新情報に基づき段階的に作成・更新していく必要がある。

---

[3] 火山の分布密度と地球物理データ（地震波速度構造，重力異常など）との地球統計学的な相関を考慮に入れたモデルのモンテカルロ・シミュレーションにより発生確率を算出する手法(Jaquet et al., 2009, 2012 など)。
[4] カーネル関数により火山からの距離や活動頻度に基づく時空間分布モデルを構築し発生確率を算出する米国ユッカマウンテン等で用いられた手法(Connor and Hill, 1995 など)。
[5] 本検討では時間的制約のため Chapman et al.,(2012)における情報を使用した。

Contents

1 Introduction

1.1 This report

This report was originally prepared by the TOPAZ international project team members as the project summary report that described the whole project activities, and was later interpreted and modified by NUMO under its responsibility. This report aims at supplementing and updating the basic ITM-TOPAZ methodology (Chapman et al., 2012) for potential practical application, by means of additional case study on the Tohoku region. The study was carried out to address specific issues in parallel by several groups of the project members, relatively in a short period. Thus, some of the following chapters may not correlate each other due to different boundary conditions and datasets (e.g. Chapter 6 and Chapter 7).

Chapter 2 updates the previous RES with new information. Chapter 3 develops SES for newly defined three example sites to include uplift and erosion in addition to volcanism and rock deformation. Chapter 4 introduces the 'Impact Scenarios' (IS) for the three sites with respect to the exhumation hazard due to uplift and erosion. Chapter 5 describes the basic methods of probabilistic volcanic hazard assessment, and a newly developed method for evaluating volcanism in evolving tectonic conditions at 1 Myr timeframe. It then demonstrates how the information from various models are aggregated to develop hazard maps for both volcanism and exhumation (uplift and erosion). Chapter 6 presents how to map frequency of a tectonic deformation scenario (occurrence of $6.5 \leq M \leq 7.5$ earthquakes). Chapter 7 explains how to use logic trees and expert elicitation approach to assign weights to hazard scenarios and their probabilities. Methods for evaluating specific exhumation hazards are also proposed. Chapter 8 summarises points and issues in applying the ITM-TOPAZ methodology to potential decision-making.

1.2 NUMO site evaluation

NUMO will need to evaluate sites that emerge either from voluntary application by municipalities or request made by the national government to municipalities, and select a preferred site for a repository (NUMO, 2013). They might also need to express preferences for regions of Japan where stable tectonic conditions would favour repository siting. Site evaluation will involve the initial Literature Surveys (LS), the surface-based Preliminary Investigations (PI) and the Detailed Investigations (DI) both on surface and underground (Figure 1.1).

Prior to the field investigations, NUMO will carry out a detailed literature-based evaluation of suitability to accept the sites as the Preliminary Investigation Areas (PIAs). A key aspect of this stage is consideration of the susceptibility of a site to future tectonic activity and tectonically driven processes and events. For repository safety evaluation, the focus is predominantly on long-term (more than thousands of years) post-closure tectonic processes leading to progressive perturbations of the repository environment. These may possibly lead to the initiation of disruptive tectonic events which may cause perturbations at repository depth, although potential impacts of other tectonic events during the multi-decade, operational period also have to be taken into account in many locations.

Whilst the nationwide evaluation factors for qualification (EFQ) [6] for PIA acceptance are designed to remove clearly unsuitable sites from consideration, they cannot guarantee that, over the next hundreds of thousands of years, the risks of tectonic hazard for a chosen PIA will be acceptable.

This is because large parts of Japan that are potentially geologically suitable for siting are directly affected to varying extents by rock deformation, uplift and erosion, the peripheral impacts of volcanic activity or the possibility of new magma intrusion or volcanic activity. The EFQ were only intended as preliminary screening guidelines to prevent obviously unsuitable candidates entering the siting process.

---

[6] The siting factors for selection of PIAs consist of factors relating to legal requirements (evaluation factors for qualification (EFQ)) and favorable factors (FF) that are not part of legal requirements (NUMO, 2004). The EFQ include earthquake and fault activity, igneous activity, uplift and erosion, unconsolidated Quaternary sediments and mineral resources.
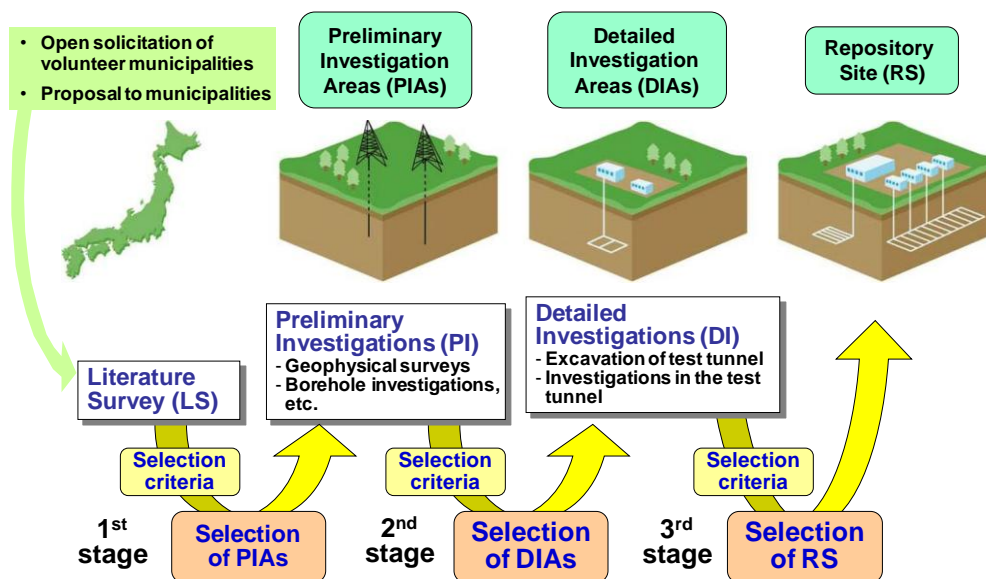
Figure 1.1: An overview of the NUMO site evaluation stages.

1.3 The ITM Methodology: probability – the likelihood of future tectonic impacts

NUMO recognised that an integration of additional and more refined techniques would be required to evaluate sites that pass the EFQ test, so that they could have a clear, quantitative indication of the likelihood and potential impacts of tectonic events and processes at each PIA. The ITM (International Tectonics Meeting) project developed such a methodology (the 'ITM Methodology') for the specific conditions of Japan, based upon state-of-the-art approaches used internationally (Chapman et al., 2009a).

The ITM methodology is essentially probabilistic in nature. A probabilistic approach was seen by the ITM expert group as the only realistic means of addressing the uncertainties in predicting possible hazards (processes or events that could lead to adverse effects) when there is marked variability in the spatial distribution, timing, intensity and style of the tectonic events being evaluated. The consequences of ignoring very low probability events with significant impacts were highlighted by the Fukushima accident after the earthquake in March, 2011.

Essentially, two approaches have been adopted internationally to address low probability, disruptive events and deformation processes that are discontinuous in time and magnitude in response to continuous regional strain.

- To calculate the health risk[7] to people in the future by combining the probability of a disruptive event occurring with its radiological consequences in terms of releases from a repository: simply, risk = probability x consequence. With this approach, regulatory standards or targets can be defined in terms of risk to an individual.
- To consider the impacts of a disruptive event and calculate the radiological doses[8] to people in the future and then, separately, to discuss the likelihood that this might happen (the so-called 'disaggregated' approach). With this approach, separate regulatory targets for radiation doses might be set for events (or scenarios) with different degrees of likelihood (often expressed qualitatively; e.g. 'likely', 'less likely', 'highly unlikely').

In either approach, an evaluation of probability is essential: in the first 'risk approach' a sound quantitative estimate will provide more confident estimation of risk; in the second, some form of quantification of 'likelihood' is needed to decide which category to place an event or scenario into. The probabilistic approach developed by ITM is based upon and strongly

---

[7] Health risk is normally defined as the risk of death or serious genetic effects.

[8] Of course, a radiological dose can also be expressed in terms of health risk, by applying accepted dose-to-risk conversion factors.

supported by deterministic models of the underlying tectonic processes that lead to magma intrusion, volcanism and rock deformation. The ITM methodology is applicable to the following situations of NUMO's repository siting programme:

- in the LS when potential PIAs are being assessed. The ITM methodology will use currently available information to allow comparison of sites in terms of confidence that they are likely to prove acceptable with respect to tectonic impacts.
- in the planning of the PIA site investigations, to identify geoscientific information requirements that will be needed to refine the LS analysis.
- at the point where DIAs are being evaluated and compared in order to select a preferred site (or sites) for disposal.

The ITM project was mainly concerned with the first and second situations, and focussed on evaluating comparative hazards of small areas (e.g. 25 km^2) within a regional or sub-regional context of 100,000 to 10,000 km^2. This is partly because the project originally developed to compare several possible alternative volunteer sites that might arise within a region. However, it is clear that regional to sub-regional scale assessment of tectonic hazard will also be required even for single sites.

Application of the methodology in the third situation is several years into the future and it is expected that it will be most efficient to carry out any necessary updates/refinements on a region-specific basis during the DIA investigations.

The overall structure of the ITM methodology is described in Chapman et al. (2009a) and consists of:

- assembling nationally available data and alternative models of the nature, causes and locations of tectonic processes and events;
- using probabilistic techniques to evaluate the likelihood and scale of future tectonic processes and events, shown as a function of their type and geographical distribution;
- feeding information on these potential likelihoods and impacts to NUMO's performance assessment team so that feedback can be provided on repository performance under tectonic stress;
- providing clearly justified and traceable input to decision-making on consequent siting.

The methodology was first tested during its development by means of a case study of the Tohoku region of northern Honshu (Chapman et al., 2008) and then further developed and tested by application to a second case study region covering the whole of Kyushu (Chapman et al., 2009b). The Tohoku case study looked into the varied strain response of the crustal plate to subduction of the Pacific Plate (the key current tectonic driver for much of Japan) and the mechanisms that underlie the apparent clustering of Quaternary volcanoes in much of Honshu. The Kyushu case study region is among the more dynamic and rapidly changing plate boundaries in the world, with the tectonic situation being intrinsically more complex than in Tohoku. The observed modes of strain accommodation in Kyushu are varied but not yet fully understood, and the style of volcanism and geochemistry of the magmas varies considerably across Kyushu, compared to the reasonably simple arc volcanism in Tohoku. Forecasting future volcanism and faulting in Kyushu is less certain because the geological setting is evolving more rapidly. The fundamental assumptions in Tohoku, that the plate boundary configurations and plate motions influencing rock deformation and volcanism are relatively stable over periods up to 1 Myr, are less appropriate in Kyushu. Consequently, these two case studies allowed development and testing of the ITM Methodology under significantly different tectonic conditions that span a significant part of the range of tectonic environments across the Japanese Islands.

1.4   The March 2011 earthquake - a "natural experiment"

On March 11, 2011, the fourth-largest instrumentally recorded earthquake, a Magnitude (M) 9.0 event, occurred offshore northeast Japan. Because of Japan's history and preparedness for earthquake shaking, the devastation was primarily a result of the subsequent tsunami. The Great 2011 Tohoku-oki earthquake was a product of the subduction of the Pacific Plate beneath the edge of the Eurasian plate at a speed of about 8.5 cm/yr along the northeast Japan trench. This trench segment extends northwards about 800 km from the triple junction

intersection with the Izu-Bonin trench and Nankai trough (36°N) and the southern end of the Kurile trench (42°N). Along this trench, an earthquake of M≤6 occurs nearly every year. The historical record indicates M7 or larger events occur every five years with events of M≤7.5 every few decades.

The 2011 M9 event was extraordinary for the Japanese islands as rapid seismogenic slip occurred along the central 400 km length of this trench segment with as much as 50-60 m of thrust-type displacement at the toe of the trench wall 85 km seaward of the epicentre. In retrospect, it is now apparent that a very similar earthquake occurred in AD869. The Jogan tsunami left a sand layer deposit in the Sendai plain that is remarkably similar in thickness and extent to that produced in on March 11, 2011. Minoura and Nakaya (1991) discovered evidence for this event in cores from the Sendai plain. This evidence was investigated more thoroughly and better dated via samples selected from trenches excavated by Minoura et al. (2001). However, these workers attributed the tsunami to nearby subduction zone earthquake of only M8.3. Sawai et al. (2008) used cores and trenches to confirm the 869 Jogan event was the largest tsunami in the past 1,500 years, with only the lesser 1611 Keicho tsunami leaving evidence in the Sendai plain. They also presented a chart indicating there is evidence for two other large tsunamis around 1,900 and 2,900 years before present. There is reason to believe 2011 M9 Tohoku-scale earthquakes recur over timescales of about 1kyr.

Prior to the 2011 M9 earthquake, the maximum expected magnitude for an event near Japan, M8.5, was based upon the historical record, considered complete for major events since AD1600. In 2005, the Japan Headquarters for Earthquake Research Promotion (HERP) released a formal report that was a "consensus opinion" of a committee of leading Japanese seismologists (Fujiwara et al., 2006). This report, with updates in 2006, 2007, and 2009 identified 98 major active faults and 15 trench parallel regions of subduction zone seismicity. Most on-land fault zones were given 30-year probabilities of earthquake-producing ruptures in the range of M7.2±0.5 of less than 7%. Probabilities as large as 16% were given to six fault zones, all of which are part of the active deformation belt that delineates the plate triple junction region in central Honshu. The Nankai Trough subduction zone, long believed as overdue for a great subduction earthquake, was given a 30 year probability of about 50% for a M8.4 event and about 60% for a M8.1 event, with a M8.5 event listed as possible if the rupture extends along the entire trenchline.

The 2005 HERP seismic hazard assessment divided the Japan Trench subduction zone into six segments. The Miyagi-oki area, the epicentre of the 2011 M9 event was given a 99% probability of a M7.5 event by 2035, the highest probability for a major earthquake anywhere in Japan! The North Sanriku-oki segment was given a 30-year probability of 70-80% for a Mw7.7 event. The entire Japan trench segment from Sanriku-oki to Boso-oki was identified as having a 20% potential of a M8.2 tsunami-generating near-trench movement with associated tsunami inundations up to about 6 m. In retrospect, the activities of the HERP committee produced an analysis that was correct in terms of probable location of major tectonic activity, but inadequate in terms of magnitude and tsunamigenic potential.

The expectation of potential M8.3± earthquakes near Japan guided the design of engineered structures and seawall defences. While the M9.0 earthquake along this subduction zone segment was about fifteen times larger (in terms of energy release) than the maximum expected and resultant tragedy from the huge 10+ m high tsunami shocked the highest levels of the geoscientific community (see e.g., Nature Comment, 2011, "Rebuilding seismology"), the scientific approach that produced the 2005 HERP report that identified the Miyagi-oki area as having the greatest probability of a major earthquake for all of Japan can be considered a success.

The possibility that subduction zones can produce great M9 thrust-type events is one of the tenants of plate tectonics theory that arose in the late 1960s (shortly after construction began on the Fukushima Daiichi nuclear power plant reactor #1). In most ways, the 2011 Tohoku event was very similar to the 1952 Kamchatka M9.0, 1960 Chile M9.5, 1964 Alaska M9.2, and 2004 Sumatra M9.1 subduction zone earthquakes and tsunami floods. From now on, all probabilistic hazard analyses near subduction zone settings must consider these kinds of multicentury to millennia-scale events.

From the point of view of the long-term (≥100 kyr) disposal of nuclear waste in Japan, the 2011 Tohoku M9 earthquake can be viewed as a "natural experiment" because it occurred in

the most intensively monitored (seismograph, GPS) portion of the planet. Already, analysis of this event has generated hundreds of professional publication that reveal much about earth behaviour (e.g., Lay et al., 2013). Such events, rare in the historical record, must be viewed as commonplace over the timescales of concern for the issue of nuclear waste disposal in Japan.

1.5   Timescales and tectonic impacts on a geological repository

The impact of tectonic events and processes on the long-term safety of a geological repository is highly dependent on the time at which they might occur. Figure 1.2 shows the declining hazard of high-level waste (HLW) and spent fuel as a function of time after production. Hazard is represented here as the ingestion radiotoxicity of all the radionuclides in the waste relative to the radiotoxicity of the amount of uranium ore required to manufacture the fuel from which the HLW was produced.

The hazard from HLW declines rapidly over the first hundreds of years and, after about 3,000 to 4,000 years, reaches the same level as the uranium ore. At this time after disposal, a repository would have a similar hazard potential (by mobilisation of radionuclides into groundwater to cause exposure to people and the environment) as a rich uranium ore body buried at a similar depth.

Worldwide, people live in close proximity to natural deposits of radioactive materials, with no apparent impacts on health. There are large variations in natural background radioactivity, giving everyday doses to people that far exceed any that might result from a geological repository in the distant future. It can thus be argued that the isolation and containment function of the geological repository for HLW has been largely fulfilled within the first ten thousand years.

Nevertheless, quantitative safety evaluations of repositories for HLW are required in most countries out to times of at least 100,000 years (100 kyr) – the period addressed in the ITM project. In several countries, even those dealing with disposal of spent fuel, which can be seen from Figure 1.2 not to reach the natural crossover point with uranium ore until about 100 kyr after disposal, only qualitative statements of safety are required after 100 kyr. Such statements are expected to discuss the longevity of safety functions into the distant future, to compare hazard to natural radiotoxic hazards and to discuss the long-term fate of the wastes as the repository degrades. The engineered barriers and the waste itself are expected to be substantially degraded in the period 100 kyr to 1 million years (1 Myr) and beyond.
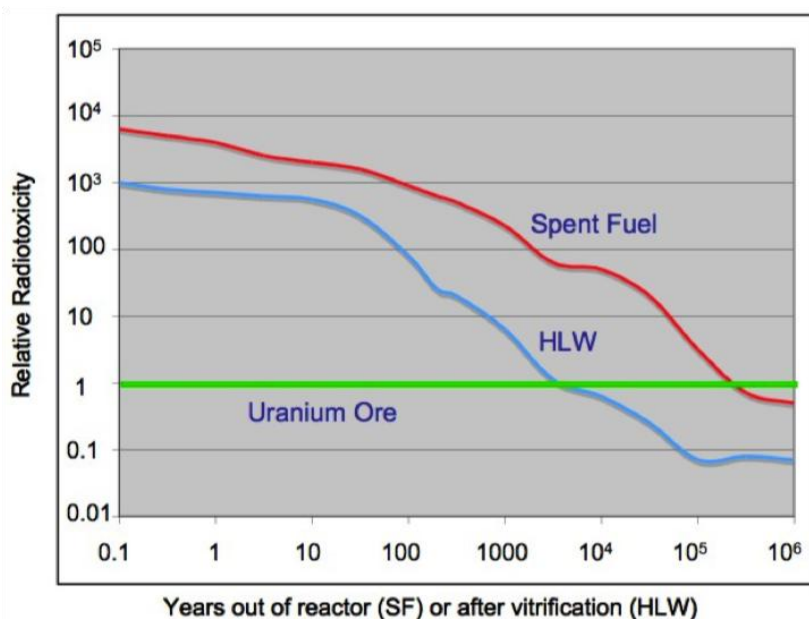
Figure 1.2: Declining radiotoxicity of HLW and spent fuel as a function of time after production: see text for description (after NUMO, 2004; Chapman and Hooper, 2012).

One of the main reasons that only qualitative descriptions are expected in many countries is that many uncertainties associated with making quantitative estimates of actual radiological health impacts increase significantly and such forecasts lose credibility as actual indicators of safety. The other main reason is that, as can be seen, the hazard potential of the waste by mobilisation into the deep groundwater system will, over these protracted timescales, eventually start to approach levels similar to naturally occurring sources of radioactivity in the environment. The concepts discussed above are shown schematically in Figure 1.3.

Returning to tectonic impacts, it can be seen that events and processes that might disrupt a repository over the first 10 kyr are critical and need to be avoided, so far as possible, by correct siting in regions of low tectonic susceptibility. Thus, the probability of occurrence of events and processes is an extremely important factor. The ITM project develops the tools to assess such probabilities up to 100 kyr – not only the period for which quantitative evaluations of doses or risk are typically required, but also the limit of confident forecasting of the tectonic framework of the Japanese islands, before major restructuring might be expected. Major restructuring refers to a change in tectonic regime for parts of Japan.

However, as the regulatory framework for geological disposal is still under development in Japan, NUMO considered it was worthwhile to prepare a measure for providing information out to longer periods – up to 1 Myr – again in the form of probabilities (or 'likelihoods') that could be used to express degrees of belief to alternative forecasts of the evolution and fate of a repository.
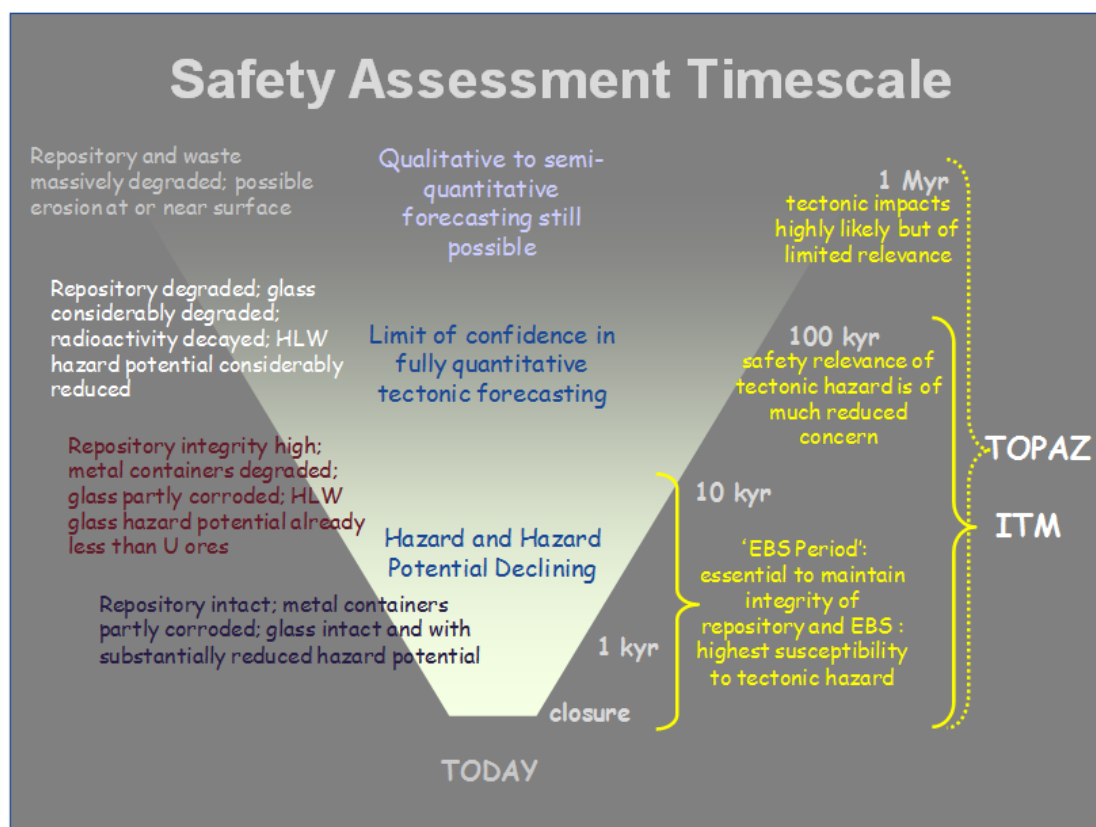
Figure 1.3: Schematic representation of the progressive degradation of a geological repository with time, the diminishing ability to make quantitative forecasts as uncertainty increases, and the decreasing importance of tectonic impacts to safety as the hazard potential also decreases. The ITM and TOPAZ project timescales are shown on the right hand side of the diagram.

1.6 Going beyond 100 kyr: the TOPAZ Project

Consequently, following the completion of the ITM project, the expert team was proposed to look at the possibilities and constraints of making forecasts of the likelihood and nature of tectonic impacts for longer periods into the future, from 100 kyr out to 1 Myr.

The TOPAZ (Tectonics Of Preliminary Assessment Zones) project was started to extend the methodology developed in the preceding ITM project for this purpose. The developed methodology in the TOPAZ project is called the ITM-TOPAZ methodology.

One of the main additional steps of the ITM-TOPAZ methodology involve the development of alternative conceptual models, 'Regional Evolution Scenarios' (RES), which characterise how the tectonic situation in a region might develop over the next 1 Myr. These, in turn, are used to develop 'Site Evolution Scenarios' (SES), which describe how an RES might 'play out' at a specific location within the region being evaluated. The degrees of belief in these RES and SES are attached using a formal expert elicitation methodology, expressed as probabilities in a logic tree, and can be superimposed on the event probabilities derived from the ITM methodology to arrive at probabilities of specified impacts in different timeframes.

The basic methodology was tested by means of the Tohoku case study (Chapman et al., 2012). A partial test of the methodology on the different tectonic setting (i.e. monogenetic volcanism) was made in the Chugoku case study (Connor et al., 2013).

Figure 1.4 summarises the outline of the ITM-TOPAZ methodology. The output of a complete analysis of a site would be an essential underpinning component of any NUMO safety assessment and comprise the following elements:

- A complete description of the tectonic situation of a site;
- Alternative conceptual models of how that situation might evolve over the period of interest to the safety assessment;
- A comprehensive list of impact scenarios for transfer to repository consequence analysis;
- The relative probabilities of each 'Impact Scenarios' (IS) affecting the repository, which can be incorporated into a risk-based safety assessment and used to generate either radiological risks (to compare to regulatory standards) or probabilities of occurrence of scenarios to present along with dose consequences in a disaggregated dose-likelihood approach to regulatory standards.
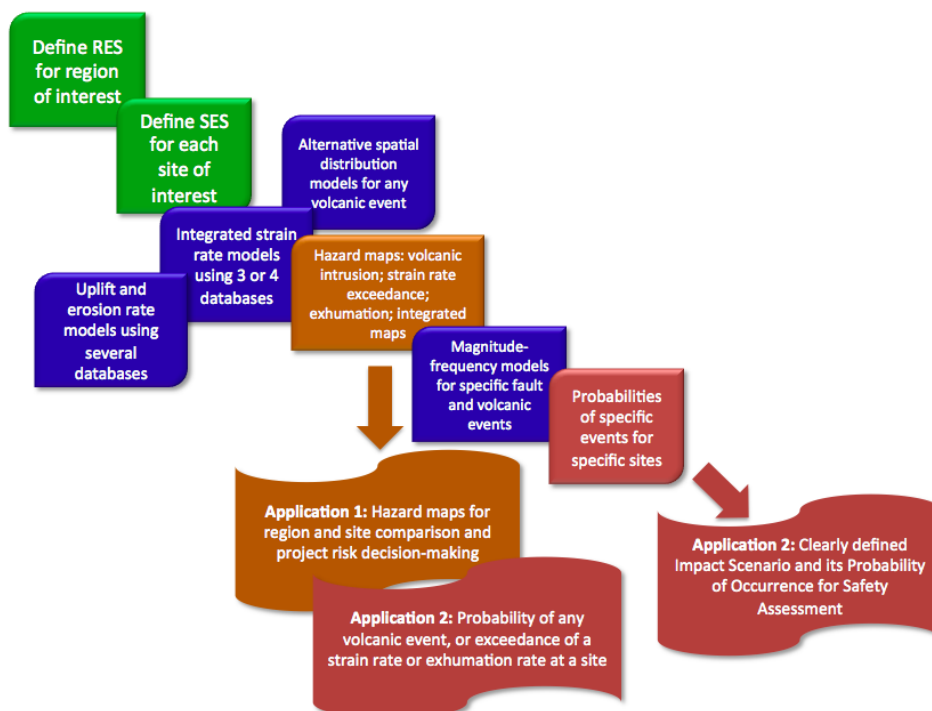
Figure 1.4: The outline of the ITM-TOPAZ methodology.

The Project involved the close interactions of Japanese and international experts to gain the necessary understanding to carry out the methodology development and testing. The international experts came from the organisations in Table 1.1.

Table 1.1: An overview of the International Project Team Members for the TOPAZ Project.

TOPAZ International Project Team Members (as of March 2014)		
Rock Deformation	Dr Kelvin Berryman Dr Mark Stirling Dr Nicola Litchfield	GNS Science, New Zealand
	Professor Mark Cloos Dr Laura Wallace	University of Texas, USA
Volcanism	Professor Charles Connor Laura Connor Rocco Malservisi	University of South Florida, USA
	Professor Steve Sparks Dr Sue Mahony Ellie Scourse	University of Bristol, UK
	Dr Olivier Jaquet	In2Earth Modelling, Switzerland
Interface with PA	Dr Mick Apted	INTERA, USA
Expert Elicitation	Dr Willy Aspinall	University of Bristol, UK
Project Co-ordination	Professor Neil Chapman Ellie Scourse	MCM Consulting, Switzerland

2 Regional Evolution Scenarios

In this chapter, we updated the four plausible RES presented in the previous Tohoku case study (Chapman et al., 2012) with new discussions on the implications of these scenarios. Importantly, it is noted that the RES developed here are meant as examples to demonstrate the approach. The scenarios presented here are based on our current understanding of how tectonics has evolved in Tohoku in the past. When the RES approach is eventually applied to a specific site, more exhaustive RES should be developed by a panel of experts, who are expected to back the RES up with more extensive and robust data.

2.1 Major issues to consider in developing future tectonic evolution scenarios

In a regional sense, the first-order features to consider in the future tectonic evolution of Japan are: the configuration and sense of relative plate motion at the plate boundary, the migration of triple junctions between tectonic plates, and the dynamics of the subducting slabs and mantle in the region. All of these things will strongly influence the distribution and evolution of rock deformation and volcanism. We have developed four RES for the Tohoku region in the previous TOPAZ report, each of which assumes a different future tectonic evolution that we consider to be plausible. One of the most important aspects of future evolution to consider is whether or not the Sea of Japan convergent zone will evolve into a subduction margin. Thus, tracking the location and depth of the leading edge of the underthrusting Sea of Japan crust is one of the features we highlight for the northern Japan RES. At a more detailed and local-scale level, processes such as fault zone evolution and development of magmatic centres should be accounted for. In terms of the backbone range domain, the potential for the development of new volcanic centres and uplift associated with that is very important to consider, as is the on-going evolution of active faulting in that region. A suite of geodynamic and numerical models is recommended to inform RES development, particularly in terms of how active deformation and the distribution might evolve with time, in response to the evolving tectonic boundary conditions.

To assess future tectonic evolution, we must also consider the possibility that relative plate motions can change over time scales of a few million years; such a scenario will strongly influence the results for RES developed for the 1 Myr timescales. We know that the Pacific Plate has changed its motion (in an absolute sense) numerous times throughout its history. Most of these plate motion changes arise from forces exerted on the boundaries of the plates. For example, Wessel and Kroenke (2000) suggested that collision of the Ontong Java Plate with trenches bordering the Pacific Plate in the southwest Pacific initiated a change in Pacific Plate motion ~6 Ma. Similar to the Pacific Plate, the Philippine Sea Plate motion has changed numerous times throughout its history (Sdrolias et al., 2004; Hall et al., 1995). Part of our RES development involves consideration of scenarios where reasonable changes in relative plate motion occur at various stages in the future. A recent study (Regalla et al., 2013) suggest that changes in convergence rates of the Pacific Plate has impacted Pacific slab dynamics in the past, leading to stages of uplift vs. subsidence. To properly assess the influence of changes in plate motion on the future uplift and subsidence scenarios in the Tohoku region (e.g., Regalla et al., 2013), geodynamic modelling is required. Moreover, for more robust assessment of likely future changes in tectonic plate motion, calculation of the forces acting on the plate boundaries and modelling of how these forces are expected to influence future rates of motion of the Pacific Plate are recommended.

2.2 RES 1: Tectonic boundary conditions remain the same

In this scenario, we assume that the overall tectonic boundary conditions in the Tohoku region remain the same as they are today for the next 1 Myr (Figure 2.1). As part of this scenario, we assume that the rate of permanent plate boundary deformation occurring within the upper plate (>15 mm/yr) remains similar to what occurs today, and that the subducting Pacific slab maintains its current configuration (configuration defined by Hasegawa et al., 1994) with respect to the upper plate. We also assume that the crust underlying the Sea of Japan continues underthrusting beneath Honshu at its current rate of ~15 mm/yr, eventually evolving into a subduction margin (cf. Tamaki and Honza, 1985). The results of this RES for the various timeframes are shown schematically in Figure 2.2.
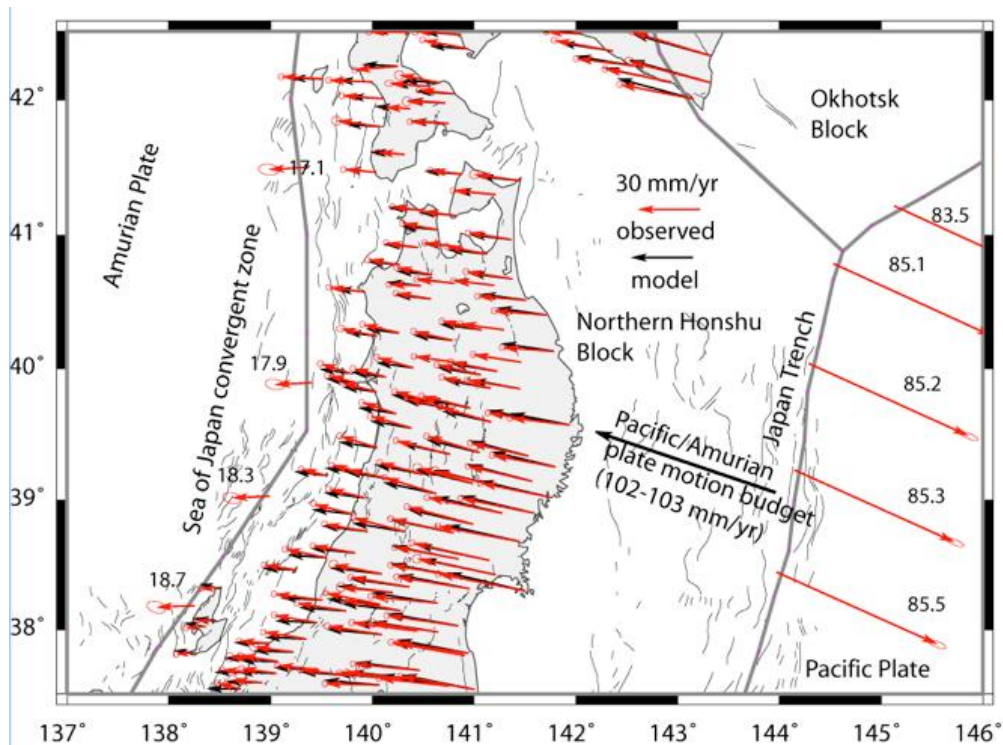
Figure 2.1: Tectonic setting and GPS velocity field in Northern Honshu (shown relative to a fixed Eurasian plate). Thinner grey lines are active fault traces. Ellipses show uncertainty at 65% confidence level. Velocities are derived from daily solutions provided by Geographical Survey Institute of Japan. Block boundaries (heavy grey lines) used in the elastic block modelling to interpret GPS velocity field in terms of long-term block motion (Pacific, Amurian, and northern Honshu Block) and fits to the GPS velocities (red arrows) from the best-fitting model (black arrows) (from Wallace et al., 2009). Arrows on the boundaries with numbers beside them (mm/yr) show the motion of the Northern Honshu block relative to the Amurian and Pacific Plates. Interpretation of the GPS velocities also suggest that 3-4 mm/yr of contraction occurs in the backbone range of northern Honshu (Miura et al., 2004; Wallace et al., 2009)

Although this scenario assumes relatively constant tectonic boundary conditions, it could lead to some degree of temporal and spatial change in the distribution of faulting and volcanism with time. For example, as the convergent margin and associated fold and thrust belt evolves near the west coast of Tohoku, more localization of deformation onto particular structures could be expected, and/or spatial changes in distribution of active deformation could occur as a result of the natural evolution of the fold and thrust belt there. This could lead to substantial changes in rock deformation strain and uplift rates in the evolving contractional domain associated with underthrusting of the Sea of Japan (western contractional domain) and the currently active backbone range domain, out to longer time periods. It is also likely that any optimally oriented bedrock faults (i.e., approximately north-south striking) could become reactivated. Although we expect the location of volcanism in the arc to be relatively stable over the timeframes presented, it is possible that volcanism could move into the "gap" region between volcanoes, possibly driven by temporal and spatial changes in magmatic supply and mantle wedge flow regimes over longer timeframes (e.g., Honda et al., 2007).

Present day – 10 kyr scenario. We do not expect this scenario to be significantly different from what is observed today, particularly in terms of the location of deformation, uplift, and active volcanism. We recommend that hazard calculations derived from the ITM methodology will be reasonable for this timeframe.

10 – 100 kyr scenario. We do not expect this scenario to be significantly different from the present day to 10 kyr scenario, although it is possible that some spatial changes in the rates

and location of volcanism, deformation, and uplift could begin to occur during this longer time period, as fault and volcanic systems evolve. We anticipate that most of the contractional deformation accommodated in the upper plate during this period will continue to occur within the backbone range domain (Hasegawa et al., 2000) and along the evolving convergent margin adjacent to the Sea of Japan. In terms of the backbone range domain, which has bedrock faults within a few hundred meters of it, it is certainly plausible that bedrock structures within this domain will become reactivated as the contractional fault system evolves. This could lead to some combination of uplift or subsidence, depending on whether or not it is situated within the hanging wall or footwall of the evolving fault system. So for this time frame, any site located within the footwall of an active reverse fault, continued subsidence is a reasonable scenario. Volcanism is unlikely to migrate significantly outside of the current location of active volcanism on this time frame due to the likely stability of magma supply systems over these timeframes.

100 kyr – 1 Myr scenario. Over longer time periods it is possible that larger spatial and temporal changes in the distribution of volcanism and rock deformation will occur. However, we anticipate that the largest rates of rock deformation will still remain focused within the backbone range and the western part of Honshu. Radiometric dating of volcanism in the backbone range suggests that the location of volcanic centres there remains stable on timescales of 5-10 Myr, and the current volcanic centres have been in place since ~4 Ma (Honda et al., 2007). However, the locus of volcanism between the currently active areas and the "gaps" between the active arc volcanoes appears to flip-flop on 5-10 Myr timescales (Honda et al., 2007). Thus, we cannot rule out the possibility that migration of arc volcanism into the gaps between the currently active volcanoes could occur during the 1 Myr period of interest in this RES. However, given the lack of evidence for significant lateral migration of volcanism across in the arc in the last 10 Myr or more, it is highly unlikely that active volcanism will migrate significantly across the margin (for example, into the forearc domain) in this RES.

If it occurs, migration of volcanism into the "gap areas" between the currently active volcanic centres will greatly impact the backbone range domain, both in terms of disruption by magmatic intrusions and potential eruptions, as well as uplift in response to magmatic injections. However, if the locus of active faulting propagates into the basin, away from the range front, an eventual transition to uplift there is plausible. Overall, given the potential for increased magmatic influence in the gap between current volcanic centres, as well as continuing rock deformation in the backbone range domain during this time period, this area could be prone to increased uplift rates, and higher rock deformation and possibly volcanic hazard on the 1 Myr timeframe (in contrast to the present situation).

In the western contractional domain, if deformation becomes progressively localized and evolves towards an incipient subduction margin, it is possible that larger portions of the convergent component of plate motion will be shifted into the western contractional domain. This could manifest itself by (1) a larger portion of the deformation budget occurring on structures just offshore, (2) an increase in deformation rates on the already active onshore faults, or (3) by reactivation of other properly oriented structures onshore, or some combination of all three options. Potential future increases of the plate motion budget being focused into the western contractional domain will depend on the details of evolution of the associated fold and thrust belt, and the distribution of optimally oriented bedrock structures. Out to longer time periods, we expect continued evolution of contractional deformation (growing anticline), and for continued uplift, erosion, and rock deformation to impact that site out to 1 Myr.

If the Sea of Japan is evolving into a subduction margin (e.g., Tamaki and Honza, 1985), we expect that 1 Myr into the future the leading edge of the underthrusting Sea of Japan crust will have migrated eastward by ~15 km, and will have deepened by several km, compared to ~30 km depth that we assume for its current depth (loosely based on seismicity). We note that the location of the leading edge of the underthrusting Sea of Japan (and its likely future location) is not well-constrained, and requires further geophysical investigation. Encroachment of the leading edge of the Sea of Japan crust beneath western Honshu could also impact future volcanic development in that region (perhaps inhibiting it beneath the west coast, pushing

currently active west coast volcanoes eastward). Underthrusting Sea of Japan crust may also perturb the dynamics of the mantle wedge beneath both the western contractional domain and the backbone range domain, leading to some reorganization of the locus of active volcanism within the arc andbackarc. Numerical modelling studies to assess the influence of the underthrusting Sea of Japan crust on the mantle wedge and subsequent volcanic evolution in northern Honshu is recommended.

RES 1, 0-10 kyr

Western contractional domain: patterns of uplift, rock deformation and volcanism likely to be similar to present day

Backbone range domain: patterns of volcanism, uplift, and rock deformation likely to be similar to present day

Forearc domain: Uplift patterns and low rates of rock deformation likely to persist for this time

0-10kyr into the future, with assuming tectonic boundary conditions stay the same

Amurian Plate

Sea of Japan

15 mm/yr

15 mm/yr

100 km contour of the subducting Pacific slab

Forearc region

leading edge of underthrust Sea of Japan crust (~30 km depth)

plate motion vector (plate motion budget ~100 mm/yr)

85 mm/yr

Pacific Plate

85 mm/yr

▲ = volcanoes

10-100 kyr

Western contractional domain: patterns of uplift rock deformation, and volcanism may evolve within this timeframe

Backbone range domain: patterns of volcanism, uplift, and rock def. likely to evolve within this timeframe.

Forearc domain: Uplift patterns and low rates of rock deformation likely to persist for this time

10-100kyr into the future, assuming tectonic boundary conditions stay the same

15 mm/yr

15 mm/yr

leading edge of underthrust Sea of Japan crust (~30 km depth at 100 kyrs into the future)

r

plate motion budget ~100 mm/yr

85 mm/yr

85 mm/yr

100 kyr-1 Myr

Western contractional domain: uplift, rock deformation, and migration of volcanism possible throughout region

Backbone range domain: volcanism, uplift, rock def. on active and pre-existing bedrock structures possible throughout region

Forearc domain: Uplift patterns could evolve depending on deep-seated tectonic processes

100 kyr to 1 Myr into the future, assuming tectonic boundary conditions stay the same

15 mm/yr

15 mm/yr

Current leading edge

leading edge of underthrust Sea of Japan crust at 1 Myr (~37 km depth)

plate motion budget ~100 mm/yr

85 mm/yr

85 mm/yr

Figure 2.2: Schematic of major tectonic domains and likely evolution for the three timeframes of RES 1. Light green :evolving contractional domain associated with underthrusting of the Sea of Japan, light orange: backbone range domain of currently active arc, dashed black line: current likely leading edge of the underthrusting Sea of Japan crust, red line: likely position of the leading edge at the end of each timeframe, red triangle: Quaternary volcanoes (Committee for the Catalogue of Quaternary Volcanoes in Japan, 1999).

2.3 RES 2: Rate of upper plate motion doubles

In this scenario we assume that the rate of long-term (e.g., >1 kyr) horizontal deformation accommodated within the upper plate doubles from its current value (~15 mm/yr) in a linear fashion to ~30 mm/yr at 1 Myr into the future. This is similar to the increase in upper plate deformation that occurred in northern Honshu around 2.4 Ma (Sato and Amano, 1991). There are a number of potential triggers for this scenario, including: (1) an increase in the convergent component of Pacific/Eurasian plate motion in the Tohoku region (this could occur by a anti-clockwise shift in Pacific-Eurasia relative motion vector, or by acceleration of the motion between the two plates); (2) the subducting Pacific slab flattens its subduction angle (similar to what currently occurs along parts of the Andean margin), causing transmission of a larger component of plate boundary strain into the upper plate; (3) the Sea of Japan convergent zone evolves into a self-sustaining subduction plate boundary with a negatively buoyant slab, allowing a progressively larger amount of the plate motion budget to be accommodated in the Sea of Japan due to the evolving slab pull forces.

In this RES (see summary in Figure 2.3) we expect that most of the onshore rock deformation budget will still be accommodated in the backbone range and within western Honshu, but it is very likely that any optimally oriented bedrock structures (approximately north-south striking) anywhere in Tohoku (such as the forearc domain) could be reactivated to accommodate these changes in plate tectonic boundary conditions. In this scenario, it is plausible that rock deformation rates and uplift rates could double[9] in the regions of current active deformation. Increased uplift and erosion could lead to decompression melting of the crust and triggering of ignimbrite and caldera formation. For the most part there is unlikely to be a major change in the position of the volcanic arc in this RES during the time period of interest. However, if an onset of flat slab subduction occurs, the volcanic arc could migrate westward of its current position (Figure 2.3). Perturbation of the flow regime in the mantle wedge is also likely to occur in the flat slab scenario, as well as the scenario where the Sea of Japan evolves into an early stage subduction margin. This should be considered in the context of the volcanic evolution of the region. This RES could open up the possibility of future volcanism anywhere in the backbone range and western northern Honshu during the longer timeframes of interest (e.g., 100 kyr- 1 Myr).

0-10 kyr timeframe. We do not expect this scenario to be significantly different from what is observed today, particularly in terms of the location of deformation, uplift, and active volcanism. Hazard assessments using the ITM methodology will be appropriate for this time period.

10-100 kyr timeframe. We do not expect this scenario to be significantly different from the present day to 10 kyr scenario, although it is possible that some spatial changes in the rates and location of volcanism, deformation, and uplift could begin occurring later in this time period, as fault and volcanic systems evolve. We anticipate that most of the contractional deformation accommodated in the upper plate during this period will continue to occur within the backbone range domain and along the evolving convergent margin adjacent to the Sea of Japan. The steady increase in horizontal convergent rates accommodated within the upper plate during this period (from 15 up to 17 mm/yr) could cause rates of faulting on known active faults to increase correspondingly, or for optimally oriented bedrock structures to be reactivated to accommodate this. This scenario could begin to impact the western contractional domain and the backbone range domain towards the end of the 100 kyr time frame, leading to a larger rock deformation hazard, and potentially larger uplift rates depending on how the fault systems near those locations evolve. Volcanism is unlikely to migrate significantly outside of the current arc on this time frame, although the beginning stages of changes in mantle wedge dynamics (if a flat slab situation has driven the increase in upper plate deformation rate) could lead to the start of volcanic migration into the gap between currently active volcanic centres. At the latest part of this time frame, a change in mantle wedge dynamics could lead to increasing volcanic influence at the backbone range domain, and possible onset of increasing uplift rates due to magmatic contributions. We also note that the increase in contractional deformation that has been observed over the last few million years has been accompanied by an increase in uplift rates along the east coast

---

[9] This value was tentatively set for a demonstration purpose, and requires detailed analyses for actual assessment.

(Regalla et al., 2013). Under RES 2, we expect the forearc domain to begin to experience an increase in uplift rates.

100 kyr – 1 Myr timeframe. During this period the convergent component of plate motion accommodated in the upper plate increases from 17-30 mm/yr. During this time we anticipate that rock deformation will still remain focused within the backbone range and the western part of Honshu, with some reactivation of optimally oriented bedrock structures across the Tohoku region. Rates of deformation in those regions will increase dramatically (perhaps doubling by the end of the timeframe). It is highly likely that migration of arc volcanism into the gaps between the currently active volcanoes will occur during this period, particularly if the increase in convergence rates is accompanied by a change in slab and mantle wedge dynamics. If a period of subducted Pacific slab flattening occurs, then the location of active arc volcanism could be expected to migrate westward from its current position (probably by no more than 20-40 km during this period). If the Sea of Japan convergent zone deformation becomes progressively localized and evolves into an incipient subduction zone, it is possible that larger portions of the convergent component of plate motion being accommodated within the upper plate could shift into the Sea of Japan region during this time, possibly localizing on structures just offshore. Alternatively, larger components of the plate motion budget could be accommodated on the onshore western contractional domain and backbone range domain faults, which would greatly increase the rock deformation and uplift and exhumation hazards at the western contractional domain and the backbone range domain. The future localization of plate boundary deformation into the Sea of Japan region will depend on the details of evolution of the associated fold and thrust belt, and the distribution of optimally oriented bedrock structures. If the Sea of Japan is evolving into a subduction margin, we expect that 1 Myr into the future the leading edge of the underthrusting Sea of Japan crust will have migrated eastward by ~23 km, and will be ~10 km deeper than today, compared to ~30 km depth that we assume for the its current depth (rough estimate based on seismicity). The incipient Sea of Japan subduction scenario would significantly perturb the flow regimes and magma supply within the mantle wedge, and we expect that this scenario could lead to a shut down of active volcanism near the west coast of northern Honshu as the underthrusting Sea of Japan encroaches on and perturbs the magma supply to those regions. This could also have effects on the location of volcanism in the backbone range domain. The impacts of future Sea of Japan subduction on mantle wedge dynamics and future volcanism should be investigated with geodynamic modelling. We also anticipate increasing uplift rates for the forearc domain throughout this time period of enhanced upper plate contraction.

Another consideration for RES 2 in particular (but is also a relevant scenario for all RES discussed here) is that rifted continental fragments exist within the Sea of Japan, based on P-wave velocity anomalies (e.g., Sato, 2013; No and Kodaira, 2013). As convergence between the Sea of Japan and northern Honshu progresses, episodes of collision between these fragments and northern Honshu will occur. Collision of these fragments will lead to more complex collisional deformation in the collision zone in the western contractional domain. Moreover, these collisional events are also expected to perturb the locus and style of current volcanism; in particular, it could also lead to production of collision zone rhyolite or granitic magmas along the Sea of Japan coast, analogous to what has been proposed for Miocene partial melting and intrusive complexes that occurred during the Izu-Bonin arc collision with central Honshu (Tamura et al., 2010). Assessment of the likelihood of continental fragment collision with the Sea of Japan coastline is needed for all RES (especially RES 2) via detailed mapping of the current location of these fragments using existing data, and projection of their likely future point of collision (given reasonable convergence rates and kinematic scenarios) is required.

RES 2, 0-10 kyr

Western contractional domain: patterns of uplift, rock deformation and volcanism likely to be similar to present day

Backbone range domain: patterns of volcanism, uplift, and rock deformation likely to be similar to present day

Forearc domain: Uplift patterns and low rates of rock deformation likely to persist for this time

10-100 kyr

Western contractional domain: patterns of uplift rock deformation, and volcanism may evolve within this timeframe

Backbone range domain: patterns of volcanism, uplift, and rock def. may evolve within this timeframe.

Forearc domain: Uplift patterns and low rates of rock deformation likely to persist for this time

100 kyr-1 Myr

Western contractional domain: accelerated uplift, rock deformation, and west-ward migration of volcanism likely in region

Backbone range domain: volcanism, uplift, increased rock def. on active and pre-existing bedrock structures likely in region

Forearc domain: Uplift patterns could evolve depending on deep-seated tectonic processes

0-10kyr into the future, with assuming tectonic boundary conditions are similar to today

Amurian Plate

Sea of Japan

15 mm/yr

15 mm/yr

100 km contour of the subducting Pacific slab

Forearc region

plate motion vector (plate motion budget ~100 mm/yr)

85 mm/yr

Pacific Plate

85 mm/yr

▲ = volcanoes

leading edge of underthrust Sea of Japan crust (~30 km depth)

10-100kyr into the future, assuming a steady increase in upper plate short-ening rates

15-17 mm/yr

15-17 mm/yr

plate motion budget 100-102 mm/yr

~85 mm/yr

~85 mm/yr

leading edge of underthrust Sea of Japan crust (~30 km depth at 100 kyrs into the future)

100 kyr to 1 Myr into the future, assuming an steady increase in upper plate shortening rates from 17-30 mm/yr over that timeframe

17-30 mm/yr

17-30 mm/yr

possible 100 km contour if slab shallowing occurs

plate motion budget 100-115mm/yr

70-85 mm/yr

70-85 mm/yr

current 100 km contour

original leading edge

leading edge of underthrust Sea of Japan crust (~40 km depth)

Figure 2.3: Schematic of major tectonic domains and likely evolution for the three timeframes of RES 2. Light green :evolving contractional domain associated with underthrusting of the Sea of Japan, light orange: backbone range domain of currently active arc, dashed black line: current likely leading edge of the underthrusting Sea of Japan crust, red line: likely position of the leading edge at the end of each timeframe, red triangle: Quaternary volcanoes (Committee for the Catalogue of Quaternary Volcanoes in Japan, 1999).

16

2.4   RES 3: Relative plate motion becomes more oblique

Pacific Plate absolute motion has undergone a number of changes throughout the Cenozoic (Wessel and Kroenke, 2007, and references therein). In particular, at ~6 Ma Pacific absolute plate motion (APM) underwent shift in direction of motion, leading to more rapid northerly absolute motion of the Pacific Plate, although in northern Japan the result was to shift Pacific Plate APM to a more southerly direction (by ~15 degrees) (Wessel and Kroenke, 2000). It is suggested that this change occurred due to a change in plate boundary forces related to Ontong Java Plateau collision with the Pacific/Australia Plate boundary in the western Pacific and on-going subduction at the northern and western boundaries of the Plate (Wessel and Kroenke, 2000, 2007). This change was not likely to be abrupt, and we expect that it occurred more gradually over a period of ~1 Myr.

In this RES, we assess the possibility that Pacific Plate motion could take a similar shift in the opposite direction over the next 1 Myr period, leading to more oblique relative motion with more northerly-directed Pacific Plate motion in the northern Japan region. In RES 3, we assume that the relative motion vector between the Pacific and Eurasian Plates undergoes a 15 degree clockwise shift from present to 1 Myr in the future; the effect of this shift is to have a larger northward component for the motion of the Pacific Plate relative to Eurasia. This would shift the angle between relative plate motion and the direction perpendicular to the trench (e.g., obliquity angle) from 10⁰ (currently) to 25⁰ at 1 Myr. At subduction plate boundaries such as Sumatra, partitioning of the margin-parallel component of relative plate motion onto strike-slip faults within the upper plate begins to occur when the obliquity angle exceeds some critical angle (dependent on the strength of the upper plate, and the shear stresses acting on the plate boundary; McCaffrey, 1992). In Sumatra and the Philippines, this critical angle is ~20-25⁰, while it is as high as 25-45⁰ in Alaska (McCaffrey, 1992; McCaffrey et al., 2000). One of the major outcomes of an increase in plate motion obliquity suggested in this RES is the potential for reactivation of bedrock structures in the Tohoku region such as the Hatagawa Tectonic Line and the Hizume-Kesennuma Fault (Figure 2.4).
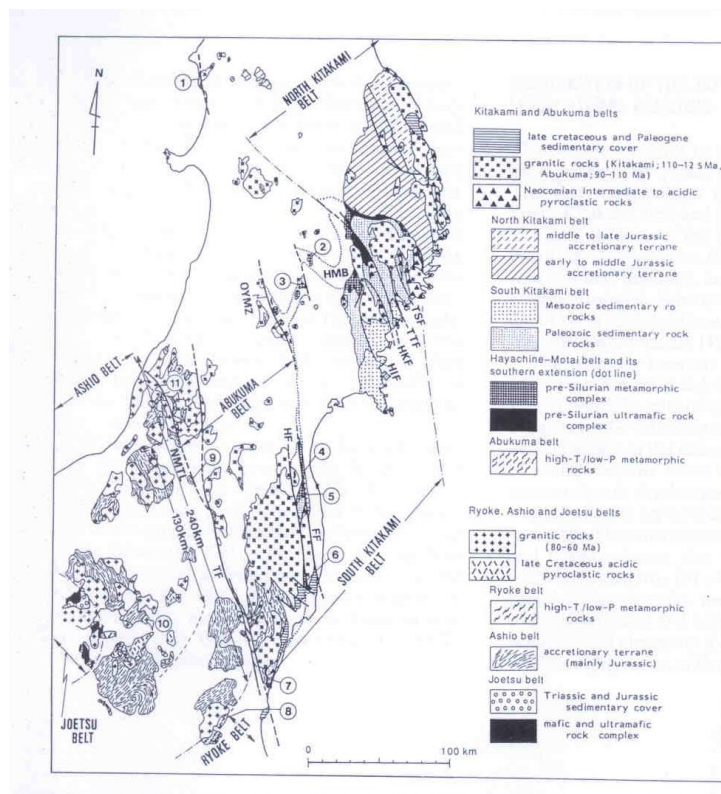
Figure 2.4: Bedrock and fault map from Otsuki (1992). This figure illustrates much of the pre-existing bedrock faulting, including extensive NNW striking faults in the forearc region. It is possible that such faults could become reactivated if there is a change in orientation of relative plate motion.

These currently inactive bedrock structures strike NNW, and are in an ideal orientation to accommodate a more northerly component of Pacific-Eurasia relative plate motion. The results of this RES for the timeframes are summarized schematically in Figure 2.5. We note that this RES has a larger impact on the forearc domain, and is unlikely to be very different from RES 1 for the western contractional domain and the backbone range domain.

0-10 kyr timeframe. We do not expect this scenario to be significantly different from what is observed today, particularly in terms of the location of deformation, uplift, and active volcanism.

10-100 kyr timeframe. We do not expect this scenario to be significantly different from the present day to 10 kyr scenario, although it is possible that some spatial changes in the rates and location of volcanism, deformation, and uplift could begin occurring during this longer time period, as fault and volcanic systems evolve. We anticipate that most of the contractional deformation accommodated in the upper plate during this period will continue to occur within the backbone range domain (Hasegawa et al., 2000) and along the evolving convergent margin adjacent to the Sea of Japan. Volcanism is unlikely to migrate significantly outside of the current volcanic arc.

100 kyr – 1 Myr timeframe. As relative plate motion becomes more oblique to the plate boundary through this time period (the obliquity will increase from just above 10º to 25º by 1 Myr), the potential for reactivating NNW trending bedrock faults in the Tohoku region (Figs. 4 and 5) such as the Tanakura fault increases. We expect that this will particularly come into play during the latter half of this time period (>500 kyr into the future). The point at which slip partitioning in the upper plate begins will depend on the details of the strength of the upper plate and the shear stresses acting on the plate boundary interface and other major faults in the system. Over longer time periods it is possible that some spatial and temporal changes in the distribution of volcanism and rock deformation could occur, but we anticipate that most rock deformation will remain focused within the backbone range and the western part of Honshu, and along optimally oriented NNW trending bedrock faults such as the Tanakura fault. Reactivation of NNW trending structures in the forearc could increase rock deformation hazard at the forearc domain over longer timeframes. It is possible that migration of arc volcanism into the gaps between the currently active volcanoes will occur during this period particularly as the overall plate kinematics change, but it is unlikely that active volcanism will migrate substantially relative to its current position, or migrate across the margin (for example, into the forearc domain). If deformation in the Sea of Japan convergent zone becomes progressively localized and evolves towards an incipient subduction margin, it is possible that larger portions of the convergent component of plate motion being accommodated within the upper plate could shift into the Sea of Japan region, possibly localizing on structures just offshore. The future localization of slip in the Sea of Japan region will depend on the details of evolution of the associated fold and thrust belt, and the distribution of optimally oriented bedrock structures. If the Sea of Japan is evolving into a subduction margin, we expect that 1 Myr into the future the leading edge of the underthrusting Sea of Japan crust will have migrated eastward by ~15 km, and will have reached several km deeper, compared to ~30 km depth that we assume for the its current depth (based on seismicity). Overall, the likely impact of this RES on the western contractional domain and the backbone range domain are similar to those for RES 1.
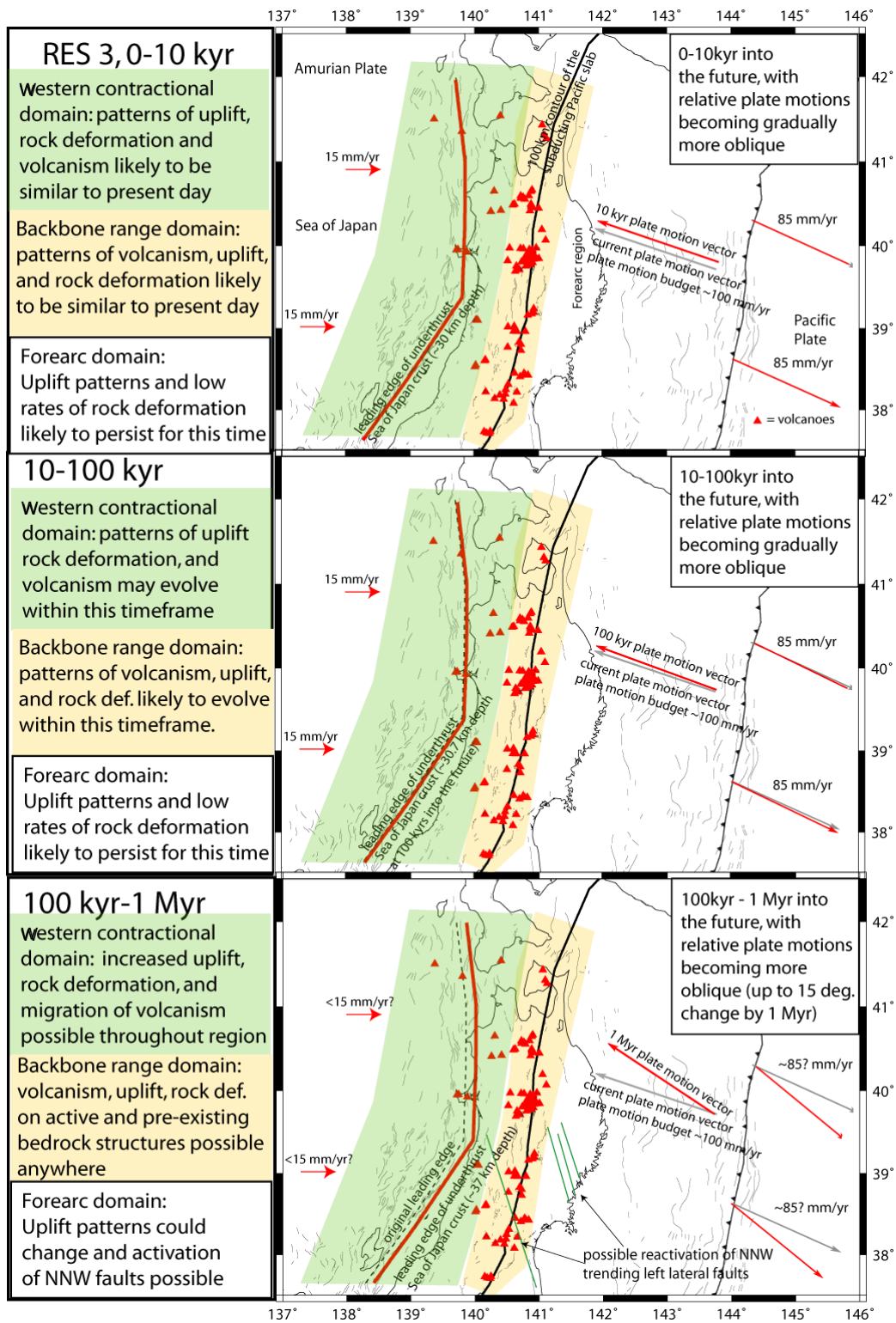
Figure 2.5: Schematic of major tectonic domains and likely evolution for the three timeframes of RES 3. Light green :evolving contractional domain associated with underthrusting of the Sea of Japan, light orange: backbone range domain of currently active arc, dashed black line: current likely leading edge of the underthrusting Sea of Japan crust, red line: likely position of the leading edge at the end of each timeframe, red triangle: Quaternary volcanoes (Committee for the Catalogue of Quaternary Volcanoes in Japan, 1999), dark green lines: some of the NNW trending bedrock structures (e.g. Hatagawa Tectonic Line).

2.5   RES 4: Upper plate shorting decreases to a neutral state

Tectonics in northern Honshu throughout the Cenozoic have been dominated by alternating periods of extension and contraction (Sato and Amano, 1991, among others). From 22-13 Ma, northern Japan tectonics was strongly influenced by backarc rifting in the Sea of Japan, while 13-2.4 Ma was a period of transition from upper plate rifting to upper plate contraction. 2.4 Ma to present has seen a shortening dominated regime in Tohoku upper plate tectonics. Extension in the upper plate of the Sea of Japan region and northern Honshu was most likely driven by the initiation of a phase of rollback of the subducting Pacific slab, as suggested for other plate boundaries worldwide (cf. Schellart and Lister, 2004, and references therein). Oceanic crust subducting at the Japan Trench is Cretaceous in age, and is among the oldest oceanic crust on earth. It is certainly plausible that the slab could founder and that an episode of slab rollback could occur again sometime in the next few Myr. RES 4 (see Figure 2.6) considers the possibility that a phase of slab rollback and a shift to upper plate extension could occur in the near future, and that over the next 1 Myr we could see a transition from the current upper plate shortening regime to a more or less neutral state of stress in the upper plate in the lead up to a phase of backarc extension. At the western contractional domain and the backbone range domain, this would produce a progressive reduction in rock deformation rates, and most likely, a shift to subsidence (as was observed during the Sea of Japan rifting phase in the Miocene). This scenario would also impact volcanic patterns, with a likely eastward migration of the arc out to longer timeframes, possibly into the western part of the forearc domain.

0-10 kyr timeframe. We do not expect this scenario to be significantly different from what is observed today, particularly in terms of the location of deformation, uplift, and active volcanism in Tohoku. Rock deformation, volcanic, and surface uplift/exhumation hazards would be analogous to those estimated using the ITM methodology.

10-100 kyr timeframe. We do not expect this scenario to be significantly different from the present day to 10 kyr scenario, although it is possible that some spatial changes in the rates and location of volcanism, deformation, and uplift could begin occurring during this longer time period, as fault and volcanic systems evolve and the plate tectonic boundary conditions begin to change. We anticipate that most of the permanent contractional deformation accommodated in the upper plate during this period will continue to occur within the backbone range domain and along the evolving convergent margin adjacent to the Sea of Japan, although rates of rock deformation and uplift may be slightly reduced. Volcanism is unlikely to migrate significantly outside of the current volcanic arc.

100 kyr – 1 Myr timeframe. During this time, a substantial decrease in the component of plate motion accommodated as permanent deformation in the upper plate will occur, going from ~15 mm/yr to ~0 mm/yr from 100 kyr to 1 Myr. This will lead to a gradual decrease in the magnitude of contractional deformation in the upper plate. During the latter half of this timeframe (500 kyr to 1 Myr) the rates of rock deformation and uplift will decrease to nearly zero compared to the present day, and potentially transition to subsidence. With the shift to an extensional upper plate environment, volcanism could become more voluminous than is currently observed. It is also likely that the gradual onset of a phase of slab rollback would perturb the flow regime within the mantle wedge substantially, and this could cause some migration of the arc and the current location of volcanism in Tohoku. One possibility is that a small trenchward migration (on the order of a few tens of km) of the volcanic arc into the western forearc domain could occur due to slab rollback. The amount of trenchward migration will depend on the rate of slab rollback. Perturbation of the mantle wedge by the onset of slab rollback would also disrupt the "hot fingers" (Tamura et al, 2002) in the mantle wedge that are feeding the currently active volcanoes, and could lead to volcanism within the gap areas between the active arc volcanoes. Moreover, the occurrence of rhyolitic, caldera-forming volcanism will be more likely in an extensional tectonic environment, and such features could develop in the gaps between the currently active volcanoes. This could lead to increased volcanic impacts at the backbone range domain, as well as increased uplift rates there (relative to surrounding areas), if magmatism migrates significantly into that region. Overall, however, for all domains in Tohoku we expect a shift to subsidence (rather than uplift) as was observed during Miocene Sea of Japan opening (e.g., Regalla et al., 2013).
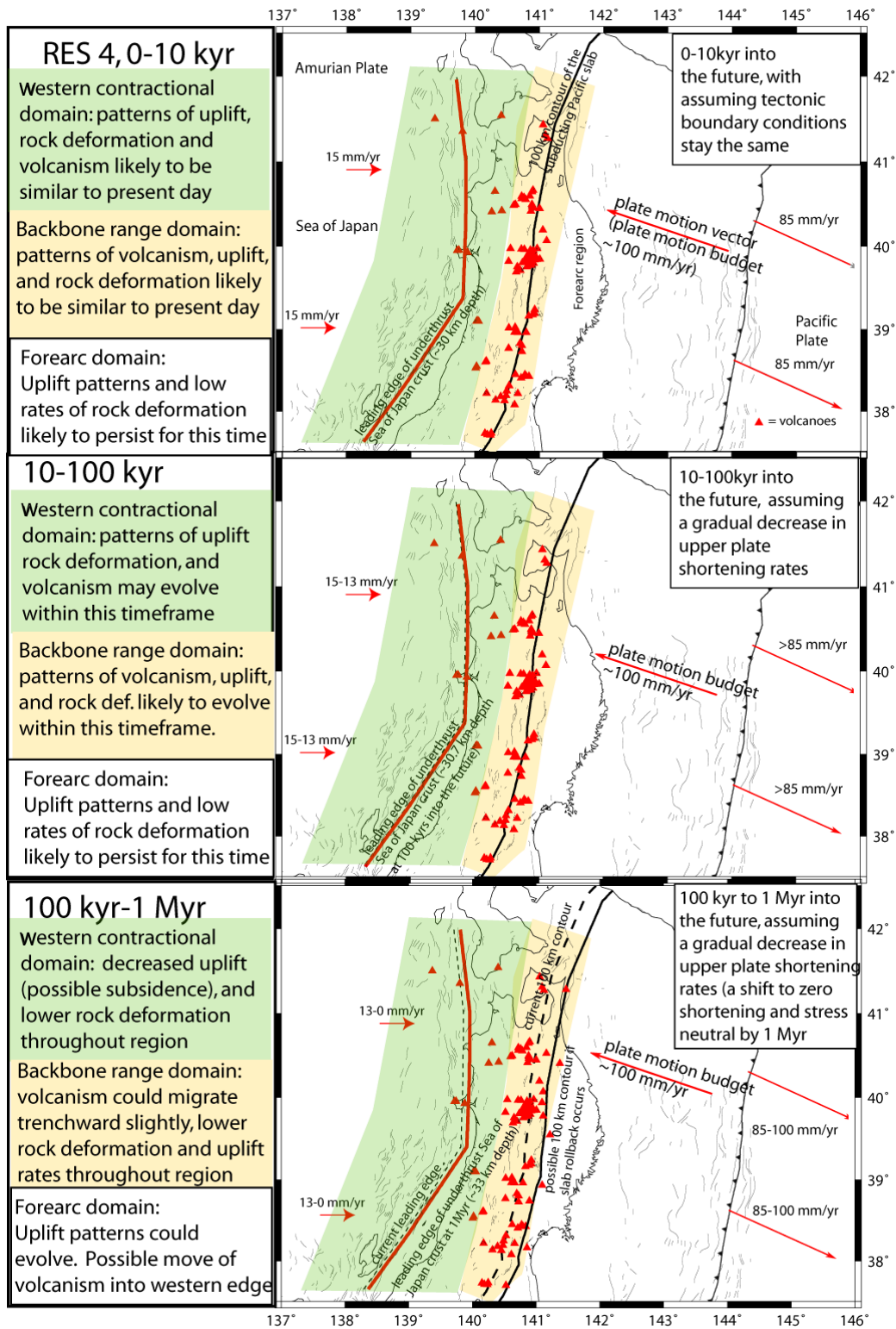
Figure 2.6: Schematic of major tectonic domains and likely evolution for the three timeframes of RES 4. Light green :evolving contractional domain associated with underthrusting of the Sea of Japan, light orange: backbone range domain of currently active arc, dashed black line: current likely leading edge of the underthrusting Sea of Japan crust, red line: likely position of the leading edge at the end of each timeframe, red triangle: Quaternary volcanoes (Committee for the Catalogue of Quaternary Volcanoes in Japan, 1999), heavy dashed black line: current position of the 100 km contour to the surface of the subducting Pacific slab, heavy line: possible position of this at 1 Myr assuming the decrease in upper plate shortening and shift to a stress neutral state related to the rollback of the subducting Pacific slab.

21

2.6   Summary of possible impacts on sub-regions (domains)

Overall, under RES 1 and 3, we expect the rock deformation hazard to stay the same at the western contractional domain and the backbone range domain, or, potentially to increase depending on the details of faulting evolution in those domains (and the potential for reactivation of bedrock faults there). RES 3 would produce a potential increase in rock deformation hazard at the forearc domain. For RES 2, we expect an increase in rock deformation hazard at the western contractional domain and the backbone range domain out to the longer timeframes. Under RES 4, there would be a reduction in rock deformation hazard with time at all three sites, going to very low rates by 1 Myr (although on the 0-100kyr timescale, we expect the rates to be comparable to today).

In terms of volcanic hazard, all RES would produce a similar scenario at all three sites seen today out to 100 kyr. Beyond 100 kyr, all RES indicate that it is plausible for volcanism to migrate into the "gap" between active volcanoes in the arc (e.g., Honda et al., 2007), producing an increased hazard at the backbone range domain. RES 2 could produce an increased volcanic hazard at the backbone range domain, if there is a westward migration of arc volcanism (related to potential slab flattening as part of RES 2). A shift to extension in the upper plate as part of RES 4 could produce more voluminous volcanism in the arc andbackarc, and we would expect elevated volcanic hazard at the western contractional domain and the backbone range domain relative to the other RES.

Increased uplift and exhumation at the western contractional domain and the backbone range domain could be due to an increase in rock deformation rates at those sites, as well as increased volcanic activity. Increased uplift rates due to changes in rock deformation rates is of most concern out to longer time periods in RES 2 (doubling of upper plate rock deformation rates), but it is certainly a plausible scenario for RES 1-3. In general, RES 4 should produce a shift to subsidence over longer timeframes at all three sites, unless a magmatic centre migrated into the western contractional domain and the backbone range domain. A shift to uplift at the backbone range domain (which includes currently in a fault-bounded basin) would be of concern during the latter periods (100 kyr- 1 Myr) for all of the RES, if there is a migration of volcanic activity into the gap areas between the currently active volcanic centres, or if the thrust front migrates basin-ward. Tables 2.1, 2.2 and 2.3 summarize the possible impacts of RES 1-4 at different timescales for all three domains.

Table 2.1: Summary of possible impacts on the western contractional domain

	0-10 kyr	10-100 kyr	100 kyr-1 Myr
RES 1	Similar to present day	Constant or increased rates of rock deformation and uplift/exhumation, no change in volcanism.	Constant or increased rates of rock deformation and uplift/exhumation, potential for shifts in the locus of volcanism and increased volcanic hazard
RES 2	Similar to present day	Increased rates of rock deformation and uplift/exhumation, no change in volcanism	Possible doubling of rates of rock deformation and uplift/exhumation, potential for shifts in the locus of volcanism (westward migration) and increased volcanic hazard. Role of incoming continental fragments in the Sea of Japan should be accounted for, as this will cause local increases in rock deformation rates, and perturbation of the present volcanic regime. The latter could be an issue for WCB site in all RES.
RES 3	Similar to present day	Constant or increased rates of rock deformation and uplift/exhumation, no change in volcanism	Constant or increased rates of rock deformation and uplift/exhumation, potential for shifts in the locus of volcanism and increased volcanic hazard
RES 4	Similar to present day	Constant or decreased rates of rock deformation and uplift/exhumation, no change in volcanism	Decreased rates of rock deformation and uplift/exhumation. Distinct shift to subsidence There is potential for shifts in the locus of volcanism and increased volcanic hazard (due to more voluminous volcanism in an extensional regime).

Table 2.2: Summary of possible impacts on the backbone range domain

	0-10 kyr	10-100 kyr	100 kyr-1 Myr
RES 1	Similar to present day	Constant or increased rates of rock deformation and uplift/exhumation, no change in volcanism.	Constant or increased rates of rock deformation and uplift/exhumation, potential for migration of volcanism into the volcanic "gaps" and increased volcanic hazard (and associated uplift)
RES 2	Similar to present day	Increased rates of rock deformation and uplift/exhumation, no change in volcanism	Constant or increased rates of rock deformation and uplift/exhumation, potential for migration of volcanism into the volcanic "gaps" and increased volcanic hazard (and associated uplift).
RES 3	Similar to present day	Constant or increased rates of rock deformation and uplift/exhumation, depending on details of fault evolution there; no change in volcanism	Constant or increased rates of rock deformation and uplift/exhumation, potential for migration of volcanism into the volcanic "gaps" and increased volcanic hazard (and associated uplift)
RES 4	Similar to present day	Constant or decreased rates of rock deformation and uplift/exhumation, no change in volcanism	Decreased rates of rock deformation and uplift/exhumation. Distinct shift to subsidence. There is potential for shifts in the locus of volcanism and increased volcanic hazard (due to more voluminous, potentially rhyolitic, volcanism in an extensional regime).

Table 2.3: Summary of possible impacts on the forearc domain

	0-10 kyr	10-100 kyr	100 kyr-1 Myr
RES 1	Similar to present day	Constant or increased rates of uplift/exhumation	Constant or increased rates of rock deformation and uplift/exhumation
RES 2	Similar to present day	Increased rates of uplift/exhumation	Constant or increased rates of rock deformation and uplift/exhumation
RES 3	Similar to present day	Constant or increased rates of rock deformation and uplift/exhumation	Constant or increased rates of rock deformation and uplift/exhumation
RES 4	Similar to present day	Constant or decreased rates of rock deformation and uplift/exhumation	Decreased rates of rock deformation and uplift/exhumation. Distinct shift to subsidence.

2.7   Examples of additional aspects of tectonic evolution for the RES

The well-developed volcanic arc in central northern Honshu (coinciding with the backbone range) has remained roughly in its current location since at least 10 Ma (e.g., Finn et al., 1994). Conceptual models have been developed to explain the distribution of arc volcanism in northern Honshu, such as the "hot finger" model (Tamura et al., 2002). The hot finger model helps to explain the clustering of volcanic centres along the arc (with non-volcanic gaps in between) as well as some volcanism in the backarc region of western northern Honshu. An important consideration for Tohoku RES is how models such as the "hot finger model" might be expected to evolve in to the future, and how this will influence the locations of future magmatism and rock deformation. Honda et al. (2007) demonstrate that the distribution of arc volcanism appears to "flip-flop" between the current location and the gaps in between the active volcanoes every 5 Myr or so. We discuss this briefly in RES 1, and in practice, this concept should be applied more fully to all RES with more precise knowledge of the distribution of volcanism for the last 10-20 Myr.

The 2011 M9 earthquake has led to a reversal in the stress field (to an east-west extensional regime) throughout Tohoku as documented by numerous seismological studies over the last years. In light of this, we should also consider the possibility that any optimally oriented bedrock faults (generally, north-south trending) could be temporarily reactivated as normal faults following a giant megathrust earthquake as has been observed following the 2011 event.

It is also important to consider the impact that deep-seated processes could have on rates of tectonic uplift in Tohoku. For example, processes such as deep underplating of subducted sediment can lead to rapid uplift at subduction margins (e.g., Walcott, 1987). In contrast, deep basal subduction erosion can lead to subsidence of the margin, as has been suggested for the east coast of northern Honshu by Heki (2004) in order to explain observed subsidence at continuously running GPS sites. A more recent study (Regalla et al., 2013) suggests that changes in the rate of Pacific Plate convergence (and the impact of this change on slab dynamics) has led to periods of uplift and subsidence in the past. Assessment of the potential influence of these and other deeply seated subduction zone processes on the future vertical tectonic motion in the Tohoku region can be incorporated into alternative RES and/or as options within the suggested RES presented here.

3   Site Evolution Scenarios

We redeveloped Site Evolution Scenarios (SES) for three example sites, in which uplift and erosion rates were estimated based on regional data, that had not previously been investigated. The scenarios are shown as the storyboards in Figure 3.2 to Figure 3.4 for example sites described below. The storyboards are intended to demonstrate visually how each of the RES might manifest itself as a variety of site evolution scenarios, which may impact the repository footprint during the time periods of interest. These are largely intended to demonstrate the use of storyboards to develop these scenarios. These are not considered as complete or detailed descriptions of the impact of the various RES at any of the example sites. Undoubtedly, there is a larger variety of SES that could be considered at these sites than are shown in this demonstration.

3.1   Example sites for SES demonstration

Three example sites for the SES demonstration were selected to represent the three tectonic domains described in Chapter 2. These are the West Coast Backarc (WCB), Inland Basin (IB) and East Coast Forearc (ECF) (Figure 3.1), based mainly on the availability of data on uplift and erosion.

West Coast Backarc (WCB):

Example site WCB is located within the crest of a growing anticline, on the Sea of Japan Coast, within the fold and thrust belt comprising a contractional zone. This site is identical with the Site C in the previous TOPAZ Tohoku case study (Chapman et al., 2012) and the Site 8 in the ITM Tohoku case study (Chapman et al., 2008).The area is marked by high historical seismicity rates and high GPS crustal strain rates. It is located within 500 m of the active Noshiro Fault (on the hanging wall of the fault), which has a vertical slip rate of 0.4-1.4 mm/yr. Blind thrusts and flexural slip faulting may be widespread in this area. Okamura et al. (2007) have shown that the folds in the Niigata area to the south are forming above steep reverse faults that are mostly reactivated normal faults formed during Miocene rifting. The site is located north-west of the Sengan Cluster, in the low-lying inter-cluster region, and the nearest volcano (Kampu Volcano) is 32 km distant.

The geology of this area is characterized by Quaternary (marine terrace) sediments (mud, sands, and gravel) over Tertiary sediments (mid-late Miocene and Pliocene sandstone and siltstone). The Tertiary sediments would be the likely host rocks for a 300 m deep repository.

Inland Basin (IB):

The IB site is situated within an actively subsiding basin in the backbone range, within a volcanic 'gap' region between the Sengan and Chokai clusters, and near to an active fault. This site is close to but in between the Site 1 and Site 12 in the ITM Tohoku case study (Chapman et al., 2008). The nearest volcano is 30 km to the northeast (Inai-Takahachi). It is located in an area of high historical seismicity and high contractional strain from GPS.

The geology of the area consists of Quaternary (alluvial fan) sediments overlying Late Miocene-Pliocene shales, sands, gravels, and clays, as well as early-middle Miocene tuff, mudstone, and sandstone.

East Coast Forearc (ECF):

Example site ECF is on the Sanriku (Pacific) Coast in the forearc region of Tohoku, on the relatively stable Kitakami Block. This site is identical with the Site 12 in the ITM Tohoku case study (Chapman et al., 2008).This is in an area of no volcanism; the nearest cluster (Sengan) is 100 km to the west, while the nearest volcano is 88 km to the northwest (Iwate). The nearest major active fault is 53 km to the northwest, although there is a possibility of unmapped near-coast submarine faults. A NNE-trending inactive bedrock fault exists adjacent to the site.

The bedrock geology is characterized by Mesozoic crystalline rocks, mostly consisting of Paleocene to early Eocene dacite, welded tuff, and tuff breccia. The Mesozoic rocks would be the likely host for a 300 m deep repository. Nearby there are also early Cretaceous dacite to rhyolite lavas, pyroclastic rocks, granodiorite, and granite. Relatively thin (a few metres) Quaternary marine terrace deposits likely overlie the site.
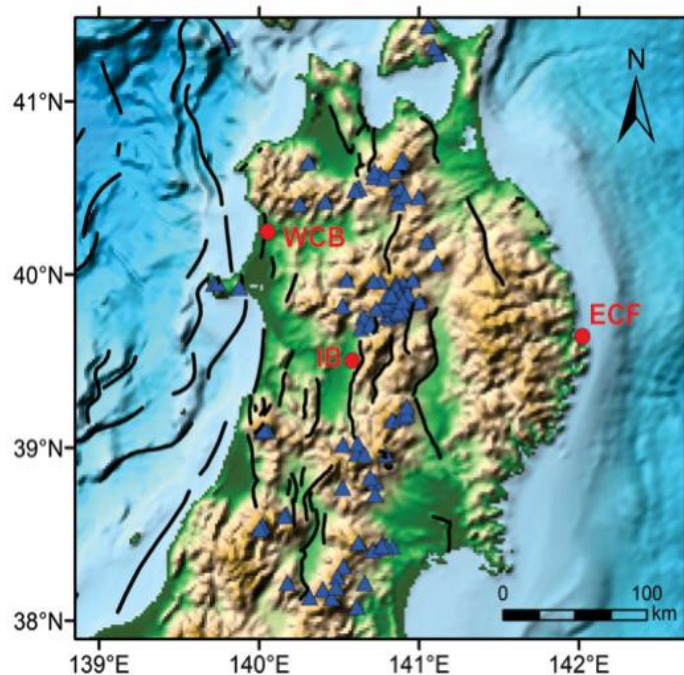
Figure 3.1: Example site locations for the SES demonstration. WCB: West Coast Backarc; IB: Inland Basin; ECF: East Coast Forearc. Blue triangles: Quaternary volcanoes (Committee for Catalogue of Quaternary Volcanoes in Japan, 1999), solid ines: active faults (AIST, 2013).

3.2   Data on regional scale uplift and erosion

The Tohoku area is undergoing both local and regional scale uplift. Local scale uplift is occurring on the upthrown side of reverse faults (tectonic uplift), which are often characterised by fault-associated anticlines, and above volcanic intrusions (volcanic uplift). These localised uplifts predominantly occur along the (Ou) backbone range (tectonic and volcanic uplift) and along the Sea of Japan coast (tectonic uplift). Regional scale uplift also appears to be occurring across the majority of Tohoku and is likely related to the Japan Subduction Zone, possibly by an isostatic response to crustal thickening (e.g., Matsu'ura et al, 2008, 2009).

Uplift rates along the Tohoku coast are generally well constrained from Pleistocene and Holocene marine terraces (e.g., Miyauchi, 1988; Ota and Omura, 2009; Ota 2010). By contrast, and like most places around the globe, uplift rates inland are less well constrained. One dataset that has been used is the vertical spacing between fluvial terraces (Yoshiyama and Yanagida, 1995; Tajikara and Ikeda, 2005). Tajikara and Ikeda prepared a map of uplift across Tohoku using a combined marine (125,000 year) and fluvial terrace (≤140,000 year) dataset (Figure 3.2; Koike, et al., 2005). Although some of the fluvial terrace ages have subsequently been questioned (Matsu'ura et al. 2008), we consider this the best available dataset for regional scale uplift rate in the Tohoku area. We have therefore calculated uplift rates from this dataset by dividing the uplift values by the age of the marine terrace or the time between fluvial terraces, 125,000 years.

With regard to regional scale erosion dataset for the Tohoku region, Fujiwara et al. (1999) constructed an erosion rate map for the whole of Japan derived from the relationship between (contemporary) sediment delivery rates to reservoirs and the dispersion of altitude of the drainage basin (Figure 3.3). However, although this is based on a 6 x 6 km grid (similar to the 5 x 5 km grid used in this study) the drainage basin scale means it is too coarse for use in this study.

26
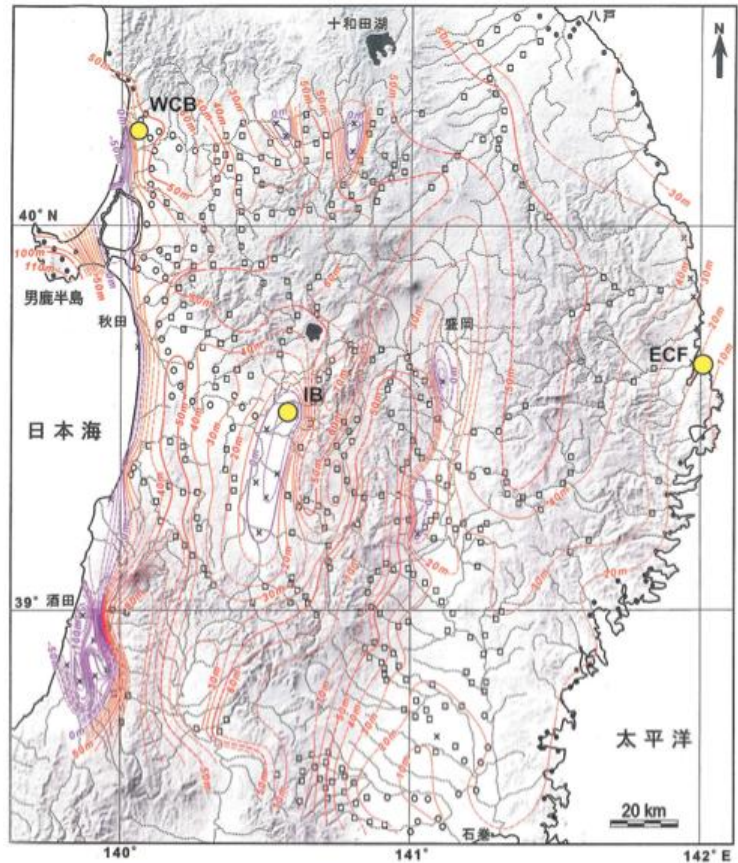
Figure 3.2: Map showing uplift in metres of a normalised 125,000 timeline across the northern Tohoku area, derived from marine and fluvial terraces (Koike et al., 2005; prepared by M. Tajikara). The locations of the example sites are also shown.
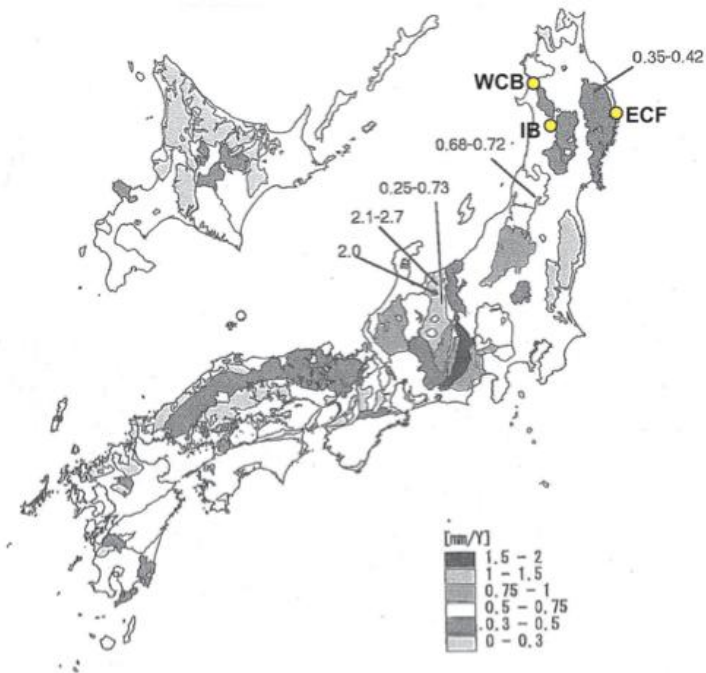
Figure 3.3: Erosion rate map for the Japanese Islands derived from sediment delivery rates and the dispersion of drainage basin altitude (Fujiwara et al., 1999). The locations of the example sites are also shown.

3.3 Estimation of uplift and erosion rates for the example sites

West Coast Backarc (WCB):

The mean uplift rate is relatively well constrained from the current altitude (~50 m - Figure 3.2; also Miyauchi, 1988; Shiraishi et al., 2008) of the 125,000 year old marine terrace strandline (~landward cliff above the terrace), at ~0.4 mm/yr. We infer uncertainties of ± 0.2 mm/yr, mainly to take into account likely uncertainties in the terrace altitude (from terrace coverbeds and the fact that the site is not at the strandline).

There are no erosion rate data, but we infer an erosion rate of 0.2 ± 0.1 mm/yr, which is half the uplift rate and takes into account the soft to moderately hard bedrock beneath the marine terrace (i.e., the likely host rock for a repository). Over longer timeframes, the erosion rate could increase through river and coastal erosion.

Inland Basin (IB):

The mean uplift (subsidence) rate, rate is -0.15 mm/yr, and is derived from the regional scale uplift map (Koike, et al., 2005; Figure 3.2). The rate appears to be from the vertical spacing between fluvial units, which are presumably from drill hole or geophysical data. A relatively large uncertainty of ±0.1 mm/yr is assigned to reflect the likely uncertainty on the dating of the fluvial units.

There is no erosion (burial) rate data, and so we infer a rate of -0.1 ± 0.05 mm/yr, which is slightly less than the subsidence rate. This rate reflects likely incomplete filling of the basin and little to no compaction if the sediments are mostly alluvial gravels. It is possible that the erosion rates could increase with time, particularly if the nearby Senya Fault migrates basin-wards, leading to uplift at the site, or the rivers migrate to the site.

East Coast Forearc (ECF):

The mean uplift rate is relatively well constrained from the current altitude (~15 m – Figure 3.2; also Miyauchi et al., 2005; Miyauchi, 2011) of marine terraces, at ~0.1 mm/yr. We infer an uncertainty of ±0.05 mm/yr, mainly to take into account likely uncertainties in the terrace altitude (from terrace coverbeds and the fact that the site is not at the strandline).

There is no erosion rate data, but the site is situated on relatively hard early Tertiary volcanic rocks, and so we infer a very low mean erosion rate of 0.05 ± 0.05 mm/yr, which is half the uplift rate. Over longer timeframes (>100 kyr), lateral coastal erosion could impact the site.

The estimated rates for each site are summarised in Table 3.1.

Table 3.1: Uplift and erosion rates estimated for the three example sites for use in this study.

Site	Uplift rate (mm/yr)		Erosion rate (mm/yr)	
	Mean	Uncertainty	Mean	Uncertainty
WCB	0.4	0.2	0.2	0.1
IB	-0.15	0.1	-0.1	0.05
ECF	0.1	0.05	0.05	0.05

3.4 Site Evolution Scenarios for the West Coast Backarc (WCB)

See storyboard at Figure 3.4

RES1

- *SES1:* The repository lies within a growing anticline in mid Miocene sedimentary rocks. Over the 1 Myr timeframe the anticline becomes tighter, and fault displacement accumulates at the margins, as well as secondary faulting, and possible flexural slip faulting within the repository footprint. Up to 400 m of uplift and 200 m of vertical erosion results in exhumation of the repository by 1.5 Myr. Volcanism could also initiate nearby within longer timeframes (>500 ky).
- *SES2:* As for SES1 except more rapid uplift and erosion rates result in more rapid rock deformation and repository exhumation—exhumation of the repository occurs by 750 kyr.
- *SES3:* Anticline development and associated deformation and uplift decreases over time as convergent deformation becomes increasingly localised offshore. Vertical erosion over the 100 kyr - 1 Myr time period leads to 50 m of erosion, and 200 m of uplift.

RES2

- *SES1:* As for RES1/SES1.
- *SES2:* As for RES1/SES2.
- *SES3:* As for SES2 above, but further increased contraction deformation in the vicinity of the west coast related to possible slab flattening results in even more intense rock deformation in the repository area. Uplift of up to 1500 m, and vertical erosion of up to 750 m results in repository exhumation by 400 kyr. Possible initiation of volcanism nearby.

RES3

- *SES1:* As for RES1/SES1
- *SES2:* As for RES1/SES2
- *SES3:* As for RES1/SES3

RES4

- *SES1:* As for RES1/SES3

Figure 3.4: Storyboard showing the site evolution scenarios for the WCB site.

3.5 Site Evolution Scenario for the Inland Basin (IB)

See storyboard at Figure 3.5.

RES1

- *SES1:* The repository lies within Miocene sedimentary rocks, and beneath the centre of an actively deepening basin. Over the million-year timeframe the basin slowly deepens as a result of progressive fault displacement at the basin margins. Basin margin volcanism could also initiate in the 100 kyr - 1 Myr timeframe, if the arc volcanism migrates into the volcanic gap region. Deposition within the basin increase the repository burial depth by up to 100 m throughout the 1 Myr time frame of basin development.
- *SES2:* As for SES1, except that accelerating rock deformation rate over time produces secondary fault displacement within the basin and potentially through the repository. Increased slip rates on basin bounding faults may cause the basin to deepen more rapidly, resulting in additional repository burial—up to 200 m by 1 Myr.
- *SES3:* As for SES1 except that volcanism develops more rapidly and intensely due to lateral migration of volcanism into this 'gap area'.

RES2

- *SES1:* As for RES1/SES1
- *SES2:* As for RES1/SES2
- *SES3*: As for above SES2 except that deformation rates, including secondary faulting within the basin, become even more intense. Lateral migration of volcanism could occur earlier due to possible large-scale tectonic perturbations on the system.

RES3

- *SES1:* As for RES1/SES1.
- *SES2:* As for RES1/SES2.
- *SES3:* As for RES1/SES3.

RES4

- *SES1:* As for RES1/SES1.
- *SES2:* Rate of development of the basin decreases over time, with cessation of all rock deformation by 1 Myr. Burial rates in the basin are much smaller due to decreasing deformation on basin bounding faults, with cumulative burial of the site up to 25 m by 1 Myr.

Figure 3.5: Storyboard showing the site evolution scenarios for the Inland Basin site.

32

3.6 Site Evolution Scenarios for the East Coast Forearc (ECF)

See storyboard at Figure 3.6.

RES1

- *SES1:* The repository lies within Mesozoic bedrock and beneath a stable marine platform on the east coast. The area continues its low and uniform rates of uplift and erosion over the next 1 Myr. The main potential impacts on repository integrity over time are bedrock fracturing due to shaking from regional earthquakes, and chemical weathering in the near-surface bedrock, particularly along fractures. Over the 1 Myr time period the platform continues to be gradually uplifted and eroded, achieving 100 m of uplift, and up to 50 m of erosion (assuming erosion rates of 0.05 mm/a).
- *SES2:* As for SES1, except with more rapid rates of uplift (up to 500 m over 1 Myr) and consequent erosion (up to 100 m out to 1 Myr).
- *SES3:* Platform uplift decreases to nil by 500 kyr, with an accompanying decrease in erosion rates. This yields up to 50 m of uplift and up to 20 m erosion achieved by 1 Myr.

RES2

- *SES1:* As for RES1/SES1.
- *SES2:* As for RES1/SES1, except greater uplift (up to 300 m) and erosion (up to 100 m) of marine platform achieved by 1 Myr.
- *SES3:* As for SES 2 above, except for even more rapid rates of uplift and erosion at later stages, due to higher upper plate deformation rates due to possible slab flattening. Uplift of up to 500 m and erosion of up to 250 m suggest that if maximum uplift and exhumation rates are reached, the repository could be exhumed by ~1.2 Myr.

RES3

- *SES1:* As for RES1/SES1.

RES4

- *SES1:* As for RES1/SES1.
- *SES2:* As for RES1/SES3.
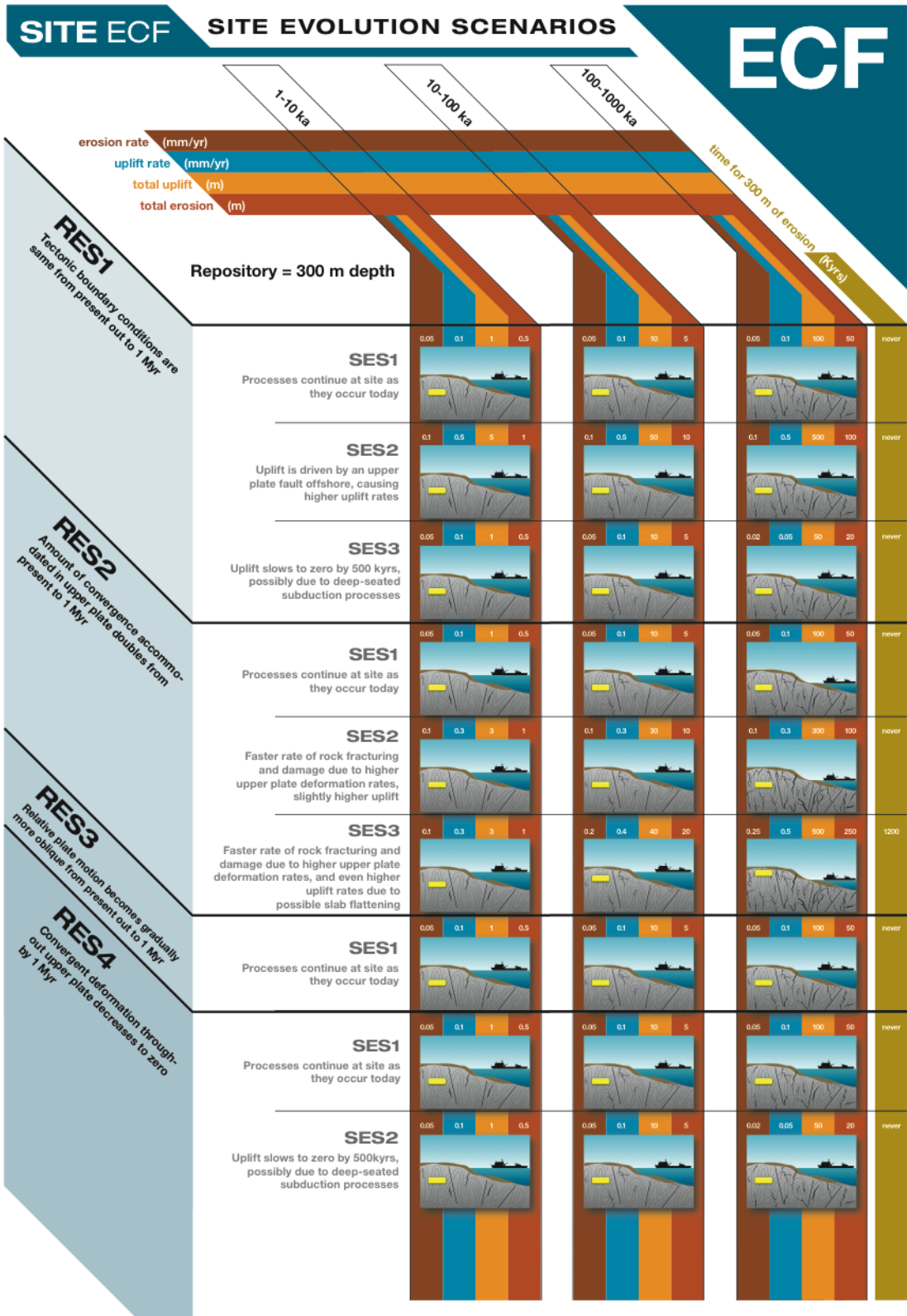
Figure 3.6: Storyboard showing the site evolution scenarios for the East Coast Forearc site.

4   Introduction to the Impact Scenarios

The purpose of this chapter is to present site-specific considerations that would be factored into natural-event Impact Scenarios (IS) for the three illustrative sites considered in Chapter 3. The previous report (Chapman et al., 2012) presented a detailed examination of impacts on a repository arising from faulting and volcanism. Therefore, this section focuses on presenting illustrations of exhumation scenarios for each of the three sites.

4.1   Evolution of a HLW repository

As previously discussed, there are several aspects of timescale and the evolution of a deep geological repository that must be kept in mind when examining natural-event scenarios. First and foremost, within several thousands of years (a relatively short timeframe compared to evolving volcano-tectonic conditions in Japan), the radiological hazard of HLW diminishes to extremely low levels.

Furthermore, consider the evolving physicochemical characteristics of the engineered barriers leading to degradation of their safety functions. After 1 kyr to 5 kyr, the initial mild steel overpack will have corroded to the point of failure, allowing groundwater to contact and initiate dissolution of the HLW borosilicate glass. The dissolution time for the HLW glass depends on a number of factors, including degree of cracking/enhancement to surface area, but a conservative estimate would be about 70 kyr. Thus, within several tens of thousand years, the initial safety functions of the EBS barriers (metal overpack and borosilicate waste-form) are no longer operative or needed. The original EBS materials will have basically converted to a thermodynamically more-stable assemblage of insoluble, slightly radioactive oxides, hydroxides and silicates surrounded by iron hydroxides/ oxides of the corroded overpack, in turn surrounded by a compacted layer of clay. More soluble radionuclides will have been released, yet dispersed and diluted throughout the rock volume surrounding the EBS. At ambient environmental conditions, the residual phases remain unreactive over the million-year timescales or more, as evidenced by numerous geological and natural analogue studies. In essence, the engineered repository will have evolved to a 'natural state' that is relatively inert with respect to plausible thermal-hydrological-mechanical-chemical (THMC) impacts that might arise from natural-event scenarios. Off course the isolation provided by the natural rock barrier of 300m depth will continue beyond this period.

Of particular importance to long-term isolation of radioactivity in a 'natural-state' repository is the low redox potential (Eh) that prevails for deep repository sites. Low Eh assures extremely low solubilities (retention) and high sorption behaviour (retardation) for many safety-significant radioelements, such as U, Pu, Np, Tc and Se. Prolonged elevated temperature, for example from nearby intrusion of magma, could also elevate the solubility of residual radionuclide-bearing solids. The leading concern of any longer term (>50,000 years) combined RES/SES scenario, however, would be if a natural event led to transport of the residual, insoluble radioactive phases to the near-surface or exposure at the ground surface.

4.2   General Impact Scenarios for exhumation (uplift and erosion)

Figure 4.1 shows a schematic cross section of a hypothetical site in which a HLW repository has been emplaced at an initial depth of 300 meters at a present day site. For this illustrative case, it is further assumed that the site has a present-day mean uplift rate of 0.1 mm/year, as possibly determined through a set of independent, complementary geophysical and geodetic methods. This illustrative site also has topography, hence erosional processes that operate to reduce the height and lateral face of terrain as it is uplifted. Uplift rate and erosion rate can be viewed as more-or-less independent processes that depend on a number of site-specific factors, such as regional strain rate, lithology, existing structural features, climate, topography, etc. For the purpose of a simple schematic illustration, it is assumed in Figure 4.1 that the erosion rate matches the uplift rate. Therefore, the 'exhumation rate', the rate at which the buried repository might approach the surface, would be equal to the uplift rate[10].

---

[10] Off course some sites may be experiencing subsidence rather than uplift. For such a site, if deposition (as opposed to erosion) rate equals subsidence, the repository would become more deeply buried, equal to the subsidence rate integrated over a specific time.
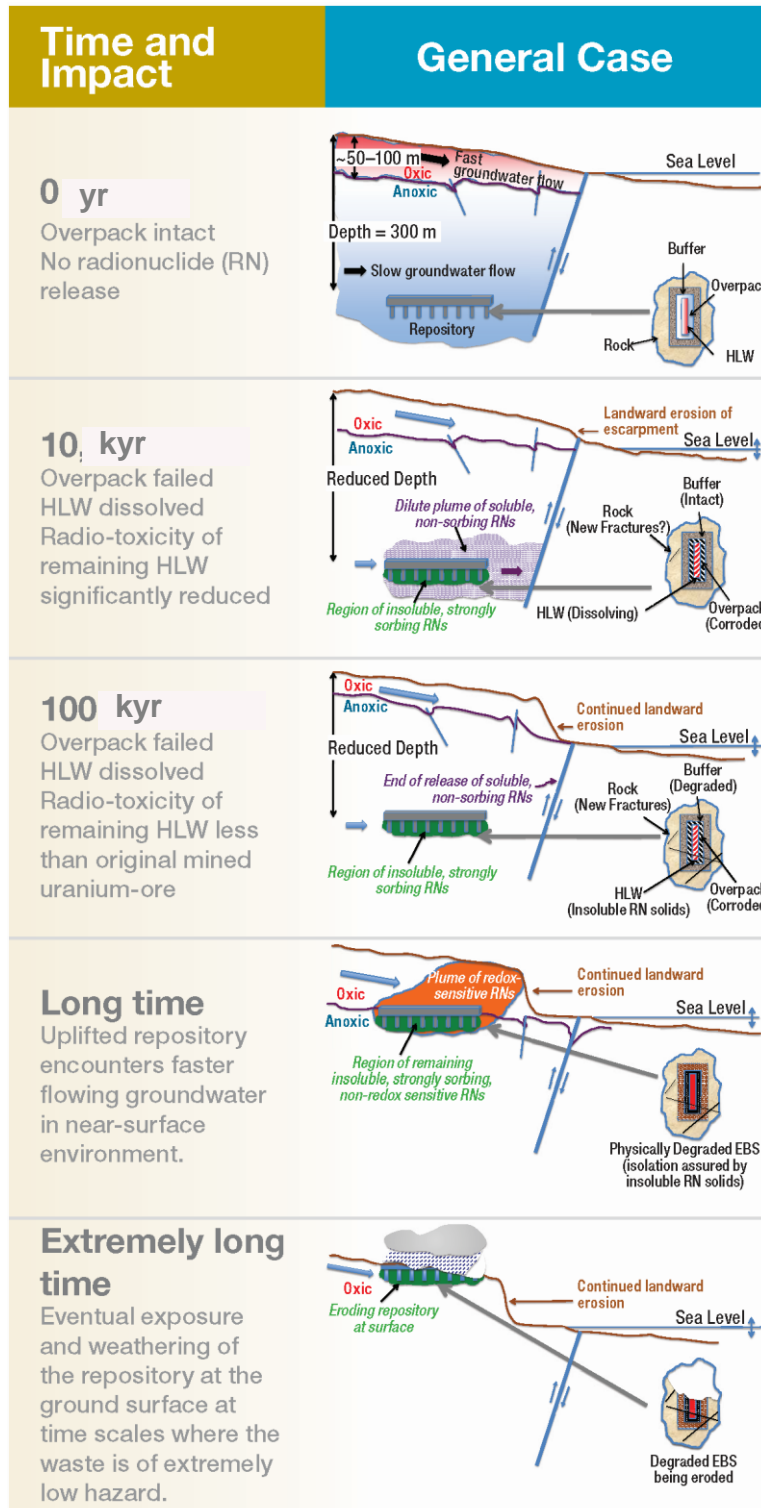
Figure 4.1: Progressive uplift of the repository at an exhumation rate of 0.1mm/year for time steps of 10 kyr, 100 kyr and beyond into the future.

At each time step, a 'cartoon' is included to illustrate the progressive degraded state of the EBS component barriers (HLW borosilicate glass, mild steel overpack and bentonite clay buffer) emplaced within a generic host rock.

Also shown in Figure 4.1 is the approximate 'fate' and 'migration' of various types of radionuclides. In the first 1 kyr to 5 kyr, the overpack has failed by corrosion, and the HLW has experienced significant dissolution. As noted previously (Chapman et al., 2012), it is a significant safety factor that the radiological hazard of HLW significantly decreases over time, within about 3 kyr reaching an equivalent radiotoxicity hazard of the original uranium ore from which the reprocessed radioactive waste was fabricated.

After about 70 kyr the HLW borosilicate glass will have been fully dissolved, and converted into more thermodynamically stable (hence less soluble) alteration solids. Highly soluble and non-sorbing radionuclides, if present, will have been released by this dissolution and transported through the hydrological system of the site to some distant sub-vertical, major water-bearing feature (e.g., a fault). These nuclides will then have been transported to the surface environment, although additional, significant dilution may occur depending on specific discharge pathway. By contrast, the great majority of radioelements will remain within the EBS, in the form of insoluble radionuclide-bearing solids that precipitate from the dissolution of the HLW glass.

Eventually about 3 Myr in the future for this case, a degraded 'natural state' repository nears the surface by means of sustained uplift and erosion. There are two factors to consider at this point with respect to enhanced radionuclide release to the accessible environment:

- Many radioelements become more soluble and less sorptive under oxidizing conditions. The depth to which O_2-rich surface waters percolate into the sub-surface hydrological setting depends on many site-specific features, and as a bounding assumption a 100m depth of oxic surface water is assumed in Figure 4.1.
- The transport pathways for radionuclides to reach the surface environment become shorter (Figure 4.1).

If uplift and erosion is taken to an endpoint, a degraded repository may be exhumed at the ground surface in this illustration. Obviously this would to significant radiological release through water, and possibly air-borne, pathways. There might also be direct exposure to future humans, although the radiological exposure-hazard of HLW at 3 Myr would be extremely low, well below that of naturally occurring uranium ore bodies for example.

4.3   Uplift, erosion and exhumation scenarios at the example sites

WCB Site

The interpreted uplift rate for the WCB site is 0.4 +/- 0.2 mm/yr, while the estimated erosion rate is 0.2 +/- 0.1 mm/yr. Figure 4.2 shows the time sequence in the evolution of a repository at such a site at 10 kyr, 100 kyr and 1 Myr and beyond 1.5 Myr into the future. If both rates are assumed to remain constant into the future, the repository at an initial depth of 300 m would rise to the level that oxic surface waters might begin to percolate down to the depth of the degrade repository. Of course sideways (landward) erosion of the escarpment of the uplifted terrain might also allow lateral access or even partial exposure of the uplifted residual repository. At this time period in the far future, however, the radiological hazard of the degraded HLW repository is significantly reduced, for example far below that for the comparable uranium ore from which the HLW was fabricated.

IB Site

For the IB site, the inferred subsidence (rather than 'uplift') rate is -0.15 +/- 0.1 mm/yr. A burial (rather than 'erosion') rate is estimated to be -0.1 +/- 0.05 mm/yr. Figure 4.2 shows the time sequence in the evolution of a repository at such a site at 10 kyr and 100 into the future. In this case, over the next 1 Myr, the repository at an initial depth of 300 meters would become deeper over time. Certainly the potential for intrusion of oxidizing groundwater from the surface becomes evermore less likely because of such subsidence. Increasing depth would increase overall system pressure on the repository, however such a pressure increase would have a negligible impact on isolation. Change in pressure has only a minor impact on the

solubility of condensed phases, such as the residual radionuclide-bearing solids. Hydrological path lengths for any radionuclide migration might become ever longer with increasing depth.

ECF Site

The ECF site has an estimated uplift rate of 0.1 +/- 0.05 mm/yr, with an inferred erosion rate equal to 0.05 +/- 0.05 mm/yr. This is similar to the general illustrative case presented; with the exception that erosion rate is lower (half) than the uplift rate. Figure 4.2 shows the time sequence in the evolution of a repository at such a site at 10 kyr, 100 kyr, 1 Myr, 4 Myr and beyond 6 Myr into the future. At about 4 Myr, the repository would approach the level of the initial ground surface, and could experience contact with oxic surface water percolating to depth. Lateral (landward) erosion of the escarpment of the uplifted terrain might allow sideways intrusion or even exhumation of the repository. At extremely long time periods into the future the degraded repository might be exposed at the surface, although radioactive decay will have reduced the radiological hazard of the degrade HLW substantially.
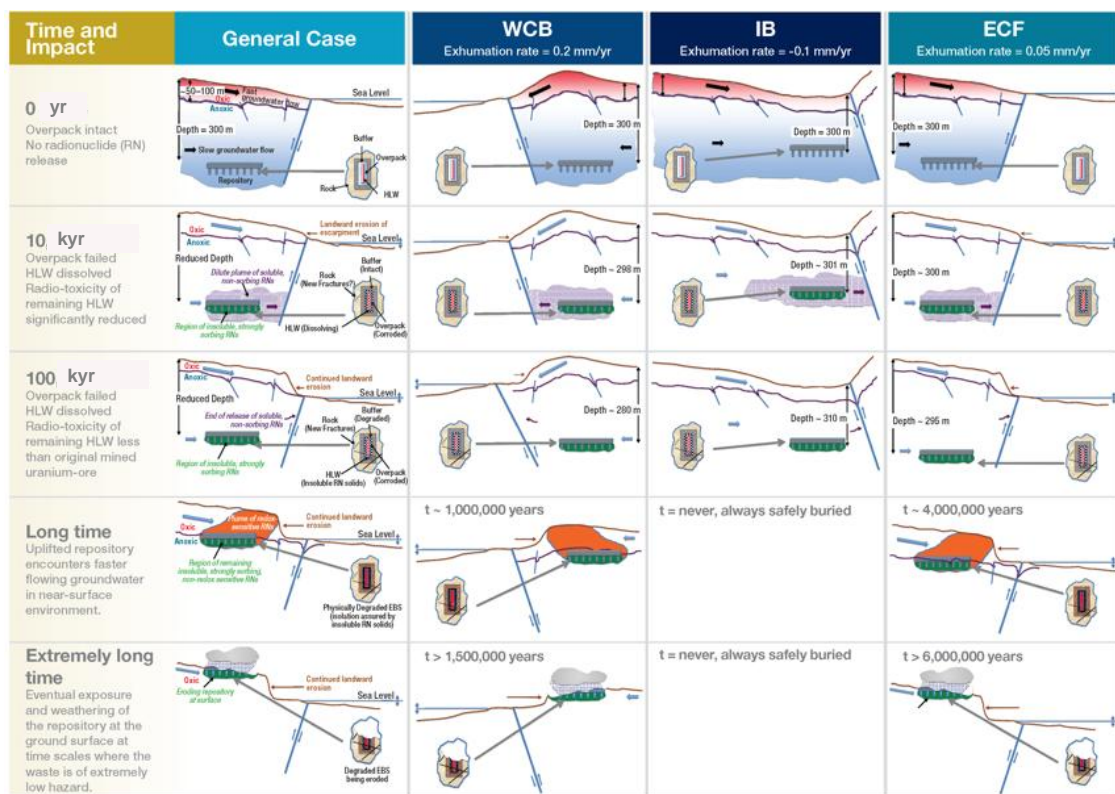
Figure 4.2: A demonstrative storyboad for the evolution of a repository at example sites WCB, IB and ECF at 10 kyr, 100 kyr and beyond 1 Myr into the future.

38

5 Hazard maps for volcanism and exhumation

In the following, we present the developed ITM-TOPAZ methodology could potentially be used for assessment of project risk. We focus on the methodologies for forecasting two potentially disruptive phenomena. These are potential volcanism and potential exhumation or near-exhumation due to uplift and erosion. For both phenomena, a variety of alternative models and data may be used to assess the potential for specific events. We present a method for aggregating these assessments to estimate project risk, recognizing that the methodology may be extended to encompass all potentially disruptive geologic phenomena for a particular site.

5.1 Introduction

The goal of geologic hazard assessment for HLW repository sites is to provide quantitative, probabilistic estimates of the occurrence of potentially disruptive geological phenomena. Potentially disruptive geologic hazards for HLW repositories include volcanism, tectonic uplift and erosion, fault displacement and related processes. In this context, volcanic hazard is defined as the probability of a specific volcanic event (e.g. volcanic eruption of a specific size) or volcanic phenomena (e.g. the occurrence of igneous dyke intrusion at a specific location during a specific time interval). Similarly, faulting displacement hazard for HLW repositories may be defined as the probability of fault displacement exceeding some magnitude during the assessment period of the site. Uplift and erosion hazard may be defined as the probability that the repository is exhumed, or reaches a shallow oxic environment during some assessment interval.

The rise of probabilistic geologic hazard assessments and their application to HLW repository sites during the last several decades has relied on developments in several aspects of geoscience. First, vastly improved quality of available data has enabled forecasts. These are geologic data, such as high-resolution stratigraphy calibrated by radiometric age determinations, and geophysical data used to assess site stability. Second, numerical simulation of volcanic and tectonic phenomena was virtually unknown more than 30 years ago, but has rapidly developed through our understanding of the physics of volcanic and tectonic processes, and our ability to run simulations using ever more sophisticated and faster codes and computers. These developments have allowed us to better model potentially disruptive geologic events for HLW repository performance. Third, statistical models are evolving at an equally rapid rate, allowing application of improved methods for understanding, for example, uncertainty in hazard, the application of alternative models, and incorporation of disparate data sets into forecasts using event trees, Bayesian methods and expert elicitation. The TOPAZ project has partially focused on developing new and efficient ways to assess aggregate geologic hazard for example sites in Japan, representing a range of tectonic environments.

Probabilistic geologic hazard forecasts are particularly useful to better understand, compare and communicate the potential for disruptive geologic events on various spatial and temporal scales. In this context, it is possible to use these methodologies to establish thresholds to assess project risk. For instance, probabilistic volcanic hazard assessment (PVHA) may be used to identify regions in which potential future volcanic activity is highly unlikely to occur during a given assessment period, or to figure as an issue in siting decisions. Put another way, such a site is characterized by an absence of potential for disruptive volcanic events, and therefore represents low project risk. Similarly, it is practical to use PVHA to identify regions or sites as potentially unsuitable by developing a threshold probability above which, although unlikely, potential future volcanic activity is sufficient to raise concern, and has potential to become a siting issue. This approach may be extended to any number of potentially disruptive geological hazards, such as fault displacements and uplift. Aggregate project risk, in this context, is estimated from the union of these assessments. That is, a site with low project risk is one in which the assessment indicates that the potential for all disruptive geological phenomena are below their appropriate threshold values.

5.2 Probabilistic volcanic hazard assessment

The TOPAZ approach involves investigation of potential volcanic hazards using regional data sets, such as the AIST Quaternary database of volcanoes of Japan, and regional geophysical studies as a starting point. Such information, together with additional information from the

literature, allows for constructing a regional view of rates of volcanic activity and the potential distribution of volcanism. Most TOPAZ work, particularly with respect to construction of project risk maps for volcanism, involves analysis of data at this regional scale. This analysis is accomplished using alternative models to assess volcanic activity, both in terms of potential rates of new volcano formation and potential location of future events.

The elements of this PVHA are summarized in a logic tree for the assessment of hazard with ensemble models (Figure 5.1). Nodes of this tree represent alternative models for volcanism in the region under consideration. The transitions on the tree give credence, or weights, to particular models, usually assigned through expert elicitation. In TOPAZ PVHA, construction of the logic tree considers the following factors:

- For regional investigation and comparisons, as is appropriate for project risk maps, the area under consideration may be the entire volcanic arc. We note that the area for detailed site characterization in PVHA often extends up to 300 km from the site. This comparatively large area is appropriate in order to understand and model regional trends in volcanic activity, especially on time scales of 1 Myr.
- For Japan, it is not credible that volcanic arcs are extinct. For example, ITM and TOPAZ work has focused on developing and evaluating PVHA models for Tohoku, Kyushu and Chugoku areas. There is no credible possibility that volcanism in these regions will not occur in the future. Nevertheless, this branch of the logic tree is included because there are geographic regions of potential interest in Japan in which volcanic activity has ceased (e.g., Shikoku). Therefore, node $N_{2,1}$ represents the possibility of magmatic activity within the system and node $N_{2,2}$ assumes the magmatic system is extinct.
- Alternative recurrence rate models may be developed for volcanic events in any volcanic region. Some of these recurrence rate models are based on the known geologic history of the region and recurrence rate is estimated using statistical models of these distributions. Alternative recurrence rate models are based on RESs intended to forecast change in average rates of volcanic activity over long periods of time based on forecast changes in the tectonic setting of magmatism or in geochemistry and heat flux in the magmatic system. Nodes $N_{3,1}$ - $N_{3,4}$ represent alternative recurrence rate models of volcanism and $w_{2,1}$ - $w_{2,4}$ weight their credibility.
- Alternative models for the potential locations of future volcanic events may be developed for any volcanic region. Some of these models are based on development of statistical models of potential volcano location based on past patterns of activity. Examples of such models include the use of kernel density models and Cox process models. Such models reflect an RES that the current tectonic setting of volcanism, and areas of magma production, will persist into the future. Alternative models may be developed that account for shifts in the location of volcanoes through time, for example associated with the roll-back of the subducted slab, as portrayed in alternative RES. Nodes $N_{4,4}$ - $N_{4,12}$ represent alternative spatial density models and $w_{3,4}$ - $w_{3,12}$ weight their credibility.
- The probability of a new volcanic event within a <100 km^2 area about the site is calculated by following each individual branch of the logic tree from left to right, and by assigning weights to the transitions that connect each of its nodes, thus, incorporating and weighting all alternative models represented by the tree to estimate the aggregate probability.

Thus, the heart of the analysis involves identification of credible alternative models and their weights. Once these are known, estimating event probabilities associated with each node is straightforward.
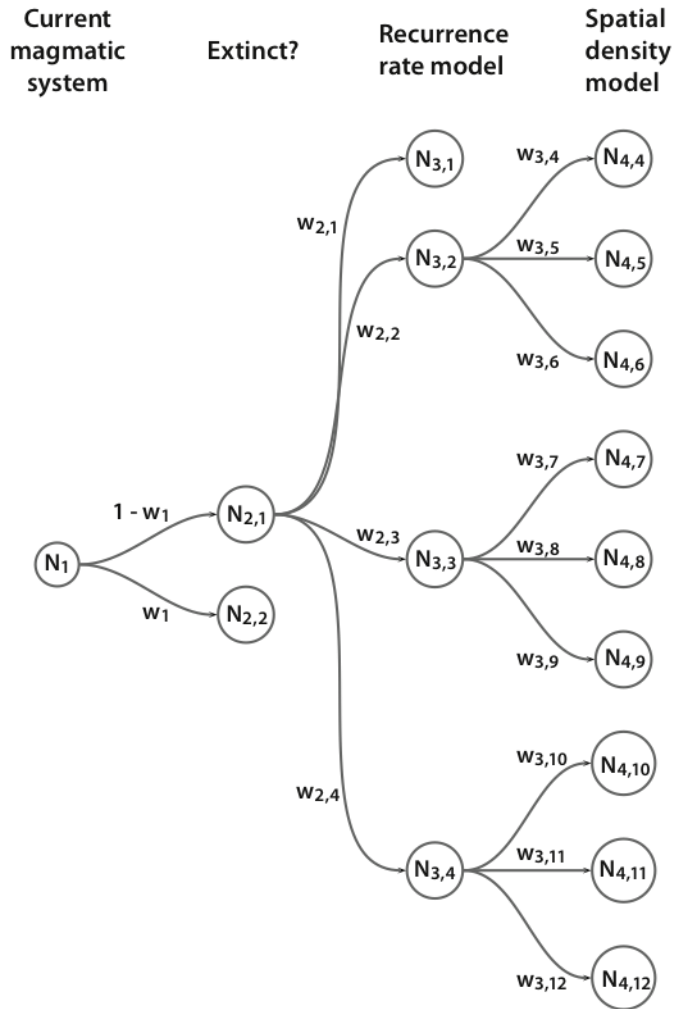
Figure 5.1: Logic tree of alternative models for the formation of a new volcano within a given timeframe and within given area area about a given site. Node N_1 represents the current state of the magmatic system. Node $N_{2,1}$ represents the possibility of magmatic activity within the system and node $N_{2,2}$ assumes the magmatic system is extinct. Nodes $N_{3,1}$ - $N_{3,4}$ represent alternative recurrence rate models of volcanism and $w_{2,1}$ - $w_{2,4}$ weight their credibility (see discussion of expert elicitation). Nodes $N_{4,4}$ - $N_{4,12}$ represent alternative spatial density models and $w_{3,4}$ - $w_{3,12}$ weight their credibility. The probability for the formation of a new volcano within a given timeframe due to one particular recurrence rate model and within a given area due to one spatial density model is represented by each branch, or path, of the tree, followed from left to right.

5.2.1 Recurrence rate of volcanic events

(1) General model structure

Long-term volcanic hazard assessment requires estimation of the recurrence rate of volcanic activity, defined as the expected number of volcanic events within a given time interval. For the purposes of HLW repository hazard assessment, a volcanic event is the occurrence of a new igneous intrusion at, or near repository depths, and the disruption of waste packages by this intrusion, either through mechanical disruption (e.g., transport of waste package fragments to the surface in a volcanic conduit) or secondary effects (e.g., development of a hydrothermal system leading to accelerated waste package degradation). Recurrence rate estimates of volcanic events are based upon the frequency with which these events occurred

in the past for a specific region. These estimates are then used to forecast future volcanic activity. A key component of long-term hazard assessment is the assumption that future rates of activity can be extrapolated from the past rate, at least throughout some time scale of interest.

Consider a sequence of volcanic events – the formation of new volcanoes within an arc. An estimation of the current recurrence rate at time t, $\lambda_{H_{S,T}}(t)$, is derived from the history of volcano formation within the arc, $H_{S,T}$, between times S and T. The early limit S, might be defined as the age of the oldest event in the entire volcanic system, or a readily identified geologic time interval – such as the Quaternary. The later limit T is typically the time at which the calculation of the recurrence rate was done, which could be the time of the youngest event in the sequence, or perhaps the present time. The number of events known to have occurred during the interval between S and T is denoted $N_{S,T}$. The probability of renewed eruptions during some time period, u (e.g., the next 1 Myr) is:

$$Pr[N(T, T+u) \geq 1] = 1 - \exp\left[-\int_T^{T+u} \lambda_T(t)dt\right]. \tag{1}$$

Then the probabilistic analysis becomes a matter of estimating at time T the recurrence rate, $\lambda_T(t)$ for times $t > T$. In practice, this approach must be further generalized so that the recurrence rate depends on the history of the volcanic system, $H_T = H_{S,T}$:

$$\lambda_T(t \mid H_T) = \lim_{\Delta t \to 0} \frac{\Pr(N(t, t+\Delta t) = 1 \mid H_T)}{\Delta t} \tag{2}$$

where the history H_T is reduced to the oldest age of each volcano, $S \leq t_0, t_1, t_2 ...., t_n < T$. Events may additionally be considered in terms of eruption volume, v_i, eruption magnitude or explosivity, m_i, or composition, x_i. Such time-volume predictable models are often applied in volcanology, but it is emphasized that for HLW repositories we are generally interested in the potential occurrence of any event, with less emphasis on volume, magnitude or composition.

Although this general model structure is straightforward, there is nearly always ambiguity in defining the time of formation of individual volcanoes, t_i, and the start time of the series, S, are defined. These uncertainties are discussed in the next section.

(2) Data Requirements for Estimating Recurrence Rates

Determining the long-term recurrence rate of new volcano formation in an arc involves large uncertainty. The most fundamental data required are geologic maps, stratigraphic studies and samples from boreholes for understanding the thickness of the volcanic section and the timing of onset of eruptive activity. For many volcanic systems only the most recent volcanic events are known. For many volcanoes, the most recent eruptive events are the best known, simply because the products of these eruptions mantle the topography and comprise the most accessible rock outcrops. As a result, in the geological literature and volcano databases, often only the ages of the most recent activity have been reported. Conversely, the oldest volcanic units are often not exposed or are unrecognized, so the onset of activity, S, and the total duration of volcanic activity are often uncertain. Similarly, eruptive data tends to be biased toward the largest eruptive events, simply because these large eruptions leave copious deposits with a greater chance of being preserved in the rock-stratigraphic record. It is often unclear when the onset of activity at a particular volcano occurred.

For the Tohoku arc, for example, the Quaternary volcano database of Japan (Committee for the Catalogue of Quaternary Volcanoes in Japan, 1999) lists approximately 65 Quaternary volcanoes has having formed since 2 Ma. Many additional volcanoes are found in the arc, but there age of formation is unknown. Some of these ages likely reflect the actual time of formation of the volcano, others suggest age of formation based on stratigraphic relationships.

That is, some volcanoes are known to have formed before or after a given data, based on stratigraphic relationships. Thus, even when ages are reported, there is considerable uncertainty in their meaning.

(3) Steady-state models

Whether or not some statistical models (e.g., Poisson process or renewal models) can be applied to estimate recurrence rate and probability of new volcano formation within a given time period depends on determining if this sequence of events is in steady-state. Lack of steady state may reflect sampling bias or may reflect the nonstationary nature of volcano formation in some arcs. If a sequence is in steady state, then the level of activity in the future is well-represented by activity in the past. Mathematically, this means that estimated probabilities of future events will be independent of t, the time at which they could occur. If t is a factor in the probability forecast, then the system is not in steady state.

The Kolmogorov-Smirnov test may be used to determine if the eruption sequence is steady state. This test is ideal because usually there are few events comprising the sequence (e.g., the 65 known ages of volcano formation in Tohoku) and because the test is simple. For the cumulative number of volcanic events in the sequence:

$$F_n(t) = \frac{\#(t_i \leq t)}{n}, i = 1....n, S < t < T \tag{3}$$

then the Kolmogorov-Smirnov test statistic is:

$$D_n = \max_{t \in [S,T]} \left[\mid F_n(t) - \frac{t-S}{T-S} \mid \right]. \tag{4}$$

In other words, in the Kolmogorov-Smirnov test statistic, the maximum deviation from the expected frequency of events determines whether the process is steady state or not. The 95 % confidence bounds are given as $1.36/\sqrt{N_{S,T}}$.

Consider the history of volcano formation in Tohoku, basing this history on the oldest ages reported for 65 volcanoes. For this series, $N_{S,T} = 65$, and $D_n = 0.38$, at 900 ka (Figure 5.2).

The cumulative distribution function for Tohoku volcanic events shows significant deviation from steady state, based on the Kolmogorov-Smirnov test at the 95 % confidence level. Volcanic events prior to approximately 900 ka apparently occurred at a significantly lower rate than subsequent events. This suggests that a different recurrence rate applies to the two different regimes, before and after 900 ka. It is conceivable that this result indicates an actual increase in volcanic events with time in Tohoku (e.g. Umeda et al., 1999), but an alternative explanation is possible that age determinations for volcanoes formed in the early Quaternary are less frequently made and are perhaps less reliable than age determinations made on younger volcanoes. Also, there may be bias in reporting the relative lack of accessibility of older strata in these volcanic systems.
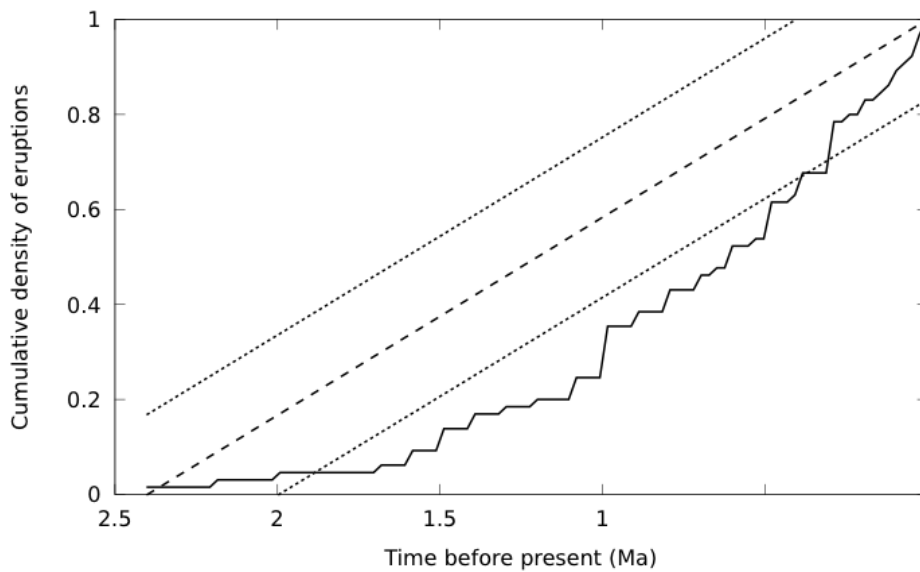
Figure 5.2: Cumulative distribution function for oldest reported volcano ages for 65 Quaternary volcanoes in the Tohoku arc. The dashed line indicates a steady state model with the confidence interval for this steady-state model shown by finer dashed lines. The Kolmogorov-Smirnov test indicates that this series not in steady state, with these volcanic events occurring at a significantly increased frequency after approximately 900 ka.

A different picture emerges if the series is filtered to include only volcanoes ≤ 900 ka. For volcanoes with oldest ages reported to be ≤ 900 ka in the Tohoku arc, $N_{S,T} = 42$, and $D_n = 0.17$, at approximately 300 ka (Figure 5.3). In this case, the series appears to be steady-state. Changing the start time of the analysis, S, changes interpretation of rate of new volcano formation. One conclusion is that a steady-state model may be used to model rates of activity over the last 900 kyr. Note, however, that even on this time scale there is an increase in activity during the last 50 kyr, presumably the best dated portion of the time series. Therefore a second conclusion is that there is significant uncertainty in the recurrence rate of new volcano formation for the Tohoku arc. The most recent time interval yields the highest recurrence rate, suggesting that additional research on the age of formation of these volcanic systems will likely lead to a higher estimate of the average recurrence rate overall.
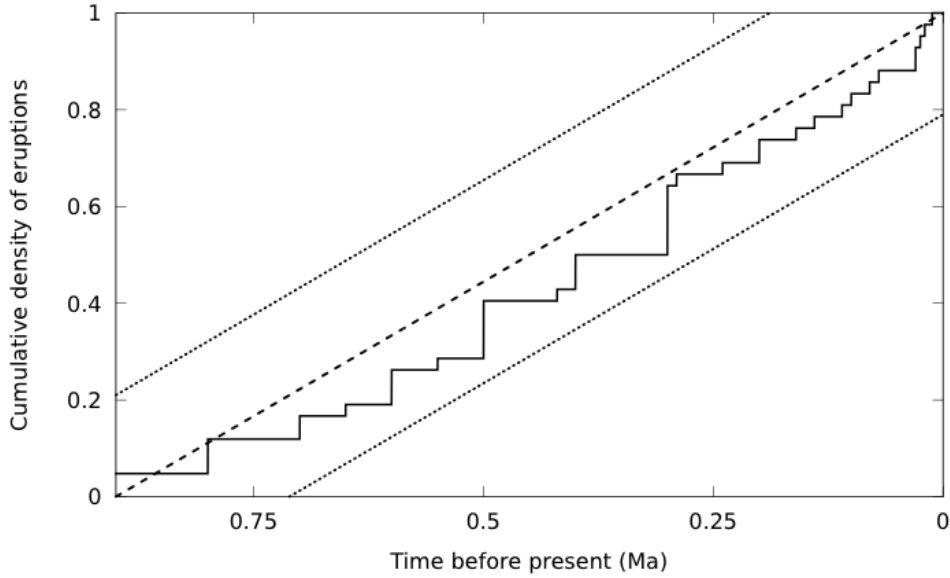
Figure 5.3: Cumulative distribution function for oldest reported volcano ages for 42 volcanoes thought to have formed during the last 900 kyr in the Tohoku arc. The dashed line indicates a steady state model with the confidence interval for this steady-state model shown by finer dashed lines. The Kolmogorov-Smirnov test indicates that this series is steady state, but note the apparent increase in activity during the best dated portion of the series during the last 50 kyr.

(4) Statistical models

The simplest approach to steady-state recurrence rate estimation is to average the number of events that have occurred during some arbitrary time period. An alternative approach, especially appropriate when the total number of known events is small, is to calculate recurrence rate using the repose-time method, in which the time range is restricted by the estimated ages of youngest and oldest events:

$$\hat{\lambda}_T = \frac{N-1}{T-S} \tag{5}$$

where $\hat{\lambda}_T$ is the recurrence rate (identical for all t), N is the number of events, occurring between S, the age of the first (oldest) event, and T, the age of the most recent (youngest) event. This is the Poisson process estimate, and is a Maximum Likelihood Estimate (MLE), provided that an event occurs at time S. If the distribution of repose intervals in a volcanic system show Poisson behavior, then the probability of a given number of events, k in some time interval u is:

$$Pr[N(t+u)-N(t)=k] = \frac{e^{-\lambda_T u}(\lambda_T u)^k}{k!}, \qquad k=1...n \tag{6}$$

for all t (the definition of stationarity), and the probability of zero events in the time interval, u, is:

$$Pr[N(t)=0] = e^{-\lambda_T u} \tag{7}$$

indicating that repose intervals between eruptive events have an exponential distribution, the memoryless property of which implies that there is no possibility of using patterns of activity in the past history to improve on the forecast.

Using volcanoes thought to have formed during the last 900 kyr in the Tohoku arc, the interval which appears to be steady-state based on available data, $\hat{\lambda}_T = 5 \times 10^{-5}$ yr^{-1}. If we

consider even the comparatively short-term assessment period of a HLW repository in the Tohoku region, $u = 10$ kyr, the probability of *no* new volcano forming in that period of time is about 60%. When longer assessment periods are considered there is a much greater chance of a new volcano forming in the Tohoku arc during that period. For example, when assessment periods are estimated for 100 kyr, the probability of a new volcano forming in the Tohoku arc is approximately 99%. Put another way, based on these rates it is expected that 5–6 new volcanoes will form in the Tohoku region within the next 100 kyr, and 50–60 new volcanoes will form in the Tohoku region within the next 1 Myr. To summarize:

- There is great uncertainty in the rate of new volcano formation in the Tohoku arc because of difficulty resolving the timing of onset of eruptions at a particular volcano or volcanic system. No age estimates for the onset of activity is available for many volcanoes in the Tohoku arc.
- Nevertheless, the time series of new volcano formation can be assessed using 62 volcanoes for which the data are available. This series is not steady-state, showing an increase in rate of new volcano formation for times less than approximately 900 ka. This change may reflect a change in activity in the arc, but likely reflects a change in data quality. For example, the onset of activity for any volcanoes in the arc is reported to be approximately 1 Ma. In many cases this is likely an educated guess based on available geological data.
- For the 42 volcanoes thought to have formed since 900 ka, the series is steady-state.
- Because the series is steady-state, it is possible to estimate recurrence rate using a MLE model. The estimated recurrence rate of new volcano formation in the arc, approximately $\hat{\lambda}_T = 5 \times 10^{-5}$ yr^{-1}, is biased because some volcanoes in the arc have no date for the onset of activity. Nevertheless, it is interesting to note that assuming all Quaternary volcanoes found in the arc formed in the Quaternary yields $\hat{\lambda}_T = 6.5 \times 10^{-5}$. This range of values appears to do a reasonable job of bounding the regional recurrence rate of volcano formation in Tohoku.

As the probability of a volcanic event in the region is relatively high for the long assessment period of a HLW repository, it is necessary to consider the potential locations of these volcanoes. Alternative models for potential volcano location is considered next in the ITM-TOPAZ PVHA methodology.

5.2.2 Location of eruptive vents

Alternative models for the potential location of new eruptive events were developed as part of the ITM-TOPAZ methodology. These include kernel density methods and Cox process models. Both nonparametric statistical models of potential volcano distribution are based on the assumption that the distribution of volcanism in the past is a guide to future volcano distribution. For each type of model may be modified to include additional data, using Bayesian methods, such as the distribution of seismic tomographic anomalies. Each method may be modified to account for shifts in the location of volcanism with time. Thus, many alternative models of spatial density are considered as part of the PVHA.

A simple approach relies on the distribution of mapped vent locations that have erupted in the past. Like in probability models of the timing of future eruptions, this assumption assumes a steady-state model for the distribution of new volcanic vents is appropriate. Kernel density estimation is a non-parametric method for estimating the spatial density of future volcanic events based on the the locations of eruptive vents. Two important parts of the spatial density estimate are the kernel function and its bandwidth, or smoothing parameter. The kernel function is a probability density function that defines the probability of future vent formation at locations within a region of interest.

A two-dimensional elliptical kernel with a bandwidth that varies in magnitude and direction is given by:

$$\hat{\lambda}(\mathbf{s}) = \frac{1}{2\pi N \sqrt{|\mathbf{H}|}} \sum_{i=1}^{N} \exp\left[-\frac{1}{2}\mathbf{b}^T\mathbf{b} \right] \tag{8}$$

where,

$$\mathbf{b} = \mathbf{H}^{-1/2}\mathbf{x}.$$

The local spatial density estimate, $\hat{\lambda}(\mathbf{s})$ is based on N total events (vent locations). The bandwidth, $\mathbf{H}$, is a 2×2 element matrix that specifies the bandwidth as an ellipse, with major and minor axis lengths, and a rotation. This bandwidth matrix is both positive and definite, important because the matrix must have a square root; $\mathbf{x}$ is a 1×2 distance matrix, $\mathbf{b}$ is the cross product of $\mathbf{x}$ and $\mathbf{H}^{-1/2}$. The resulting spatial density at each point location, $\mathbf{s}$, is usually distributed on a grid that is large enough to cover the entire region of interest.

A special case of the kernel function is a two-dimensional radially-symmetric Gaussian kernel:

$$\hat{\lambda}(\mathbf{s}) = \frac{1}{2\pi h^2 N} \sum_{i=1}^{N} \exp\left[-\frac{1}{2}\left(\frac{d_i}{h}\right)^2 \right] \tag{9}$$

that depends on the distance, d_i, to each event location, N, from the point of the spatial density estimate, $\mathbf{s}$, and the smoothing bandwidth, h that is constant in all directions.

The bandwidth is selected using some criterion, often visual smoothness of the resulting spatial density plots. Bandwidths that are narrow focus density near the locations of mapped vents. Conversely, a large bandwidth may over-smooth the density estimate, resulting in unreasonably low density estimates near clusters of past events, and overestimate density far from past events. This dependence on bandwidth can create ambiguity in the interpretation of spatial density if bandwidths are arbitrarily selected. Several methods have been developed for estimating an optimal bandwidth matrix based on the locations of the event data, such as the least-squares cross validation (LSCV), smoothed asymptotic mean squared error (SAMSE) and modified asymptotic mean integrated squared error (AMISE) methods. Such optimization methods are extremely useful because, although they are mathematically complex, they find optimal bandwidths using the actual data locations, removing subjectivity from the process. That said, alternative optimization methods result in alternative spatial density maps (Figure 5.4), so an important part of the hazard assessment is evaluation of the sensitivity of vent spatial density to different model assumptions. It is also important to select or set priorities of models considering the scale of evaluation (e.g. accross the arc, a specific region or a volcanic cluster).

A potential disadvantage of these kernel functions and similar methods is that they are not inherently sensitive to geologic boundaries and to ancillary data. For example, the distribution of earthquake hypocenters or zones of high strain observed during magma intrusion should inform and update the spatial density estimate as this information becomes available. Various schemes have been developed to weight spatial density estimates in light of geological or geophysical information in a Bayesian framework. A difficulty with such weighting is the subjectivity involved in recasting geologic observations as density functions. Furthermore, geologic insight is not always consistent with event distributions. Developing such weighting schemes remains an important area of research. In addition, note that this statistical structure uncouples the temporal forecasting problem from the spatial forecasting problem. That is, estimates of the recurrence rate are not mathematically linked to estimates of the spatial density. This assumption may be inappropriate on some volcanoes where there is migration of activity. An area of significant future research is the formulation of spatio-temporal models, which make this link explicitly.
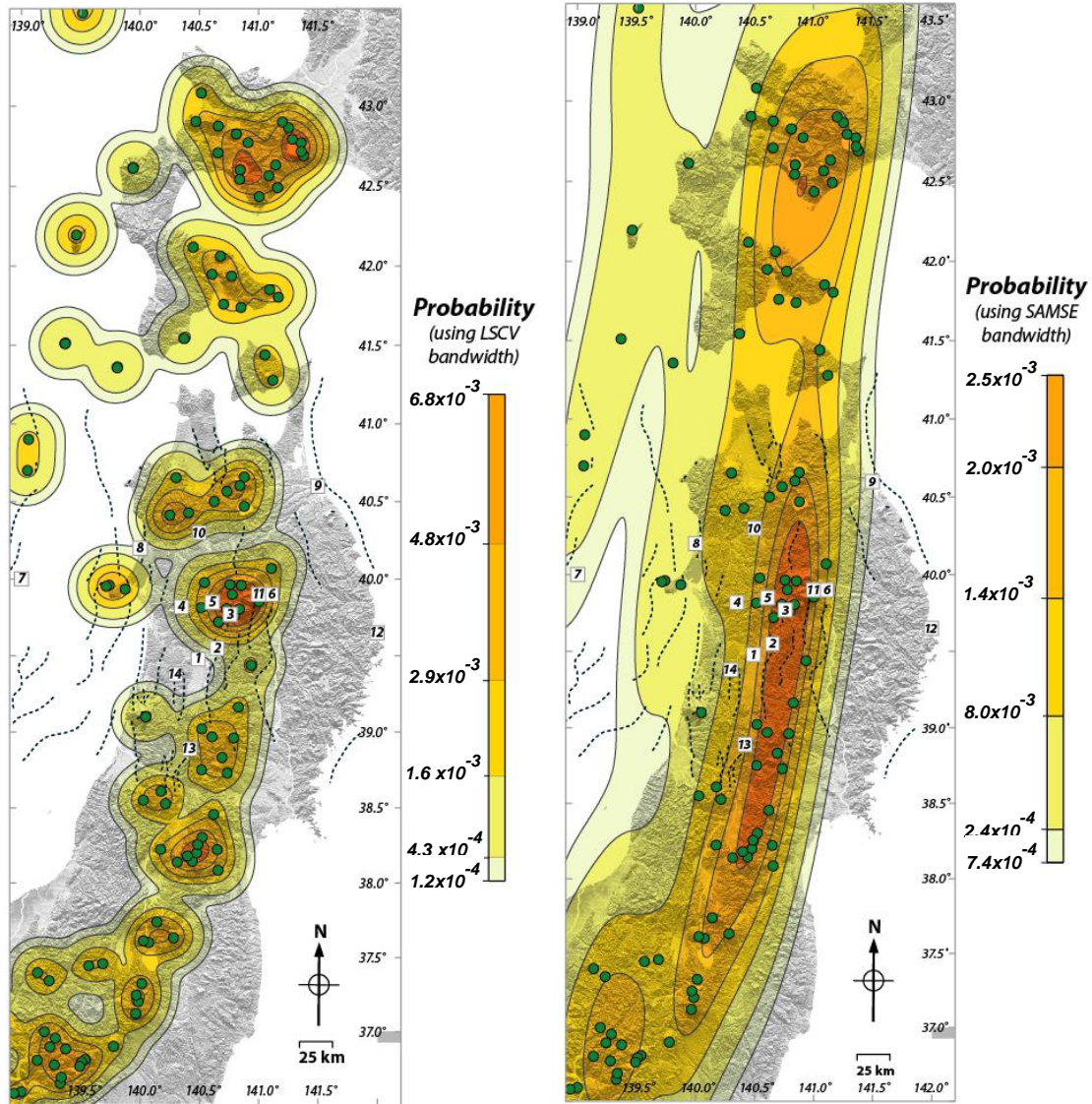
Figure 5.4: Alternative spatial density models of Quaternary volcano distribution in the Tohoku arc, northern Honshu Japan (modified after Chapman et al., 2008). Both maps are prepared using kernel density estimation, with alternative kernel bandwidths estimated using different optimization algorithms. An isotropic, short bandwidth by LSCV (left) emphasizes clustering along the volcanic arc, possibly in response to along-arc variations in magma productivity and heat transfer in the mantle wedge. An anisotropic, long bandwidth by SAMSE (right) smooths volcano distribution, and emphasizes relatively uniform melt production along the arc. Hazard assessments need to consider such alternative models, which are linked to our understanding of volcanological processes on various scales.

5.3 Estimation of volcanic hazard under evolving tectonic conditions at 1 Myr timeframe

In order to become fully TOPAZ compatible, the ITM probabilistic volcanic hazard assessment methodology needs to be extended to account for timeframes up to 1 Myr. Accordingly, new developments were performed for the stochastic model to account for various tectonic evolution scenarios likely to occur at the million-year time scale. With the results that volcanic hazard maps at 1 Myr timeframe were produced using the region of Tohoku as an illustration example.

5.3.1 Migration scenarios

Kondo (2009) has evaluated the evolution of volcanism by investigating the distribution of Middle Miocene to Quaternary igneous rocks for the northern part of Tohoku. The cumulative maps of igneous rocks produced for four periods show significant trends in the distribution of volcanism over time (Figure 5.5). It appears that at the million-year time scale, volcanism migration has occurred; in particular, towards the west in the backarc and as well between the volcano clusters of Quaternary age. Such long term patterns in the distribution of volcanism can be described using the hot finger model of Tamura et al. (2002); i.e. some variability is added in terms of the distribution of volcanism along the fingers or in relation to local lateral migration of volcanism towards the gap regions. The general 3-dimensional structure of the hot fingers model remains as it is likely to last for millions of years (Tamura et al., 2009).
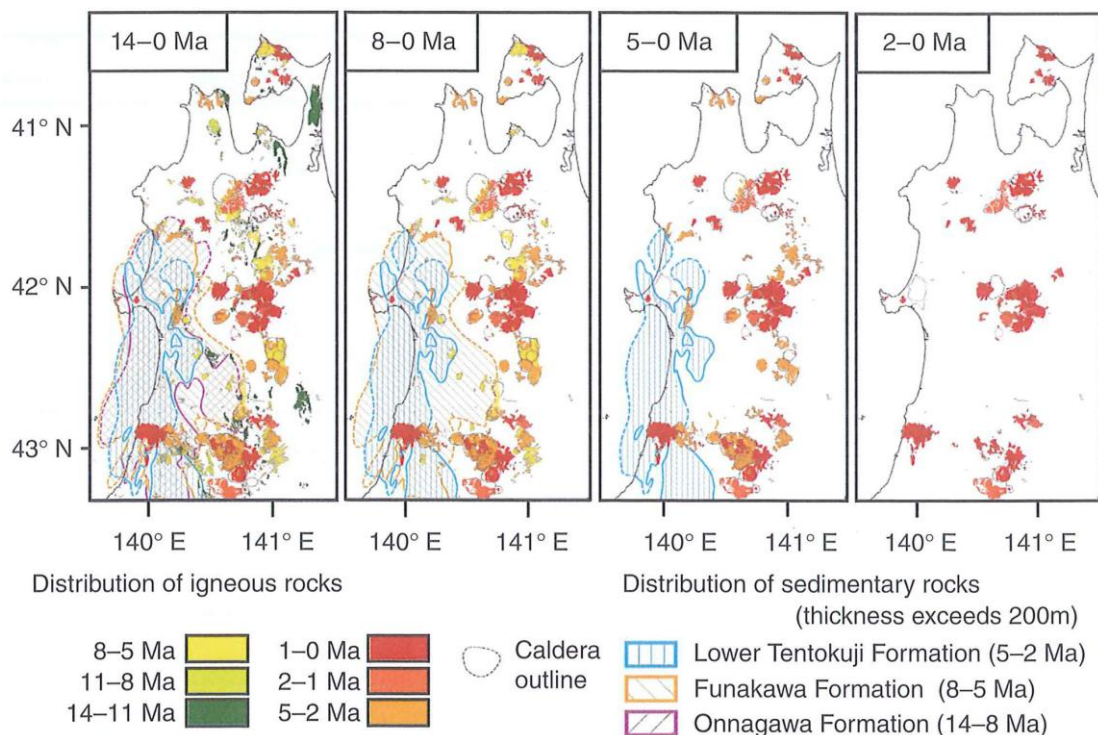
Figure 5.5: Northern Tohoku: cumulative distribution of volcanism for four periods after Kondo (2009).

Estimation of long-term volcanic hazard relies on Regional Evolution Scenarios (RES). They constitute the conceptual description of the expected behaviours of tectonic evolution. A representative range of four plausible RES was produced with various tectonic conditions likely to capture the main evolution trends in terms of rock deformation and volcanism for Tohoku (See Chapter 2). The four RES provide a description of the future behaviour of arc volcanism in Tohoku region at 1 Myr timeframe (Figure 5.6).
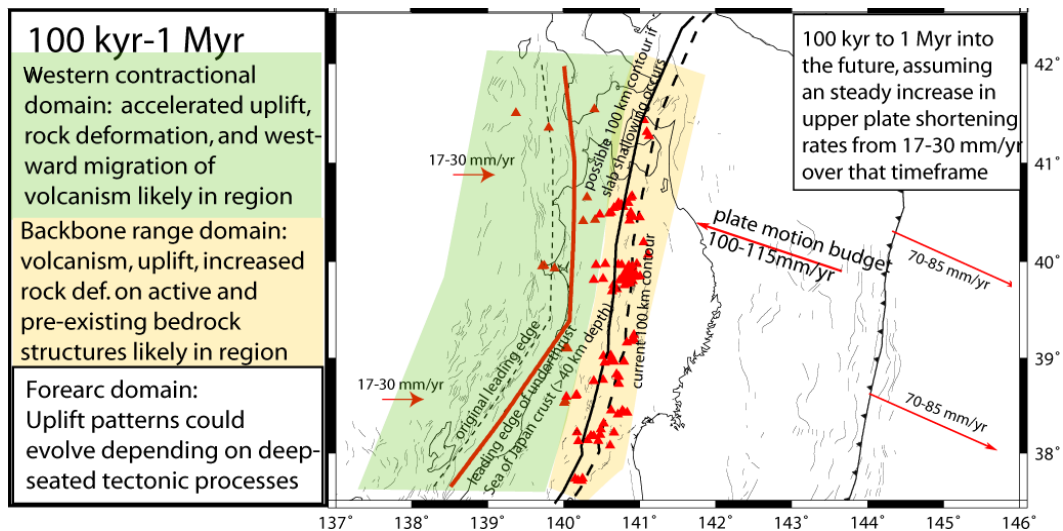
Figure 5.6: Example of Regional Evolution Scenario for Tohoku: RES 2 where the amount of relative plate convergence accommodated in the upper plate doubles from present to 1 Myr in the future (See Section 2.3 for detailed description).

Although the above evidences and models support that the current location of volcanism could continue for the next 1 Myr, the potential of migration in the four RES cannot be ruled out. The three potential Migration Scenarios (MS) in relation to arc volcanism are thus defined as below:

- MS1: migration of volcanism likely occurring towards the west.
- MS2: migration of volcanism likely into gaps between Quaternary volcanoes.
- MS3: migration (small) of volcanism likely occurring towards the trench.

The relationships between the Migration Scenarios and the RES are given in Table 5.1.

Table 5.1: Characteristics of Migration Scenario in relation to Regional Evolution Scenarios

Regional Evolution Scenarios	Migration direction			Migration Scenarios
	Westward	Gaps	Trenchward	
RES 1 (present tectonic condition ↔)	–	X	–	**MS2**
RES 2 (upper plate motion rate ↑)	X (ca. 20–40 km/Myr)*	X	–	**MS1, MS2**
RES 3 (relative plate motion oblicity ↑)	–	X	–	**MS2**
RES 4 (plate motion rate ↓)	–	X	X (small)	**MS2, MS3**

*Migration velocity.

5.3.2 Stochastic model

The developed stochastic model for the long term estimation of volcanic hazard relies on the following hypotheses: (i) the potential of volcanism is considered as evolving (non stationary) in the space-time domain, (ii) the potential can be simulated using an evolution equation with a constant velocity, and (iii) the translated distribution of volcanic events conserves the potential and remains depicted by a Cox process.

Within the framework of the Cox process, the potential of volcanism (Jaquet et al., 2009; 2012) – representing the propensity of a given region to be affected by volcanic events – is no longer considered as stationary. The following evolution equation is chosen for the description of the initial potential of volcanism, $Z_0(x,t)$, in the space-time domain:

$$Z_0(x,t) = Z_0(x+vt) \qquad (10)$$

where:

v : displacement (migration) velocity of volcanism.

The cumulated (integrated) potential of volcanism, $Z_c(x)$, is related to the initial potential using the following expression:

$$Z_c(x) = \int_{t_0}^{t_p} Z_0(x+vt)dt \qquad (11)$$

where:

t_0 : initial time (e.g. beginning of Quaternary)

t_p : present time.

A deconvolution of eq. (2) is required to derive the initial potential of volcanism knowing the cumulated potential estimated from the data. A statistical minimisation technique is chosen for solving the following linear system of equations:

$$\int \left[Z_c(x) - \int_{t_0}^{t_p} Z_0(x+vt)dt \right]^2 dx \rightarrow minimum \qquad (12)$$

where:

$Z_0 = (z_1,...,z_n)$: vector of unknowns representing the initial potential.

The discrete form of the linear system is written as follows:

$$F(z_1,...,z_n) = \sum_i \left[Z_c(x_i) - \sum_j a_{ij} z_j \right]^2 \qquad (13)$$

$$F(z_1,...,z_n) = \sum_i \left[Z_c^2(x_i) + \sum_j \sum_k a_{ij} a_{ik} z_j z_k - 2Z_c(x_i) \sum_k a_{ik} z_k \right]$$

The linear system is minimized with respect to z_k :

$$\frac{\partial F}{\partial z_k} = 0 \qquad (14)$$

And can be expressed using the following symmetric matrix form:

$$A^T A Z = A^T Z_c \qquad (15)$$

where:

$A = (a_{ij})$: interpolation matrix for the potential (migration velocity dependent)

$Z = (z_j)$: solution vector for the initial potential

$$Z_c = (Z_c(x_i)): \text{input vector for the cumulated potential: } Z_c(x_i) = \sum_j a_{ij} z_j$$

The resolution of the system is performed using a non-linear transformation (Gaussian anamorphosis) for the cumulated potential:

$$Z_c(x_i) = \varphi_z[Y_c(x_i)] \tag{16}$$

$$Y_c(x_i) = \varphi_z^{-1}[Z_c(x_i)]$$

where:

φ_z : monotonic increasing function (i.e. Gaussian anamorphosis function; Chilès and Delfiner, 1999).

Such deconvolution in the Gaussian space (this method is also applied in Oceanography; Simon and Bertino, 2009) allows overcoming physical limitations linked to constraints of positiveness when solving the linear system:

$$Z_c(x_i) \rightarrow \varphi_z^{-1} \rightarrow Y_c(x_i) \rightarrow numerical\ resolution \rightarrow y_j \rightarrow Y_f(x_i) \rightarrow \varphi_z \rightarrow Z_f(x_i) \tag{17}$$

where:

$Y_c(x_i)$: Gaussian cumulated potential

y_j : Gaussian initial potential

$Y_f(x_i) = \sum_j a_{ij}^f y_j$: Gaussian future potential

$Z_f(x_i)$: future potential.

The principles of evolution for the potential of volcanism are illustrated in Figure 5.7. It must be emphasized that the potential remains stationary in space when fixing the time step.
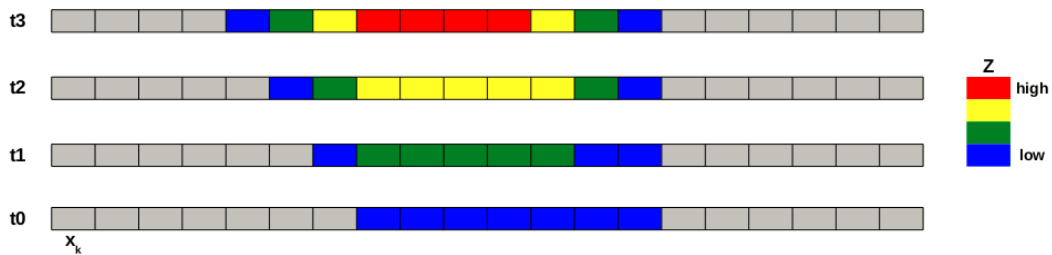
Figure 5.7: Schematic evolution for the potential of volcanism in space-time domain, where space is one-dimensional along a W–E line; and, with a migration velocity oriented towards the west.

The numerical resolution of the linear system provides the initial potential needed for the derivation of the future potential. Knowing this potential enables using the Cox process to simulate the volcanic events likely to occur in the future. The required stochastic and numerical modelling steps for the generation of probabilistic volcanic hazard maps are shown in Figure 5.8.
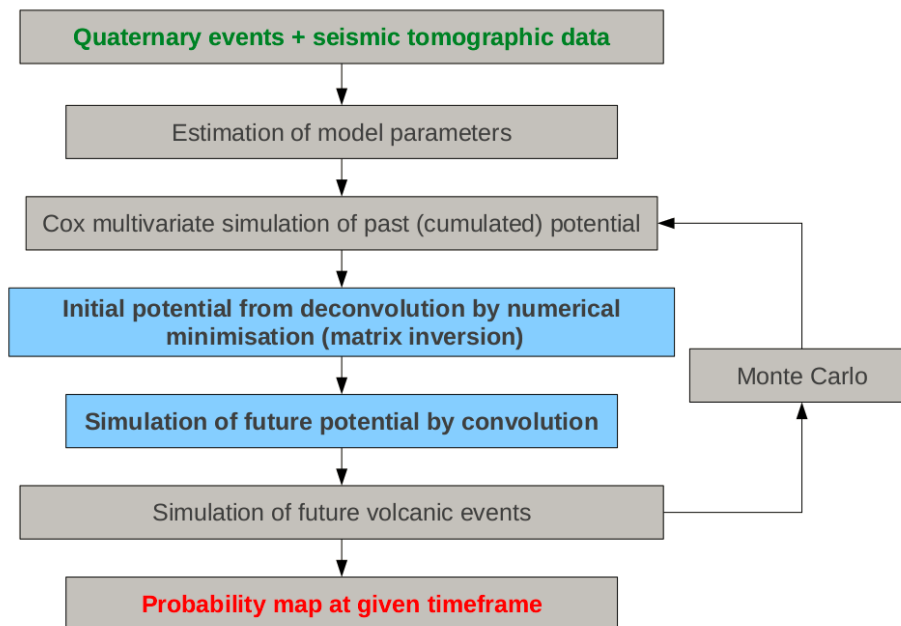
Figure 5.8: Methodology for the estimation of volcanic hazard using Cox simulation with deconvolution and Monte Carlo method.

5.3.3   Application to Tohoku data

The objective is the estimation of the probability for the formation of new polygenetic volcanoes over a proposed period of 1 Myr for Tohoku region. All Quaternary polygenetic volcanoes (those active within the last 2 Myr) of the Tohoku region are considered as representing potentially active volcanic areas for the future. The Tohoku volcanic arc is located in northern Honshu, Japan and consists of more than 100 volcanic edifices erupted during the Quaternary (Committee for the Catalogue of Quaternary Volcanoes in Japan, 1999). A volcanic edifice corresponds to the volcanic event considered for the Tohoku case study; i.e. a polygenetic volcano is composed of one or more edifices. Polygenetic volcanoes are characterized by a geomorphology and geologic structures that are created by many episodes of eruptive activity likely to affect broad areas. The formation of new polygenetic volcanoes can take place at locations up to tens of kilometres away from sites of previous eruptions; i.e. with likely future locations based on the Migration Scenarios described in the section above. The proposed probabilistic methodology is illustrated using a subset of the database of Quaternary volcanoes of Japan (Mahony et al., 2009).

According to Tamura et al. (2002; 2009), magma production may be controlled by locally developed hot regions within the mantle wedge beneath the Tohoku volcanic arc having the shape of inclined fingers with an average width of 50 km. These structures of the mantle wedge were revealed by various seismic tomography studies (Zhao et al., 1992; Zhao et al., 1994; Zhao et al., 2000; Hasegawa and Nakajima, 2004). They correspond to inclined seismic low-velocity zones located at depths shallower than about 150 km with an orientation sub-parallel to the down-dip direction of the slab. Such low-velocity zones are likely related to the upwelling–flow portion of the convection mechanically induced by slab subduction (Hasegawa and Nakajima, 2004). This upwelling flow of mantle materials encountering aqueous fluids is expected to produce partial melting in the low-velocity zones. The spatial distribution of volcanic events from the Tohoku volcanic arc is characterized by clusters, which are located above these zones of partial melting. The spacing of volcano clusters is governed by temperature variations along the Tohoku arc, ascent velocities and/or melt content in the upwelling flow of the mantle wedge underneath (Hasegawa and Nakajima, 2004; Hasegawa et al., 2005).

The cumulated potential of volcanism for the Tohoku region is believed to assimilate geological data related to Quaternary volcanic events as well as seismic tomography data

indicating zones of partial melting at depth (Jaquet et al. 2009). The latter consists of S-wave velocity perturbations along the inclined low-velocity zone in the mantle wedge of NE Japan (Hasegawa and Nakajima, 2004).

The values of the reference parameters for the simulation of the cumulated potential are taken from Jaquet et al. (2009). The main parameters are: a) the coefficient of correlation between the potential and the seismic tomography data and b) the correlation scale of the variogram, estimating the scale of the (randomly structured) spatial patterns for the potential. Sensitivity analysis is performed for these parameters as well as for the module of the migration velocity. The three scenarios of the migration direction are considered based on the Migration Scenarios in Section 5.3.1:

- **MS1: east → west**
- **MS2: south → north**
- **MS3: west → east**

5,000 Monte Carlo simulations were performed for obtaining probability maps with stable probability estimates at 1 Myr timeframe and a domain scale of 10 x 10 km; i.e. the cell size used for gridding.

Using scenario MS1, with a migration velocity of 40 km/Myr and reference parameter values, space-time dependent probability maps are produced for various timeframes. The increase effect in probability towards the west, related to the migration of volcanism, can be observed when comparing hazard maps at timeframes at 100 kyr, 500 kyr and 1 Myr (Figure 5.9).
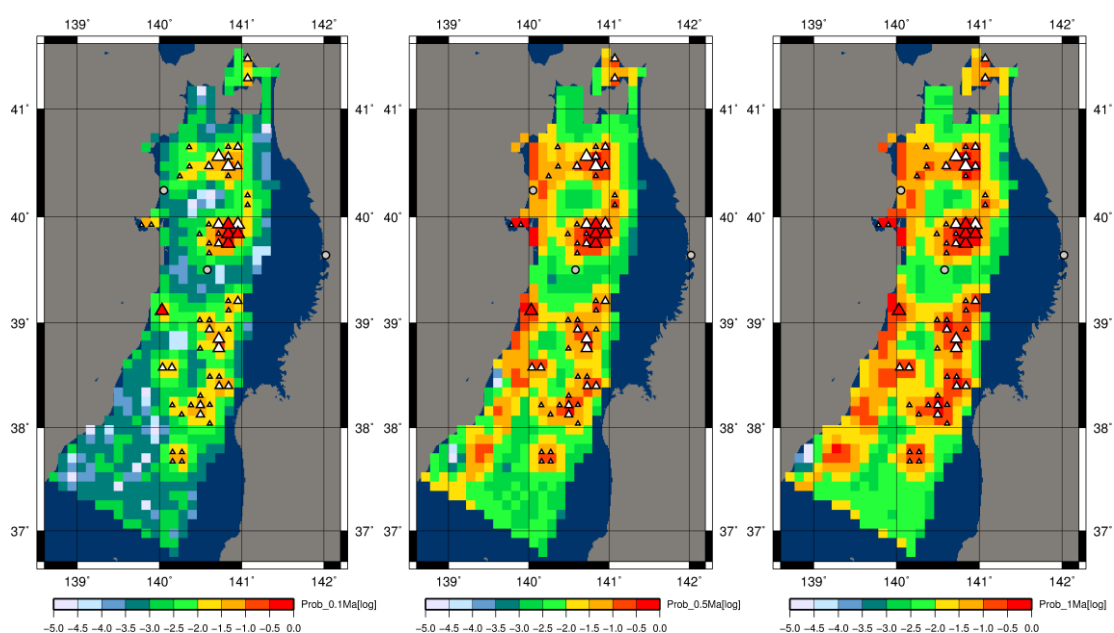
Figure 5.9: Volcanic hazard maps for Tohoku for scenario MS1 at timeframes 100 kyr (left), 500 kyr (centre) and 1 Myr (right) with migration velocity of 40 km/Myr towards the west, using reference parameter values. Triangles: location and number of Quaternary edifices (△: 0<n≤1, △: 1<n≤2, △: 2<n≤3, △: 3<n≤5, ▲: 5<n≤20). Grey dots: location of the example sites (WCB at the upper west coast, IB at the upper-middle inland, ECF at the east coast).

Hazard maps at 1 Myr timeframe were produced for scenario MS1 with different velocities of migration using reference parameter values. From a hazard point of view, it is more conservative to select velocity of migration in the range 20 – 30 km/Myr. Since a velocity of 40 km/Myr corresponds to a likely too rapid migration of volcanism for the region of Tohoku (Figure 5.10).
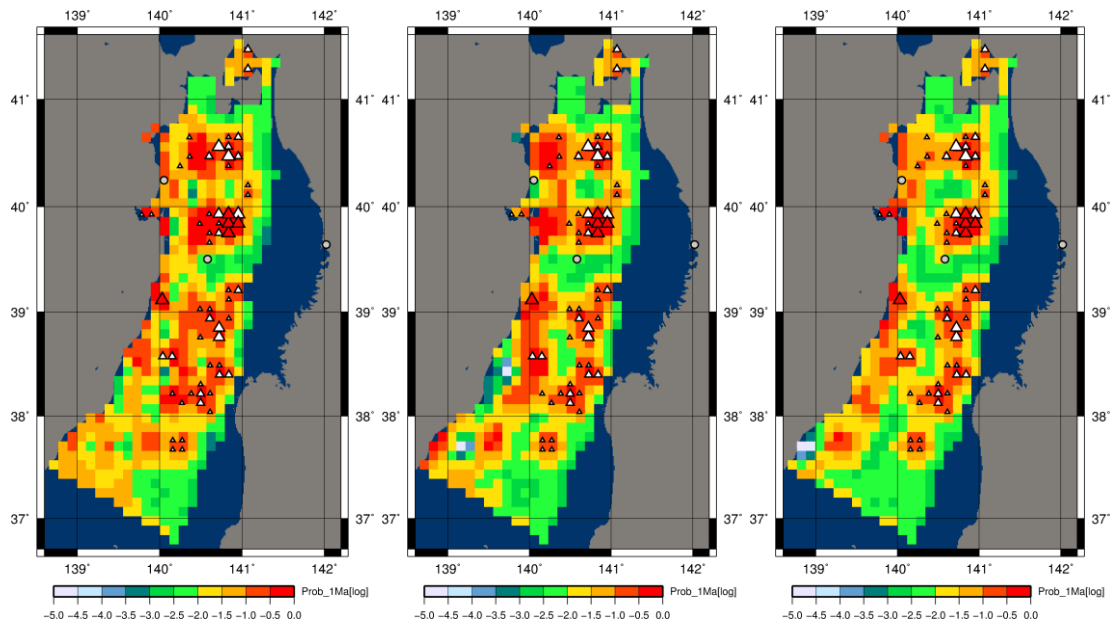
Figure 5.10: Volcanic hazard maps for Tohoku for scenario MS1 at timeframe 1 Myr with migration velocity of 20, 30 and 40 km/Myr towards the west, using reference parameter values. Triangles: location and number of Quaternary edifices (△: $0<n\leq1$, △: $1<n\leq2$, △: $2<n\leq3$, △: $3<n\leq5$, ▲: $5<n\leq20$). Grey dots: location of the example sites (WCB at the upper west coast, IB at the upper-middle inland, ECF at the east coast).

Therefore, solely the velocity values of 20 and 30 km/Myr were considered for the sensitivity analysis with respect to volcanic hazard estimation for Tohoku at 1 Myr timeframe. 18 cases were simulated based on parameter increase (Table 5.2): (i) in the correlation scale in the N-S direction (by a factor of 2); and, (ii) in the correlation between potential and seismic tomography data (by a factor of 2), the higher values mean stronger assumption that the present correlation will continue for 1 Myr. These parameter variations aim at investigating the effects of volcanism migration towards the gaps; and the impact of giving more weight to the seismic tomography, when estimating volcanic hazard at the 1 Myr timeframe.

Table 5.2: Cases with their parameters values and corresponding scenarios; 41 km and -0.3 are respectively the reference values for correlation scale and seismic correlation. The most plausible case for each Migration Scenario is given in red.

Case	Migration Scenario	Velocity [km/Myr]	Direction of migration	Correlation scale [km]	Seismic correlation	Timeframe
1	MS1	20	E→W	41–41*	-0.3	1 Myr
2	MS1	20	E→W	41–82**	-0.3	1 Myr
3	MS1	20	E→W	41–41	-0.6	1 Myr
4	MS1	30	E→W	41–41	-0.3	1 Myr
5	MS1	30	E→W	41–82	-0.3	1 Myr
6	MS1	30	E→W	41–41	-0.6	1 Myr
7	MS2	20	S→N	41–41	-0.3	1 Myr
8	MS2	20	S→N	41–82	-0.3	1 Myr
9	MS2	20	S→N	41–41	-0.6	1 Myr
10	MS2	30	S→N	41–41	-0.3	1 Myr
11	MS2	30	S→N	41–82	-0.3	1 Myr
12	MS2	30	S→N	41–41	-0.6	1 Myr
13	MS3	20	W→E	41–41	-0.3	1 Myr
14	MS3	20	W→E	41–82	-0.3	1 Myr
15	MS3	20	W→E	41–41	-0.6	1 Myr
16	MS3	30	W→E	41–41	-0.3	1 Myr
17	MS3	30	W→E	41–82	-0.3	1 Myr
18	MS3	30	W→E	41–41	-0.6	1 Myr

*Isotropic correlation scale.

**Anisotropic correlation scales with major axis orientated N-S.

The effect of parameter variations on the hazard maps are demonstrated for scenario MS1 using different values for the velocity of migration. An increase in correlation scale leads to the likelihood of more volcanism in the gap regions (Figure 5.11). And, an augmentation in the correlation between the potential and the seismic tomography data generates more variability in volcanic hazard away from Quaternary volcanic activity (Figure 5.12).
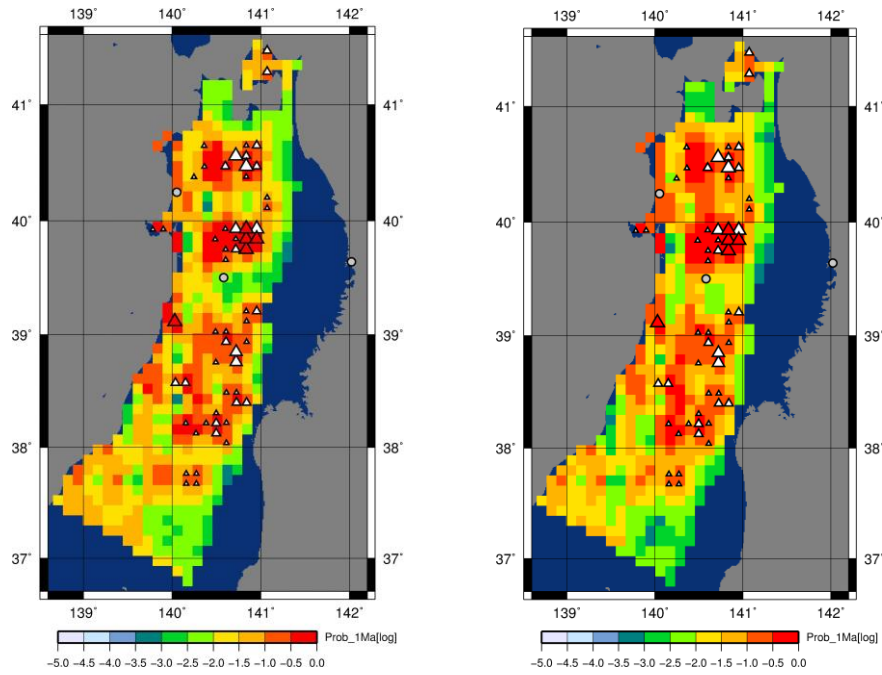
Figure 5.11: Cases 1 & 2: volcanic hazard maps for Tohoku for scenario MS1 at timeframe 1 Myr with migration velocity of 20 km/Myr (left), the effect of increased correlation scale (right). Triangles: location and number of Quaternary edifices (△: 0<n≤1, △: 1<n≤2, △: 2<n≤3, △: 3<n≤5, ▲: 5<n≤20). Grey dots: location of the example sites (WCB at the upper west coast, IB at the upper-middle inland, ECF at the east coast).
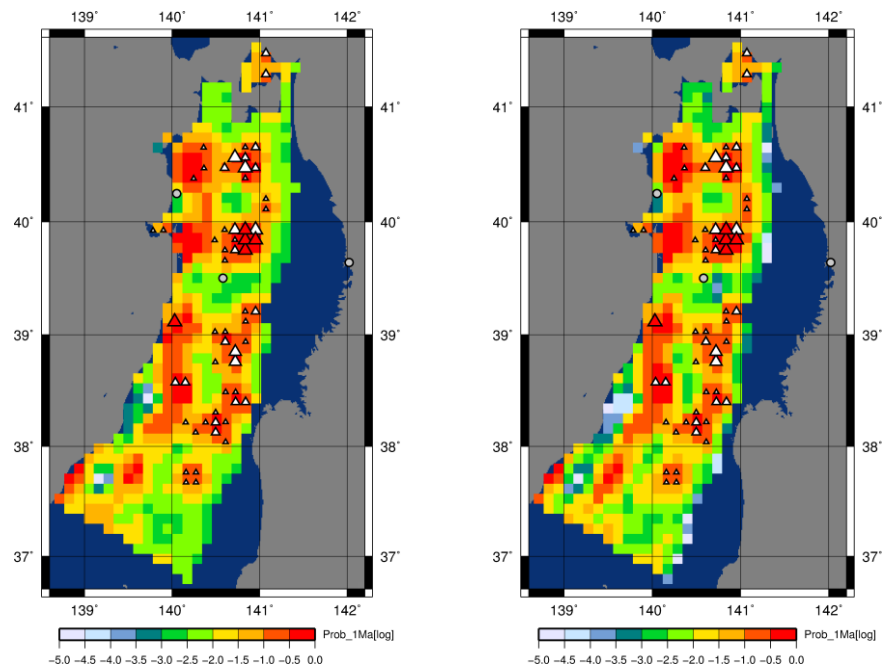
Figure 5.12: Cases 4 & 6: volcanic hazard maps for Tohoku for scenario MS1 at timeframe 1 Myr with migration velocity of 30 km/Myr (left), the effect of increased seismic correlation (right). Triangles: location and number of Quaternary edifices (△: 0<n≤1, △: 1<n≤2, △: 2<n≤3, △: 3<n≤5, ▲: 5<n≤20). Grey dots: location of the example sites (WCB at the upper west coast, IB at the upper-middle inland, ECF at the east coast).

Using the simulated results for each Migration Scenario, the most plausible case is selected in terms of migration characteristics and hazard variability (Table 5.2) for the region of Tohoku at the 1 Myr timeframe (Figure 5.13). The selected cases are associated to the following Regional Evolution Scenarios (RES):

- RES 1: Case 11 (MS2).
- RES 2: Case 6 (MS1) and Case 11 (MS2).
- RES 3: Case 11 (MS2).
- RES 4: Case 11 (MS2) and Case 13 (MS3).

Due to the differences in migration velocity and parameter values, the three plausible cases display remarkable diversity in terms of variability patterns when comparing their respective hazard maps (Figure 5.13).
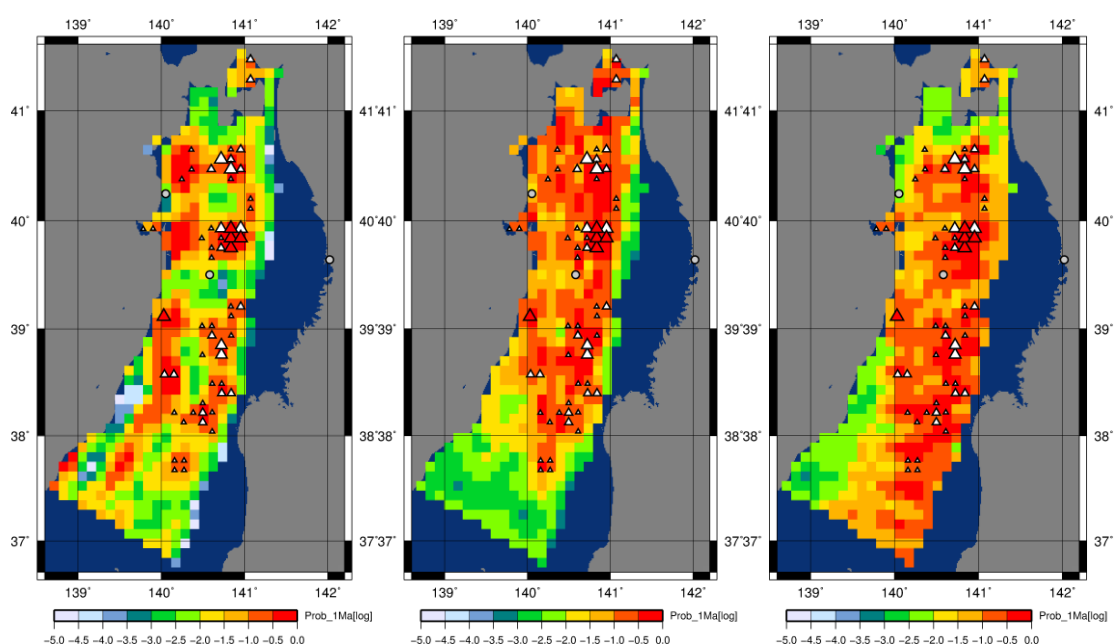
Figure 5.13: Cases 6, 11 & 13: volcanic hazard maps for Tohoku for scenarios MS1, MS2 and MS3 at timeframe 1 Myr. MS2 belongs to all RES; MS1 and MS3 are respectively solely part of RES 2 and RES 4. Triangles: location and number of Quaternary edifices (△: 0<n≤1, △: 1<n≤2, △: 2<n≤3, △: 3<n≤5, ▲: 5<n≤20). Grey dots: location of the example sites (WCB at the upper west coast, IB at the upper-middle inland, ECF at the east coast).

Hazard estimates at the following examples sites (Figure 5.13) were extracted from the simulated hazard cases:

- WCB: West Coast Backarc.
- IB: Inland Basin.
- ECF: East Coast Forearc.

The range of hazard estimates, expressed in probability at 1 Myr timeframe, for the three example sites are given with respect to Migration Scenarios (Table 5.3) and regarding Regional Evolution Scenarios (Table 5.4). The comparison of hazard range values (high & low) for Regional Evolution Scenarios (Table 5.4) shows that WCB site (high) values are generally higher by a factor of 2 compared to IB site values. Regarding the (low) site values, the opposite is observed; IB site values are generally higher by a factor of 3 in comparison to WCB values and a factor of up to 20 can be reached in case of RES 4. Such behaviour is explained by hazard range (high & low) values that are dominated by scenario MS2, with a migration direction towards the gaps, likely to occur for all RES.

Table 5.3: Volcanic hazard estimate ranges at Tohoku examples sites at 1 Myr timeframe, in relation to Migration Scenarios (MS).

Site	Migration Scenario		
	MS1	MS2	MS3
WCB	$3.4 \cdot 10^{-3} - 1.5 \cdot 10^{-1}$	$2.9 \cdot 10^{-2} - 2.2 \cdot 10^{-1}$	$3.8 \cdot 10^{-3} - 9.4 \cdot 10^{-3}$
IB	$3.2 \cdot 10^{-3} - 1.6 \cdot 10^{-2}$	$7.7 \cdot 10^{-2} - 1.3 \cdot 10^{-1}$	$3.6 \cdot 10^{-1} - 2.1 \cdot 10^{-1}$
ECF*	$< 10^{-5}$	$< 10^{-5}$	$< 10^{-5}$

*Site located outside of model domain.

Table 5.4: Volcanic hazard estimate ranges at Tohoku examples sites at 1 Myr timeframe, in relation to Regional Evolution Scenarios (RES).

Site	Regional Evolution Scenario			
	RES 1	RES 2	RES 3	RES 4
WCB	$2.9 \cdot 10^{-2} - 2.2 \cdot 10^{-1}$	$3.4 \cdot 10^{-3} - 2.2 \cdot 10^{-1}$	$2.9 \cdot 10^{-2} - 2.2 \cdot 10^{-1}$	$3.8 \cdot 10^{-3} - 2.2 \cdot 10^{-1}$
IB	$7.7 \cdot 10^{-2} - 1.3 \cdot 10^{-1}$	$3.2 \cdot 10^{-3} - 1.3 \cdot 10^{-1}$	$7.7 \cdot 10^{-2} - 1.3 \cdot 10^{-1}$	$7.7 \cdot 10^{-2} - 2.1 \cdot 10^{-1}$
ECF*	$< 10^{-5}$	$< 10^{-5}$	$< 10^{-5}$	$< 10^{-5}$

*Site located outside of model domain.

5.3.4 Conclusions and perspectives

The need of estimating volcanic hazard up to 1 Myr timeframe has led to new developments for the stochastic model. At such long time scale, arc volcanism migration is likely to occur in relation to the various tectonic evolution scenarios. Therefore, the proposed stochastic model enables to estimate long-term volcanic hazard under evolving tectonic conditions in order to produce hazard maps at 1 Myr timeframe. The mapped space-time probability of volcanic events, using Tohoku region as illustration, were obtained for three Migration Scenarios (linked to RES) with assimilation of Quaternary volcanic events and seismic tomography data. Actually for such a long timeframe, datasets that extend beyond the Quaternary, possibly up to the Middle Miocene, are required for describing the volcanic patterns likely to occur in space and time.

Remarkable diversity in volcanic hazard patterns were obtained when comparing the 1 Myr maps associated to the Migration Scenarios. Sensitivity calculations have enabled estimation of volcanic hazard ranges at examples locations for Tohoku region.

Additional developments are needed as to include various types of volcanic activity in form of selected scenarios in order to estimate their specific hazards. Using a Boolean approach coupled to a stochastic model would allow hazard estimation for explicitly described scenarios (e.g. caldera events).

5.4 Development of volcanic hazard maps

5.4.1 Consequence of volcanic events

Once temporal and spatial estimates have been made for event timing and location, respectively, it becomes possible to forecast potential event impacts and to prepare hazard curves (also known as exceedence curves or complementary cumulative density functions) for specific sites. For HLW repositories, the consequences of volcanic events include the following:

- Direct disruption of waste packages by intruding magma and transport of the HLW to the surface and dispersion. Development of volcanic conduits within the footprint of the repository would subject waste and the engineered barrier system to high temperatures (e.g., >1000°C) and high mass flow rates (e.g., >10^6kgs^{-1}), for extended periods of time (e.g., >1 yr). HLW fragments may be transported in erupted tephra plumes, in lava flows, pyroclastic density currents and by related volcanic phenomena.
- Igneous dykes and sills may intrude into the repository without necessarily venting to the surface. Such intrusions may destroy or partially destroy the engineered barrier system.
- Nearby igneous intrusions may subject the repository to high rates of deformation. Uplift and fault displacement (e.g., reactivation of long-inactive faults or slip along joint surfaces) commonly accompany igneous intrusions.
- Nearby igneous intrusions may subject the repository to changes in the level of the groundwater table, changes in groundwater flow, hydrothermal activity, and gas flux through the repository.

The ITM-TOPAZ methodology has not involved modeling most of these processes explicitly. Rather, a conservative offset distance was developed for volcanic events. For ITM-TOPAZ, the probability of new volcano formation was considered for a 100 km^2 area about the site. Any activity within this footprint was considered to be a disruptive event, without assessing its radiological consequences through a full performance assessment.

5.4.2 The aggregate probability of volcanic events

The aggregate probability of volcano formation within a given area and timeframe about a potential HLW repository site may be calculated by combining the recurrence rate and spatial density models. Probability of volcano formation can be estimated for any given scenario – any branch of the logic tree shown in Figure 5.1 – by setting the models weights along this branch equal to unity. As an example, consider the 14 sites shown in Figure 5.15, used to test and compare volcano and tectonic hazard models. At any one of these sites, probability is estimated using:

$$P[volcanic disruption] = P[number events \geq 1]P[volcanic disruption \,|\, events]$$

$$P[number events \geq 1] = 1 - e^{-\hat{\lambda}_t u}$$

$$P[volcanic disruption \,|\, Events] = 1 - e^{-\hat{\lambda}(s)A} \tag{18}$$

where u is the assessment period (e.g., 1 Myr), A is the area encompassing the site and the disruptive volcanic event (e.g., 100 km^2), $\hat{\lambda}_t$ is the estimated recurrence rate and $\hat{\lambda}(s)$ is the estimated spatial density. For example, at WCB site, the estimated recurrence rate for volcano formation, given an RES in which the tectonic setting remains unchanged and the MLE recurrence rate, is $\hat{\lambda}_t = 5 \times 10^{-5}$ volcanic events per year. Considering the spatial density estimate using kernel density estimation and the SAMSE bandwidth optimization, $\hat{\lambda}(s) = 6.6 \times 10^{-6}$ per square kilometer. With these values, the probability of disruption is:

$$P[volcanic disruption, u = 1 yr] = 3.3 \times 10^{-8}$$

$$P[volcanic disruption, u = 100 kyr] = 3.3 \times 10^{-3}$$

$$P[volcanic disruption, u = 1Myr] = 3.3 \times 10^{-2}.$$

(19)
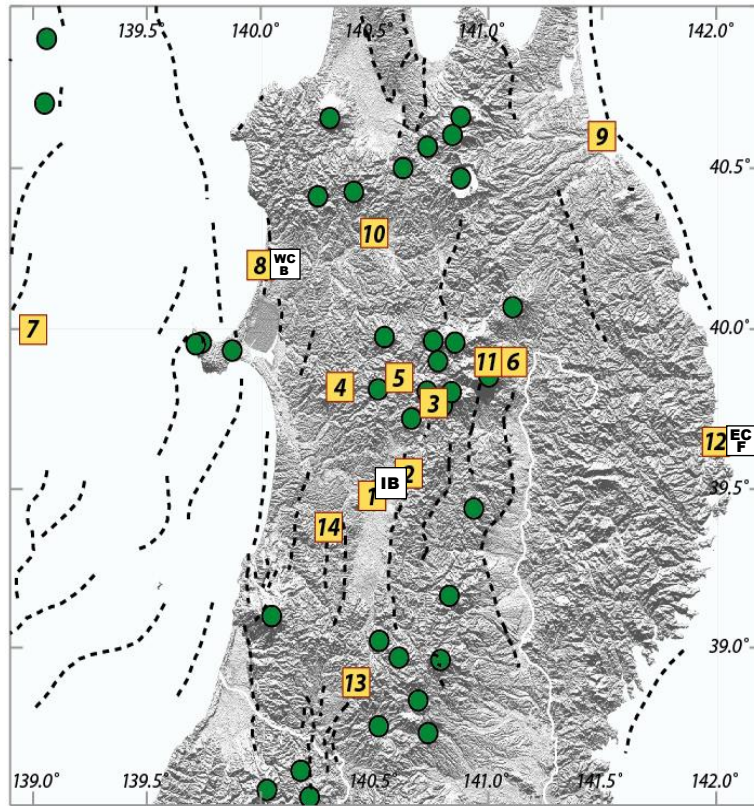
Figure 5.15: Example sites at which aggregate probabilities are calculated and threshold values are compared (yellow and white boxes) with respect to the location of Quaternary volcanoes (green circles) (modified after Chapman et al., 2009). Active faults are shown by dashed lines. Topography from Shuttle Radar Topography Mission (Jarvis et al., 2008).

This probability is estimated assuming one model scenario, that the expected values for recurrence rate and spatial density are appropriately chosen given the average recurrence rate estimated by MLE and the kernel density estimate of spatial density with SAMSE optimization. As shown in Table 5.5, other model scenarios result in other probabilities. In this example, an ensemble of 16 models results from four alternative recurrence rate models and four alternative spatial density models. The two recurrence rate models correspond to estimates of recurrence rate based on estimated λ_t during the last 900 kyr using volcanoes with estimated ages of formation (5 x 10^{-5}/yr for Senarios 1 to 4), and using all volcanoes formed in the Quaternary (6.5 x 10^{-5}/yr for Senarios 5 to 8) under RES 1. Alternatively, the recurrence rate may increase over time (10 x 10^{-5}/yr for Senarios 9 to 12) under RES 2, or decrease over time (2.5 x 10^{-5}/yr for Senarios 13 to 16) under RES 4. Four alternative spatial density models are used:

- kernel density estimate using SAMSE (large, anisotropic bandwidth; 3.5 x 10^{-5}/yr for Senarios 1, 5, 9 and 13),
- kernel density estimate using LSCV (short, isotropic bandwidth; 3.5 x 10^{-5}/yr for Senarios 2, 6, 10 and 14),
- Cox process model Case 6 (volcanism migrating toward the west; 5.2 x 10^{-5}/yr for Senarios 3, 7, 11 and 15), and
- Cox process model Case 11 (volcanism migrating along the arc into gaps; 5.1 x 10^{-4}/yr for Senarios 4, 8, 12 and 16).

These alternative models can be aggregated by assigning weights to each branch of the tree (Figure 5.1). Using the weights for the recurrence rate models (wt_{RR}) and spacial density models (wt_{SD}) in Table 5.5 yields an aggregate probability of disruption of WCB site of approximately 1.6×10^{-8}/yr. It is emphasised that these weights were temporarily set for demonstration purpose, which should be assigned through expert elicitation process in the full application of the ITM-TOPAZ methodology.

It is notable that in this example the range of annual probability of disruption of WCB site represented by these models is about one order of magnitude, providing a sense of the epistemic (model) uncertainty associated with these ensemble models. Alleatoric uncertainty could be better represented by assigning a probability distribution of recurrence rates to each model, based on uncertainty in parameter estimation.

Table 5.5: Summary of estimation for of the aggregate probability of new volcano formation at the example site WCB (site 8). Value represent mean weights, wt and modeled probabilities for 16 scenarios. The aggregate probability, AP, is the sum of the weighted probabilities.

Scenario	[1] RR model	[2] RR	[3] wt_{RR}	[4] SD model	[5] SD	[6] wt_{SD}	[7] wt Pr	[8] Pr |Scenario
1	~900 ka (RES 1)	5	0.4	SAMSE	5.1×10^{-4}	0.25	2.5×10^{-9}	2.5×10^{-8}
2	~900 ka (RES 1)	5	0.4	LSCV	3.5×10^{-5}	0.25	1.8×10^{-10}	1.8×10^{-9}
3	~900 ka (RES 1)	5	0.4	Cox (Case 6)	5.2×10^{-5}	0.25	2.6×10^{-10}	2.6×10^{-9}
4	~900 ka (RES 1)	5	0.4	Cox (Case 11)	5.1×10^{-4}	0.25	2.5×10^{-9}	2.5×10^{-8}
5	Quaternary (RES 1)	6.5	0.4	SAMSE	5.1×10^{-4}	0.25	3.3×10^{-9}	3.3×10^{-8}
6	Quaternary (RES 1)	6.5	0.4	LSCV	3.5×10^{-5}	0.25	2.3×10^{-10}	2.3×10^{-9}
7	Quaternary (RES 1)	6.5	0.4	Cox (Case 6)	5.2×10^{-5}	0.25	3.4×10^{-10}	3.4×10^{-9}
8	Quaternary (RES 1)	6.5	0.4	Cox (Case 11)	5.1×10^{-4}	0.25	3.3×10^{-10}	3.3×10^{-8}
9	increase (RES 2)	10	0.1	SAMSE	5.1×10^{-4}	0.25	1.2×10^{-9}	5.1×10^{-8}
10	increase (RES 2)	10	0.1	LSCV	3.5×10^{-5}	0.25	8.8×10^{-11}	3.5×10^{-9}
11	increase (RES 2)	10	0.1	Cox (Case 6)	5.2×10^{-5}	0.25	1.3×10^{-10}	5.2×10^{-9}
12	increase (RES 2)	10	0.1	Cox (Case 11)	5.1×10^{-4}	0.25	1.3×10^{-9}	5×10^{-8}
13	decrease (RES 4)	2.5	0.1	SAMSE	5.1×10^{-4}	0.25	3.2×10^{-10}	1.3×10^{-8}
14	decrease (RES 4)	2.5	0.1	LSCV	3.5×10^{-5}	0.25	2.2×10^{-11}	8.8×10^{-10}
15	decrease (RES 4)	2.5	0.1	Cox (Case 6)	5.2×10^{-5}	0.25	3.3×10^{-11}	1.3×10^{-9}
16	decrease (RES 4)	2.5	0.1	Cox (Case 11)	5.1×10^{-4}	0.25	3.1×10^{-10}	1.3×10^{-8}
AP							1.6×10^{-8}	

[1] dataset or assumption for recurrence rate model under the RES
[2] estimated recurrence rate (events per 10^{-5} year)
[3] weight assigned to the recurrence rate
[4] spatial density model
[5] estimated spatial density (events per $100km^2$)
[6] weight assigned to the spatial density model
[7] weighted probability of each scenario
[8] conditional probability given each scenario (unweighted probability of each scenario = RR*SD)

5.4.3　Hazard maps for volcanic disruption

The logic tree serves two roles. First, as already illustrated, the weights and scenario probabilities may be used to estimate aggregate probability, or a range of aggregate probabilities given uncertainty in model input parameters. Such weighting through expert judgment gives the best estimate of aggregate probability and uncertainty. It is, however, a different goal to assess project risk due to a particular geologic hazard, or set of geologic hazards. Although the aggregate probability for a particular site may be acceptable in terms of geologic hazard, different scenario models for the site may yield large differences in probability ($P[disruption \,|\, scenario\,]$ in Table 5.5). A project has greater risk if some branches of the logic tree have high probabilities, even if the aggregate probability is acceptable. Rather than aggregating probability to assess project risk, credible scenarios should each be investigated. A site has low project risk if individual models for hazard indicate an absence of potential for disruptive geologic events. Note that this approach does not result in a robust probabilistic assessment for any particular site. Instead, it provides a metric for comparing relative project risk among potential sites using a range of models. In that sense, the method is a project tool rather than a siting criterion.

Thus, the estimation of project risk for volcanic disruption of a given site depends on establishing threshold probabilities to define "absence of potential for disruptive geologic events" for each scenario. For volcanism, we established two thresholds to illustrate the methodology. Internationally, an annual probability of 1×10^{-8} for disruption due to volcanism has often used as a threshold – below which there is an absence of potential for volcanic events. Sites that have annual probabilities of $<1 \times 10^{-8}$ for each of a variety of alternative models are considered to carry low project risk with respect to potential for volcanism. A second threshold is established at an annual probability of 1×10^{-7}. Sites that have annual probabilities of $>1 \times 10^{-7}$ for any one of a variety of alternative models are considered to carry high project risk with respect to potential for volcanism. Intermediate sites, $1 \times 10^{-8} \le P[volcanism] \le 1 \times 10^{-7}$ carry moderate project risk. That is, detailed analysis may reveal the site carry in fact low project risk through estimation of aggregate probability, especially after detailed site investigation, but credible scenarios for potential volcanic disruption exist and must be evaluated. Potential volcanism may remain a siting concern for such sites.

For example, Scenarios 5 to 8 (Table 5.5) were used to evaluate project risk for 15 example sites in the Tohoku region (Figure 5.15) to illustrate the methodology. The results of this assessment are shown in Table 5.6. Sites with very low project risk (sites 7, 9, ECF/12) are characterized by annual probabilities $<1 \times 10^{-8}$ for all of the alternative models. The two sites of high project risk (IB, 2) are characterized by one or two scenarios yielding annual probability $>1 \times 10^{-7}$. It is notable for these sites that at least one scenario produces probabilities $<1 \times 10^{-8}$. Nevertheless, it is clear that potential for volcanic disruption of a repository at these two sites would create high project risk. Similarly, intermediate sites are characterized by a range of probabilities for different scenarios. A good example are the "gap" sites (sites 1, 13). Spatial density models that emphasize tight clustering of volcanoes (Cox and LSCV methods) produce lower probabilities than the smooth spatial density model (SAMSE). This difference reflects differences in models for volcanism in the arc. The classic subduction zone model emphasizes uniform volcano distribution along the arc, and rapid changes across the arc. This tends to increase the modeled spatial density in gaps between clusters of volcanoes in Tohoku. The "hot finger" model of volcanism emphasizes vent clustering. Thus the Cox and LSCV models tend to reduce probability between clusters. For these sites, it may be that the aggregate probability, estimated after detailed investigation and expert elicitation, may indicate such sites carry low project risk. But, there are geologic models extant in the literature that support higher probabilities. In other words these sites carry some, if moderate, project risk.

Maps may be constructed for the Tohoku region for each scenario to be compared. Four such maps are constructed for illustration, using the SAMSE, LSCV and Cox spatial density models (Figures 5.16). These maps may then be combined into a single project risk map for volcanism (Figure 5.17) to take all uncertainties in the scenarios into account.

Table 5.6: Probabilities of volcanism and project risks for the 15 example sites based on the four alternative spatial density models.

Site	Spatial Density Model				[5] Project Risk
	[1] SAMSE	[2] LSCV	[3] Case 6	[4] Case 11	
IB	9.9×10^{-8}	8.1×10^{-10}	3.2×10^{-9}	1.1×10^{-7}	H
1	7.7×10^{-8}	6.4×10^{-11}	8.4×10^{-9}	8.4×10^{-8}	M
2	1.1×10^{-7}	8.4×10^{-9}	9.8×10^{-9}	2.5×10^{-7}	H
3	1.2×10^{-7}	6.2×10^{-7}	5.1×10^{-7}	3.8×10^{-7}	H
4	4.4×10^{-8}	2.8×10^{-8}	2.5×10^{-7}	2.7×10^{-7}	H
5	9.2×10^{-8}	9.0×10^{-8}	2.1×10^{-7}	1.1×10^{-7}	H
6	5.8×10^{-8}	9.0×10^{-8}	1.1×10^{-7}	1.3×10^{-7}	H
7	7.2×10^{-9}	0	$* < 1 \times 10^{-11}$	$* < 1 \times 10^{-11}$	L
WCB/8	3.3×10^{-8}	2.3×10^{-9}	3.4×10^{-9}	$3.3. \times 10^{-8}$	M
9	4.3×10^{-9}	0	$* < 1 \times 10^{-11}$	$* < 1 \times 10^{-11}$	L
10	5.3×10^{-8}	2.0×10^{-8}	3.2×10^{-8}	2.3×10^{-7}	H
11	9.3×10^{-8}	3.4×10^{-7}	6.2×10^{-7}	5.1×10^{-7}	H
ECF/12	1.8×10^{-15}	0	$* < 1 \times 10^{-11}$	$* < 1 \times 10^{-11}$	L
13	8.7×10^{-8}	3.4×10^{-8}	4.4×10^{-9}	4.6×10^{-8}	M
14	4.4×10^{-8}	8.8×10^{-13}	1.1×10^{-8}	3.6×10^{-8}	M

[1] SAMSE method for optimal bandwith determination
[2] LSCV method using a radial bandwith of 60 km
[3] migration of volcanism from E to W during a 1 Myr timeframe
[4] migration of volcanism into the "gap" during a 1 Myr timeframe
[5] L: low; $P < 1 \times 10^{-8}$ /yr for all models
 M: moderate; 1×10^{-8} /yr $\leq P \leq 1 \times 10^{-7}$ /yr
 H: high; $P > 1 \times 10^{-7}$ /yr for any one model
 * outside the model domain for these spatial density estimates
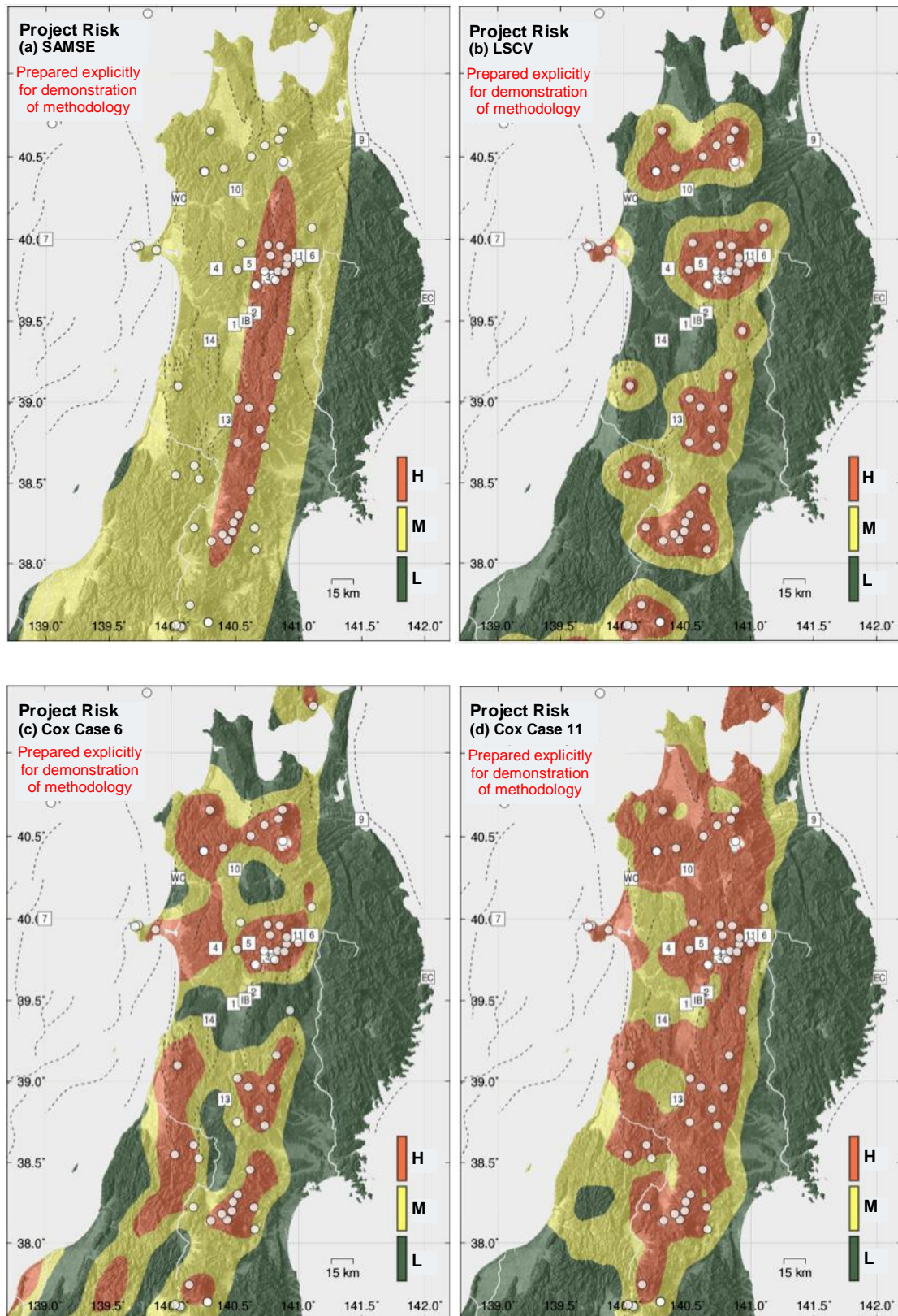
Figure 5.16: Project risk based on spatial density models (a) SAMSE, (b) LSCV, (c) Cox process Case 6 and (d) Case 11 for an area of 100 km^2 ,using a recurrence rate of 6.5x10^{-5} /yr. Green areas are characterized by very low estimated rates of volcanic activity (P<1x10^{-8} /yr). These areas comparatively carry low project risk. Red areas correspond to relatively high rates of volcanic activity (P>1x10^{-7} /yr). Sites in these areas may have a relatively high project risk due to concerns about long term rate of volcanic activity.

Figure 5.17: All four maps in Figure 5.15 are combined into a single project risk map for volcanism. Green areas are characterized by very low estimated rates of volcanic activity ($P<1\times10^{-8}$ /yr). These areas comparatively carry low project risk. Red areas correspond to relatively high rates of volcanic activity ($P>1\times10^{-7}$ /yr). Sites in these areas may have a relatively high project risk due to concerns about long term rate of volcanic activity. activity based on this model. Yellow areas have 1×10^{-8} /yr $\leq P\leq1\times10^{-7}$ /yr and carry moderate project risk due to volcanism.

5.5 Development of exhumation hazard maps

This section explores how the same approach to develop hazard map (project risk map) by assigning threshold values as for volcanism could be applicable to the evaluation of uplift and erosion. It is noted that this work was carried out in parallel with the scenario development described in the previous chapters, and thus has not been directly correlated each other.

5.5.1 Models of uplift

Like volcanism, relatively rapid uplift and erosion of a site may result in release of radionuclides into the biosphere. There are essentially two pathways leading to this release. The first involves such rapid uplift and erosion that a repository is "daylighted" within the assessment period. Assuming a repository is constructed at 500 m depth and has a 1 Myr assessment period, uplift of approximately >0.5 mm/yr is required to bring this repository to the surface during the assessment period. Here, the erosion rate is assumed to be equivalent to the uplift rate for a simple demonstration of methodology. In addition, smaller amounts of uplift may place the repository in the oxic zone, potentially creating a plume of redox-sensitive radionuclides. Two types of uplift models are used for this assessment: geological markers of regional uplift and isostatic gravity anomalies.

It is important to realize that different processes lead to long-term uplift, including compression along subduction zones, transpression, igneous intrusions and underplating of the crust, and glacial isostatic adjustments. This implies that multiple models are necessary in order to assess alternative scenarios for long term uplift. In TOPAZ, this problem has been explored using two data sets. Geomorpholocial data on uplift over the last 125 kyr provides a relatively short-term direct record of uplift resulting from any one of these processes (e.g. Koike et al., 2005, see Section 3.2). Isostatic gravity anomalies regional gravity data compiled by the Geological Survey of Japan, AIST (Komazawa et al., 2004) suggest a potential for future uplift, based on the long term compensation of topography at relatively long wavelengths. Alternative models, for example finite element models of uplift in response to compression, might certainly be developed.

We note that quantifying the disruptive potential of uplift and erosion in terms of measured vertical uplift and isostasy thresholds does simplify the problem. For a full probabilistic hazard assessment of uplift and erosion, factors need to be considered, including: (1) the average regional rate of uplift or subsidence; (2) the magnitude of differential uplift and erosion, in other words, the horizontal derivative of uplift; (3) the potential for localized extreme uplift or erosion, for example associated with igneous intrusion; (4) the balance between uplift and erosion, subsidence and burial, due to factors such as climate. Here the models used are only sensitive to the first factor.

5.5.2 Geological markers of regional uplift

Geologic markers of long term uplift and erosion include marine geologic markers including marine terraces, paleoshoreline indicators, coral reefs and marginal marine sediments. Away from coastlines, uplift markers include differential uplift across faults, flights of fluvial terraces, rates of incision, and similar criteria. In high uplift environments, geochronometry and geothermometry, for example, the annealing of fission tracks in zircon and apatite minerals, can be used to constrain long term rates.

A model of uplift and subsidence during the last 125 kyr has been constructed for part of Tohoku based on these types of data (Koike et al., 2005). Although there is considerable uncertainty in extrapolation of the uplift rates measured at local outcrops across the Tohoku region, the map can be used as one model of potential uplift to assess project risk.

Consequently, we can define two thresholds for project risk maps related to uplift and erosion. The first threshold is defined as 0.5 mm/yr – potential sites characterized by uplift exceeding this threshold are considered to carry high project risk. The second is 0.25 mm/yr – sites characterized by uplift <0.25 mm/yr are considered to be highly suitable from the standpoint of uplift and erosion. Sites characterized by intermediate values carry moderate project risk, both in the sense that there is relatively low probability of moving a repository into the oxic

zone and there is relatively low chance that the uplift at such a site is drastically underestimated.

Figure 5.18 shows uplift data for a part of Tohoku contoured using these threshold values. Roughly 50% of the area is associated with zones of subsidence or low uplift (<0.25 mm/yr). These areas are considered to be highly suitable from a project risk standpoint in terms of the absence of potential for rapid uplift. Tohoku is characterized by relatively narrow zones of relatively high rates of uplift (>0.25 mm/yr) and broad regions are characterized by intermediate values. This likely reflects uncertainty associated with measured uplift in these areas. That is, from a project risk perspective it would likely be necessary to gather additional data via detailed site investigation to characterize uplift at a site in located in these areas, and there is some potential that uplift and erosion would be of concern.
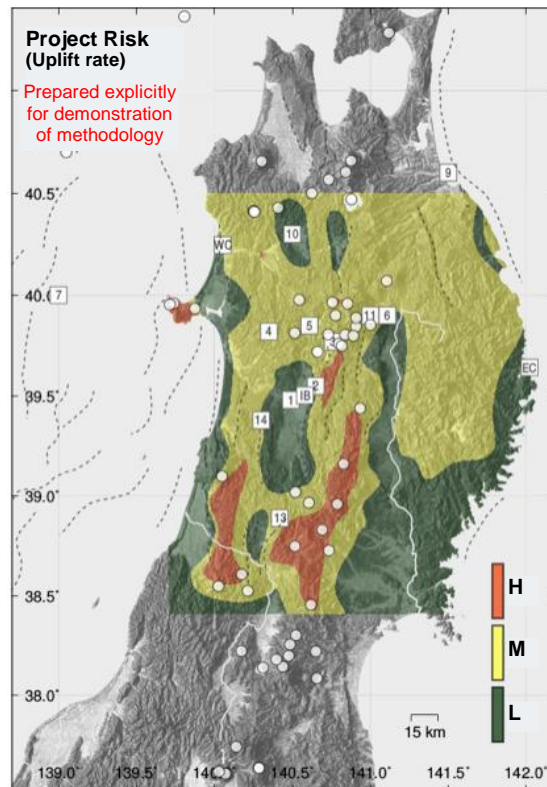
Figure 5.18: Project risk based on measured and interpolated uplift for part of Tohoku based on geomorphological data for the last 125 kyr (Koike et al., 2005). The uplift rates (mm/yr) are color-coded using threshold values. Green areas are characterized by subsidence or low rates of estimated uplift (<0.25 mm/yr). These areas carry comparatively low project risk. Red areas correspond to relatively high estimated uplift. Sites in these areas may have a relatively high risk due to concerns about long term tectonic uplift.

5.5.3 Isostatic models of uplift

Isostatic gravity anomalies result from magma underplating and differentiation at the Moho or Conrad discontinuities, or elsewhere in the crust. This process results in a negative Bouguer anomaly, no Free Air Anomaly if the crust is in isostatic equilibrium, and positive topography. Therefore, the extent of the isostatic gravity anomaly (or corresponding elevation anomaly, $g=2\pi G\rho h$, indicates potential for uplift. An absence of a negative isostatic anomaly corresponds to an absence of potential for rapid uplift as a disruptive event. Therefore, a topographic compensation, $h>0$ m is a highly suitable site using this uplift model. Uplift is proportional to topographic compensation. If $h<-30$ m, then the area is may experience rapid

uplift to compensate this topography in the future (Figure 5.19). This map and Figure 5.18 are combined into a single project risk map for uplift and erosion (Figure 5.20).
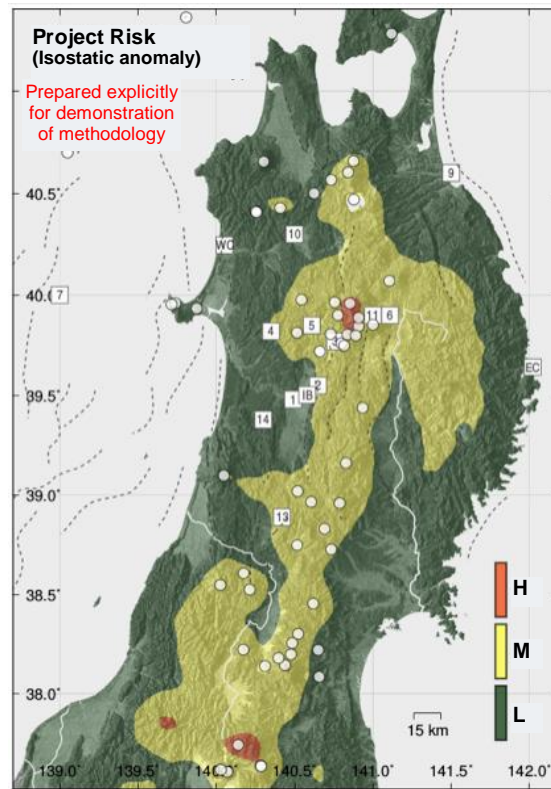
Figure 5.19: Project risk based on measured and interpolated uplift for part of Tohoku based on topographic compensation derived from the isostatic gravity anomlay map by the Geological Survey of Japan, AIST (Komazawa et al., 2004). The topographic compensation (m) is color-coded using threshold values. Green areas are characterized by subsidence or a high degree of topographic compensation ($h \geq 0$ m). These areas carry comparatively low project risk. Red areas correspond to relatively high negative topographic compensation ($h \leq$ -30 m). Sites in these areas may have a relatively high project risk due to concerns about long term uplift.
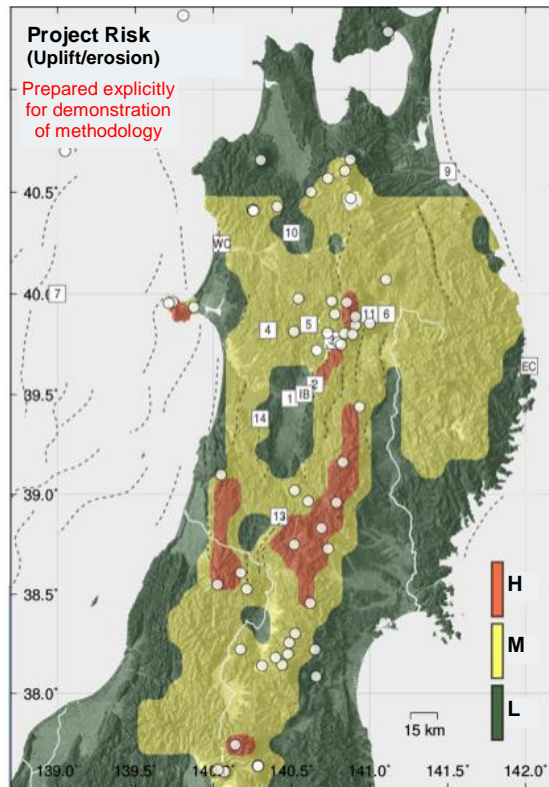
Figure 5.20: Figures 5.18 and 5.19 are combined into a single project risk map for uplift and erosion. Green zones are characterized by low observed uplift rate over the last 125 kyr and low potenital for uplift based on the isostatic model. Red correspond to relatively high rates of uplift based on at least one of the two models. Yellow areas carry moderate project risk due to uplift and erosion.

5.6 Combined project risk maps

Figure 5.21 shows relative project risk combining the volcanism and uplift maps. It is noted that this map was presented to demonstrate the idea of showing hazards (risks) of different phenomena in a single map. It is also emphasised that evaluation for exhumation hazard should be linked with the long-term evolution scenarios as same as for the volcanism, which has not been achieved in this case study.

Naturally the combined project map is rather smooth. Relatively high project risk occurs near Quatrnary volcanoes. The smooth SAMSE spatial density and the Cox process, case 11, models forecast higher rates of volcanism in gaps between current Quaternary volcano clusters. Relatively high project risk zones extend into thebackarc, especially in areas west of active Quaternatry volcano clusters. Even using these highly conservative threshold values most of Tohoku is located in zones of moderate to low project risk. Away from areas of active volcanism, sites with moderate project risk are associated with areas that have experienced uplift in the last 125 kyr. Detailed site investigations could improve the evaluation if these uplift values are the results of relatively sparse geologic data. Finally, there are large areas extending 10–50 km from the east coast of Tohoku that have very low project risk from the perspective of rapid uplift and volcanism (Figure 5.21).
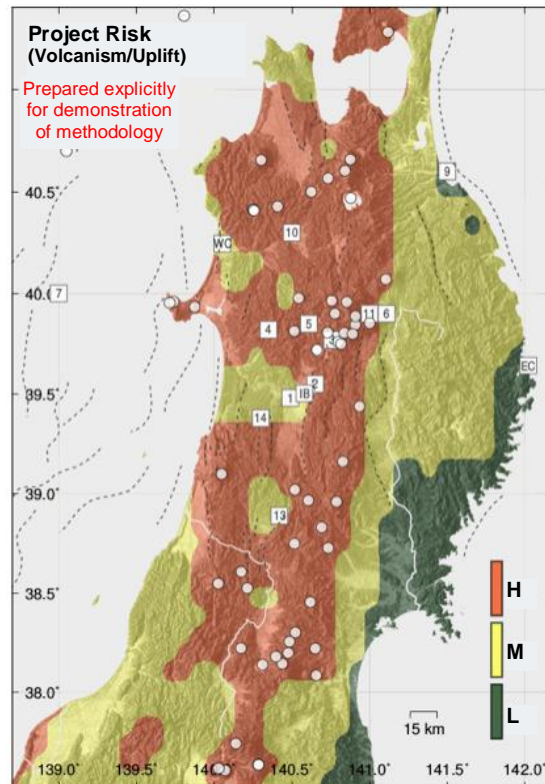
Figure 5.21: The volcano and uplift potential maps are combined into a single project risk map for Tohoku. Green zones on this map represent low project risks with respect to volcano and uplift disruptive hazards, as probabilities of disruptive events are negligible for all scenarios analyzed. Yellow zones are characterized by one or more slightly higher probability – these sites carry moderate project risk. Red zones are areas in which one or more scenario indicates high project risk.

6 Hazard maps for rock deformation

This chapter describes how the hazard maps of specific Impact Scenarios (IS) of rock deformation at any location can be developed. The example IS here is that of a large earthquake discussed in the previous report (Chapman et al., 2012), in which crustal strain is released in a 6.5 ≤M≤7.5 earthquake on a concealed deep active fault below the repository, causing shaer that could penetrate upwards into the repository.

6.1 Mapping the frequency of a tectonic deformation scenario: future 6.5 ≤ M ≤ 7.5 earthquakes

In this section we develop maps that illustrate the annual frequency of hazardous tectonic deformation across Tohoku. We use the ITM Tohoku strain rate models for surface deformation, GPS and seismicity (Chapman et al., 2009) to demonstrate how tectonic deformation can be quantified in map form. Our measure of tectonic deformation for the purposes of this demonstration model is the annual frequency of an earthquake of magnitude M6.5 to M7.5 occurring in a 3-dimensional grid cell of dimensions 5x5km, and 20km thickness. M6.5 approximates what might be the lower limit of hazardous tectonic displacements (about 0.5m displacement, depending on the magnitude scaling relationship used). We assume M7.5 is the maximum magnitude, based on the earlier ITM modelling of the region (Chapman et al. 2009).

Demonstration 6.5≤M≤7.5 maps are produced for each of the surface deformation (fault displacement, uplift and tilt), GPS and seismicity strain rate models (Figure 6.1 to Figure 6.3), for the equally weighted average of the three models (Figure 6.4), and for the maximum value of the three models (Figure 6.5). The following sections describe the method used to convert strain rates into 6.5≤M≤7.5 earthquake rates, and the resulting calculations, illustrated as a series of maps.

The method is described in Chapman et al. (2012), and summarised as below. The procedure to develop 6.5≤M≤7.5 rates is to first convert the ITM strain rates from the highest-weighted branch of the ITM logic trees for Surface Deformation, GPS and Seismicity strain rate models into seismic moment rates for a map grid of 5x5x20km resolution via the method of Kostrov (1974). The seismic moment rates are then distributed across the magnitude range of 6.5≤M≤7.5 according to a Gutenberg-Richter distribution: $logN = a - bM,$ in which N is the number of events of magnitude M, and a and b are empirical constants. The Gutenberg-Richter relationship (Gutenberg and Richter, 1944) well-describes the size distribution of earthquakes across regions, and the globe.

The maps in Figure 6.1 to Figure 6.3 show the distribution of 6.5≤M≤7.5 rates across the Tohoku region for the surface deformation, GPS and seismicity models. Also shown are combination maps for the three models; that is the average of 6.5≤M≤7.5 rates for each model, and the highest value of 6.5≤M≤7.5 rates from each model. All maps are produced for the same 5x5x20km grid cell dimension. The colour scheme is used to distinguish between high ($>10^{-4}$/yr), medium (10^{-4}-10^{-5}/yr), and low ($<10^{-5}$/yr) 6.5≤M≤7.5 rates. These divisions can also be thought of as the time span in which a 6.5≤M≤7.5 earthquake could be expected to occur (return time). There values are for demonstration purposes because it is important to consider consequences prior to defining what level of activity truly represents hazard. We have developed a threefold division to match with the number of divisions used for the volcanic hazard maps (although the rates are markedly different and cannot be compared in terms of true hazard (this would have to be done by considering consequences). Here, we refer to the three rate categories as low, medium and high tectonic hazard where high corresponds to one or more 6.5≤M≤7.5 earthquakes occurring in a 10 kyr period in that grid cell; medium corresponds to a 10-100 kyr timeframe for the occurrence of a 6.5≤M≤7.5 earthquake in that grid cell; and low corresponds to a > 100 kyr timeframe for a 6.5≤M≤7.5 earthquake occurring in that grid cell.

The surface deformation map (Figure 6.1) shows a roughly equal mix of low and medium tectonic hazard across much of the region, except for zones of high tectonic hazard along major faults in the west.
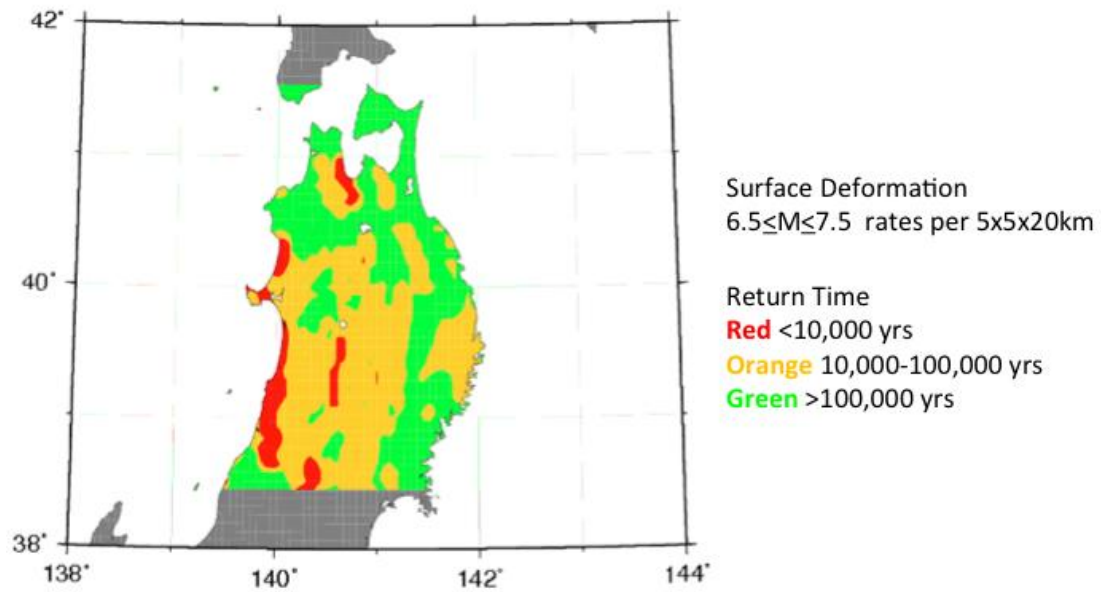
Figure 6.1: Map of 6.5<M<7.5 rates from the ITM Surface Deformation strain rate model, for a grid of cells with dimensions 5x5x20km.

The GPS map (Figure 6.2) shows largely medium tectonic hazard across much of the region, whereas the seismicity map (Figure 6.3) shows medium hazard largely confined to the central ranges (backbone ranges) of the region.
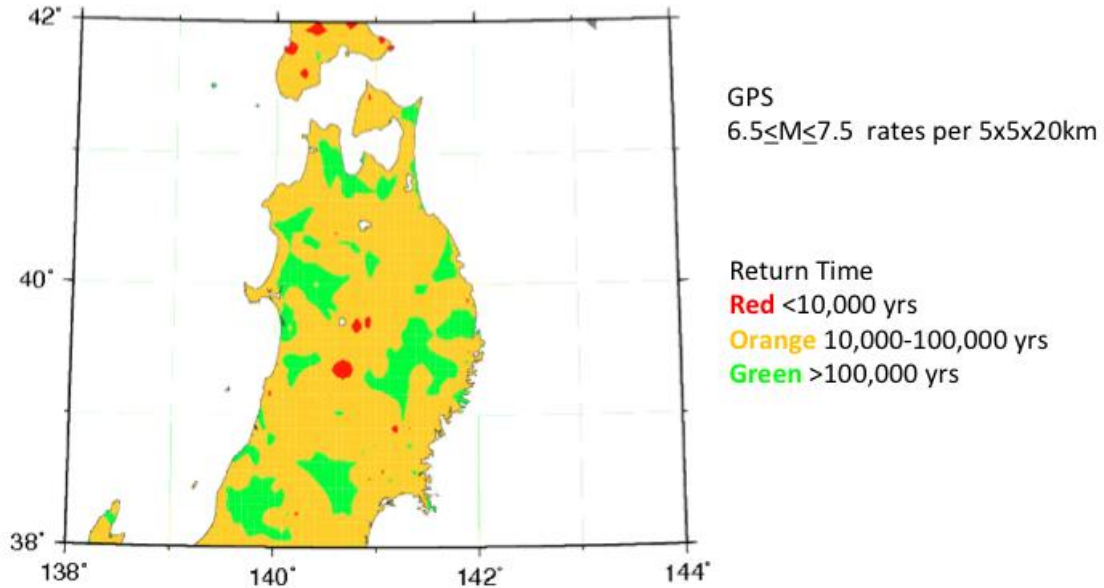
Figure 6.2: Map of 6.5<M<7.5 rates from the ITM GPS strain rate model, for a grid of cells with dimensions 5x5x20km.
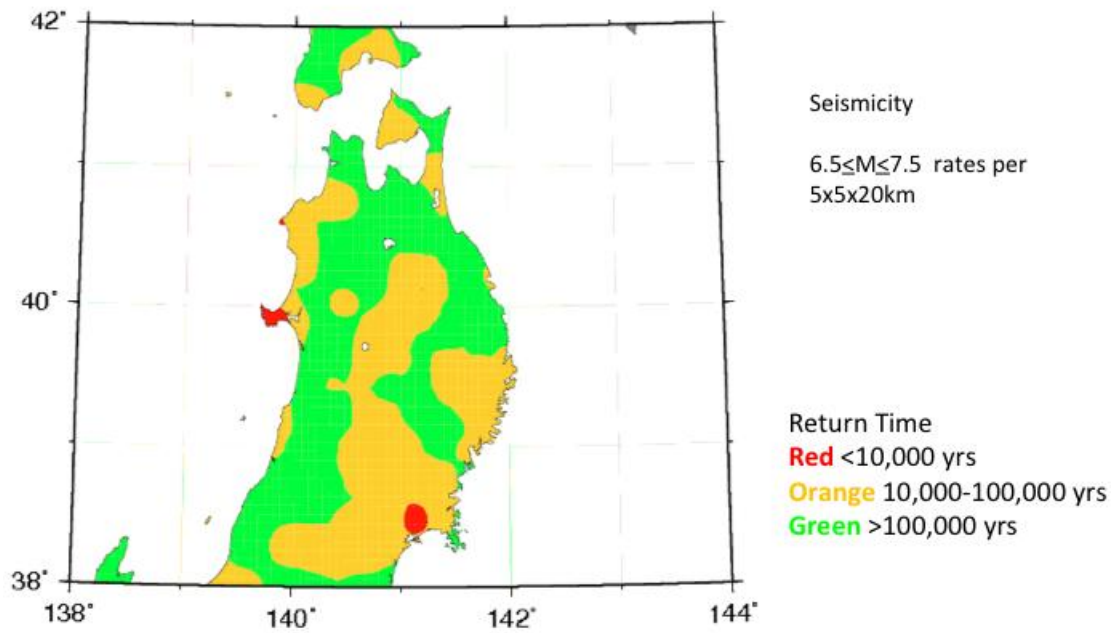
Figure 6.3: Map of 6.5<M<7.5 rates from the ITM Seismicity strain rate model, for a grid of cells with dimensions 5x5x20km.

The equally weighted (average) map for the three models (Figure 6.4) shows most of the region characterised by medium tectonic hazard, with some isolated areas of high hazard in the west, and low hazard scattered in the northwest and east. The maximum value map (Figure 6.5) shows almost no area of low tectonic hazard, but significantly more areas of high hazard where major active faults are located.
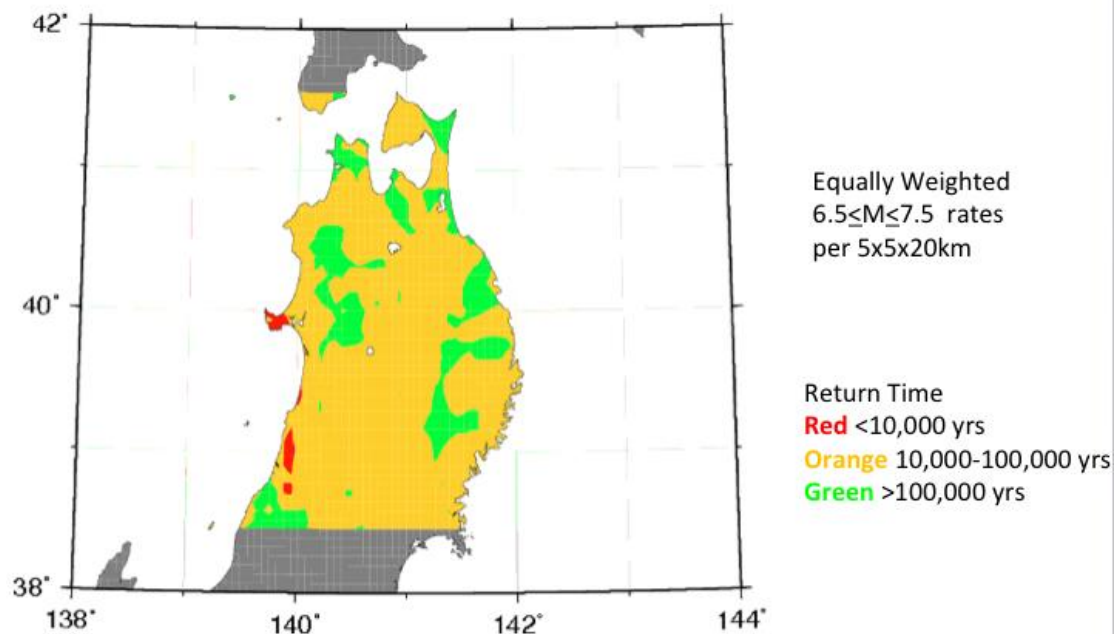
Figure 6.4: Map of 6.5<M<7.5 rates from the equally-weighted average of the three ITM Surface Deformation strain rate models, for a grid of cells with dimensions 5x5x20km.
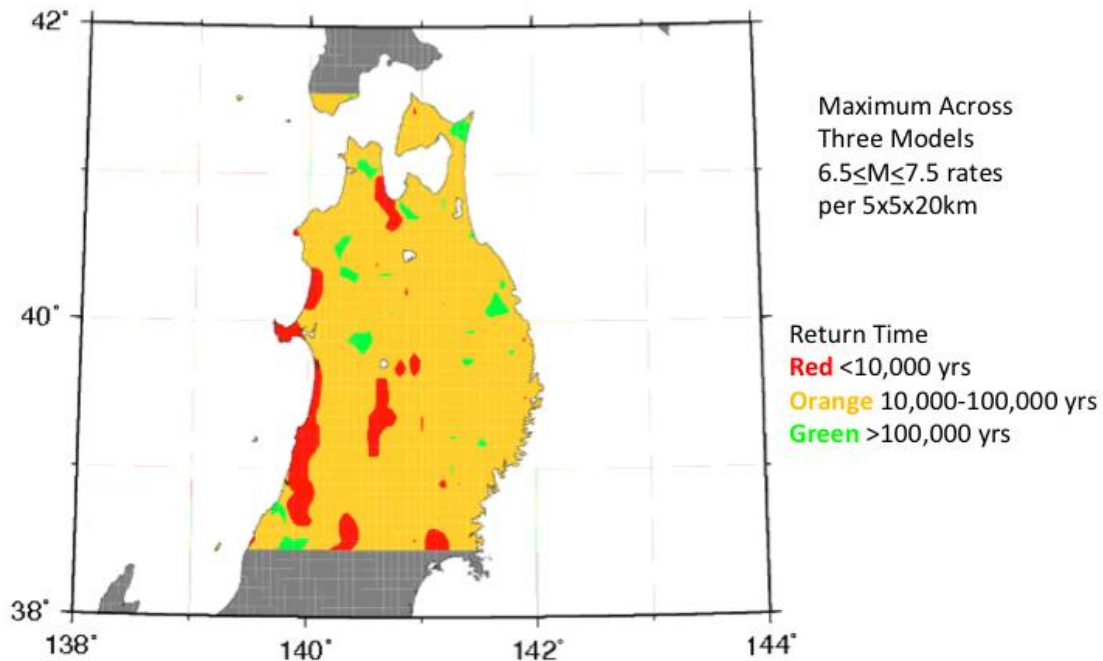
Figure 6.5: Map of 6.5<M<7.5 rates from the maximum of the three ITM Surface Deformation strain rate models, for a grid of cells with dimensions 5x5x20km.

In the context of tectonic hazard modelling from diverse datasets, we consider the maximum value map (Figure 6.5) to be the most appropriate representation of the three datasets, particularly with respect to the areas of highest hazard, which come from active fault data and are obviously muted by the averaging process seen in Figure 6.4. The GPS and seismicity datasets typically do not show elevated rates near the fault sources, which is due to seismic quiescence of the faults. This is a common observation in seismic hazard modelling, and the justification for combining datasets to build composite source models. We emphasise that the analyses developed here are to demonstrate the method rather than producing the "right" answer. The calculations we have done use early logic trees developed for each of the underpinning surface deformation, GPS and seismicity hazard models. Additionally, we have simply assumed a hazard event (the 6.5≤M≤7.5 earthquake) as a measure of "high" hazard and an implication for low prospectivity as a candidate repository site. In reality, thresholds will be very uncertain until consequence studies were undertaken for site-specific conditions. One methodological issue associated with the hazard realisations shown in Figures 6.1-6.5 is in the grid-based approach to modelling the 6.5≤M≤7.5 rates. Each 5x5x20km grid cell is modelled independently, with no ability for grid cells to interact when large sources have dimensions outside the cell volume. This is of particular concern for the fault sources, where the 6.5≤M≤7.5 rate for a fault source that crosses N grid cells is the fault rate divided by N. The net effect would be to underestimate the tectonic hazard at grid cells on or close to major active faults, and possibly in some other areas as well (e.g. near areas of high seismicity rates or GPS strain), possibly by a factor of three or more. Future work on this topic area should consider the interaction of grid cells for sources that are larger than the unit cell volume. This potential underestimation reinforces the existing NUMO criteria of avoidance of known active faults as candidate repository sites.

7 Evaluating site impact hazard probabilities using logic trees and expert elicitation

Incorporating expert opinion and uncertainties into the ITM-TOPAZ methodology is done via a formal process of expert elicitation, which was developed and tested in the first stages of the TOPAZ project (Chapman et al., 2012). The process is based on the use of logic trees that are designed to include alternative interpretations and modelling approaches and to generate scenario probabilities. This chapter updates the methodology with detailed explanation of logic trees and expert elicitation approach, followed by examples of how to use the scenario probabilities for evaluating exhumation hazard of a site.

7.1 Explanation of the method: use of logic trees to derive probability weights for site hazard maps

A *Logic Tree* is a useful framework for assessing probabilities of possible alternative future geophysical or geological scenarios and outcomes. Such trees are used extensively for volcanic hazard assessments (for example, Neri, A., et al. 2008; Newhall and Hoblitt, 2002).

There are two main sub-types of Logic Tree: *Event Trees* and *Probability Trees*, depending upon the way they are evaluated in probabilistic terms. An *Event Tree* is a graphical, tree-like representation of a series or sequence of events in which branches are logical steps from a startpoint (prior) event through increasingly specific subsequent events (with intermediate outcomes) to final events and their outcomes. For each event through the tree, a probability is assigned for its likelihood of occurrence. The product of probabilities along any one path, multiplied together, gives the probability of that endpoint event and outcome. At the most simple conceptual level, events at any particular level of the tree need not be mutually exclusive or exhaustive.

A *Probability Tree* is also a graphical, tree-like representation of alternative scenarios or events, very similar to an Event Tree, but formally the events on different branches at a specific level in the tree are exhaustive and mutually exclusive. Thus there is a requirement that the individual probabilities of these events, at that level, will sum to 1.0. This summation constraint is required if one wishes to know, for example, the total probability of a particular outcome that might occur as a result different events happening along several different possible paths.

If a situation is encountered with multiple scenarios, processes and sequential occurrences to be represented on such a tree, it is very easy for the tree to grow to have hundreds or thousands of branches and, without a structured formalism, the outcome probability evaluation problem rapidly becomes intractable. The solution is to make use of a suitable computer-based graphical package, designed for the purpose. A key benefit of this approach is that the scenario model can be made as comprehensive, or as simple, as needed, and the alternative possibilities and probability calculations become traceable and auditable – an important attribute for developing any case for geological disposal under a regulatory framework.

However, there is another important aspect to the challenge of moving from simplistic qualitative or deterministic descriptions of potential radiological impacts associated with geological disposal to more quantitative estimates. That is the ubiquitous and unavoidable presence of uncertainty in our knowledge and understanding of long-term geological processes, and how this should be tackled and characterized for site hazard evaluation. If a logic tree formulation is adopted, then it is feasible (with some software packages) to represent uncertainty on the variable values or probabilities on the tree in the form of appropriate probability distribution functions, rather than as (deterministic) single point-estimate values. These distributions can be parameterized from statistical data, where this is adequate, from conceptual model findings, or from elicitation of expert judgement, when data are too sparse and models are of limited validity. With such uncertainty distributions it is then possible to apply Monte Carlo sampling techniques to determine estimated confidence levels associated with the hazard impact or outcome assessment problem.

In the TOPAZ study, a probability tree sub-type of the logic tree concept has been adopted and implemented to create hazard scenario trees. For whichever particular form of geological or geophysical hazard is of concern, each site-specific hazard scenario tree starts from a prior

(i.e. current) condition or state at the given site, with the tree configured to depict pathways through alternative branchings that represent different defined Regional Evolution Scenarios (RES) and Site Evolution Scenarios (SES); the tree culminates in a range of hazard level values and their associated probabilities for the specific site and hazard. For example, the outcome of interest might be the total amount of exhumation of a repository that could occur at the particular site, over a number of future timescales.

In TOPAZ, hazard scenario trees have been developed for representing selected plausible regional and site vicinity patterns of geological evolution, through time and spatially, treating volcanic activity, tectonic strain and seismogenicity, and uplift and erosion (exhumation). The goal is to provide a methodology by which these strain, volcanic intrusion and uplift assessments can inform probabilistic hazard maps which then can be combined into a single tectonic hazard map, showing the overall susceptibility of a site to tectonic events over time periods of interest. In TOPAZ, the latter comprise the next 10 kyr, 100 kyr and 1 Myr.

Because the problem concerns long-term future evolutionary trends and patterns and because there are no viable forecasting models or data for this problem, in conducting a probabilistic scenario analysis the only recourse to expert judgement. The basis on which this has been done in TOPAZ, and preliminary findings in support of the hazard scenario trees are presented in the next section.

7.2 Expert elicitation approach: updating and extending elicited RES and SES probabilities

As a part of the ITM-TOPAZ methodology, the concept of incorporating differing expert views, alternative interpretations and models using a formal Expert Elicitation (EE) approach was introduced to Japanese tectonics and radioactive waste experts during the project.

This was done by means of an initial workshop, held on 25th - 26th October 2011, in Tokyo. In that workshop, selected RES and SES probabilities were elicited from a group of experts, after first calibrating the attending experts in terms of their ability to provide informative judgements for establishing probabilities and ranges of probabilities in the face of uncertainties. The outcomes of that first workshop are reported in more detail in Chapman et al. (2012).

A further elicitation was undertaken in June 2013 to update some of the RES and SES probabilities obtained at the October 2011 workshop, and to extend the scope to include further scenarios which were omitted from the first elicitation because of constraints on time and analysis resources. Further details of this follow-on exercise are provided below.

 The basis of both these TOPAZ elicitations is a structured questionnaire addressing specific scenarios, influences and factors that have been identified as pertinent for characterizing future geological processes in certain areas of Japan where a proposed geological repository for radioactive wastes might be sited. The questionnaire is completed by each participating expert, and their responses analysed with the Cooke Classical Model (below) and the EXCALIBUR software package. The main goal of the procedure is to provide a rational and defensible basis for ascribing uncertainty distributions to parameters, variables and probabilities in relation to long-term future volcanic and tectonic hazards and risks. For many of the factors addressed by the expert panel, the scientific uncertainties associated with these risk factors are large, and their quantification is a crucial element for supporting decision making related to hazards, repository siting and risk management.

Using expert judgment in this formalized manner furnishes objective quantitative estimates for identified hazard and risk factors - crucial for informing policy decision-making under conditions of severe scientific uncertainty. In addition, the elicitation exercise also helps identify major knowledge gaps, topics where definitions and terms may need clarification, and critical areas where additional research and investigation may be worthwhile.

The goal of the approach is to develop a 'rational consensus' on scientific questions of concern or significance for hazard assessment by utilizing a formalized approach based on performance-based scoring rule optimization for differentiating between the views of different experts. The group of experts involved agree that the method will produce representations of parameter uncertainty - for the purposes for which the panel was convened - without knowing

a priori the outcomes of this method. However, it is not required that each individual member adopts the results as his personal scientific belief.

To be rational, the method must comply with necessary generic conditions devolving from the scientific method; Cooke (1991) formulates the necessary conditions or principles which any such elicitation method should satisfy. These principles are implemented by adopting the Classical Model, a performance-based weighted opinion pooling model. The expert weights are derived from individual calibration and information scores, measured empirically on related subject-matter seed variables. Differentiating experts' performances with these seed items enables optimized combinations of expert uncertainty distributions to be determined for target questions that have t rely on their judgements.

In a typical application, each expert gives quantile information for his or her uncertainty distributions, such that for each calibration variable there are four distribution intervals defined by three quantiles (in TOPAZ, the 5th, 50th and 95th percentiles, respectively). The statistical accuracy ('calibration' score) of an expert is measured by looking at how far the equivalent empirical distribution given by the seed items differs from that given by the expert. The analyst wishes to identify those experts for whom the corresponding statistical hypothesis is well supported by comparison with that known distribution. Thus, the calibration score is the probability that the divergence between the expert's probabilities and the observed values of the calibration variables might have arisen by chance – a low p-value converts to a high calibration score.

Another criterion for an expert's performance is relative information (as noted earlier, sometimes referred to as 'informativeness'). Relative information represents the degree to which the expert's distribution is concentrated, relative to some user-selected background measure. The information score is a positive number, with increasing values indicating greater information relative to the background measure. Experts with distributions closest to the realization values are given higher calibration scores, and experts with smaller uncertainty bands are given higher information scores. The 'ideal' expert would have predicted close to the true value with little uncertainty; thus, 'good expertise' in this context - i.e. judging uncertainties - corresponds to high statistical likelihood and high information. In order to determine the performance-based weight that an individual expert gets, their information and calibration scores are combined together as a product. In this situation, the calibration scores are the more important: calibration dominates over relative information (or informativeness), while the relative information score serves to adjust between equally calibrated experts.

The seed questions used in the TOPAZ Project to score participating experts and the results of the calibration exercise are referenced in Chapman et al. (2012), and are not presented here.

In order to generate weights or probabilities for each hazard scenario tree, in June 2013 the TOPAZ experts were invited to provide central estimate and 90% confidence bound quantiles for those elements of the following key questions that were not elicited in 2011:

- for the four RESs, what weight should be given to each in expectation of it being an appropriate future scenario;
- given each RES, what is the probability that strain rates at the site location increase, decrease or stay the same over the next 1 Myr;
- what weight should be given to each strain dataset (in the ITM methodology) in terms of reliability for indicating strain rates;
- given each RES, what would be the expected long-term average rate of formation of new volcanoes in the Tohoku region: an increase, decrease or stay the same over the next 1 Myr;
- what weight should be given to each spatial density model (in the ITM methodology) for estimating formation rates of new volcanoes at the site location;
- what weight should be given to different spatial density models for representing an increase in long-term average rate of formation of new volcanoes.

For the target questions summarised above, performance-based weighted solutions and equal weights solutions are both reported to allow comparison, together with the facilitator's commentary on each item finding.

As with the judgments elicited from the experts, each pooled target item solution provides three values that can be used to define a unique uncertainty distribution for that particular item: the median (50th percentile) and two values marking a corresponding 90% credible interval about the central value.

After considering the nature and spread of these quantile values, a suitable functional form for the uncertainty distribution is chosen, and used for Monte Carlo analysis in concert with the relevant hazard scenario tree – see next section.

7.3   Scenario probability trees: structure and implementation

In this section, the structure and implementation of a scenario tree are exemplified by exhumation risk at 'Site C' in the previous report (Chapman et al., 2012), which is defined as WCB site in this report (see Chapter 3). The analyses were based on the uplift and erosion rates defined in the Site C Storyboard (Chapman et al., 2012; Fig. 2.11), that were independent of the updated scenario for the WCB site, because of time constraints. The software   *PrecisionTree*   [http://www.palisade.com/precisiontree/]   and   *@Risk* [http://www.palisade.com/risk/] were jointly used for the following analyses.

Figure 7.1 presents an example of the structure of the exhumation scenario probability tree for Site C using the *PrecisionTree* and *@Risk*. The exhumation risk was quantified by standard Monte Carlo technique using re-sampling of the various associated uncertainty distributions. Here, the assumption was made that the extent of exhumation, in metres, is the net result of tectonic uplift and surface erosion, with different levels of correlation between the two processes over the different timeframe, i.e. the next 10kyr; 100kyr and 1Myr. All branches of the tree incorporate elicited uncertainty distributions for scenario probabilities and indicative uncertainties for uplift and erosion rates.
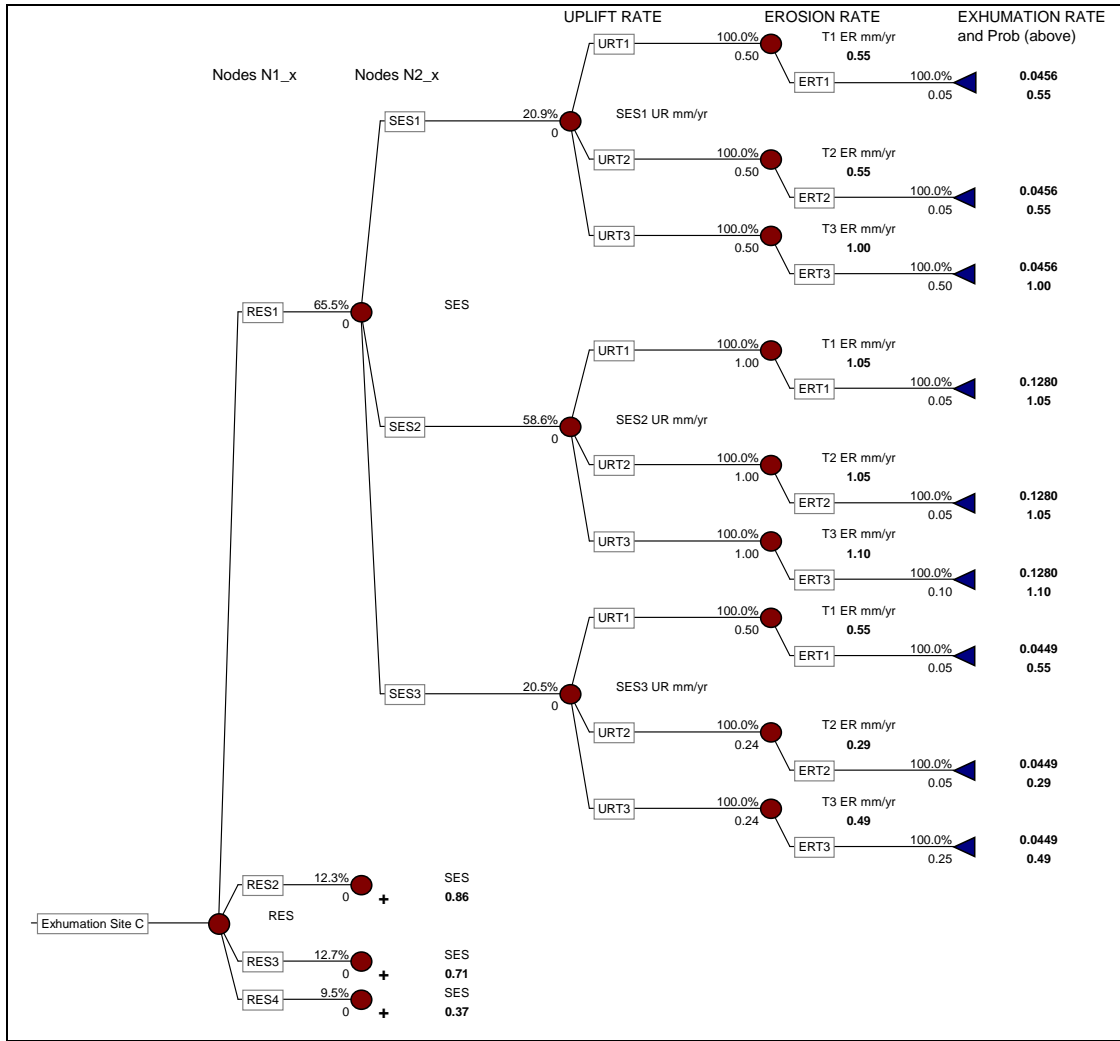
Figure 7.1: Example of the structure of scenario probability tree produced using *PrecisionTree* and *@Risk*.

Figure 7.2 presents an example of parameter set used in the analysis using *@Risk*. The column Node3_x contains Beta distributions for Uplift Rate matching the three quantiles for each RES/SES scenario, and column Node4_x does the same for Erosion Rate; these distributions are linked to corresponding Node branches on the Exhumation Tree (Figure 7.1) where sample rate values are multiplied by timeframes and summed to estimate net Exhumation over the time period. For illustration, the column with caption 'T1 T2 T3 rates Corr Coeffs' indicate Erosion Rate samples are presumed positively correlated with Uplift Rate values with the following coefficients: over 10 kyr +0.6; over 100 kyr +0.4; over 1 Myr +0.2.

Scenario Rn.Sn.Tn	UpliftRate			Node3_x	Label3	ErosionRate			Node4_x	Label4	T1, T2, T3 rates CorrCoeffs
	5%ile	50%ile	95%ile			5%ile	50%ile	95%ile			
R1S1T1	0.250	0.500	0.750	0.5000	N3_1	0.0001	0.050	0.100	0.0530	N4_1	0.60
R1S1T2	0.250	0.500	0.750	0.5000	N3_2	0.0001	0.050	0.100	0.0530	N4_2	0.40
R1S1T3	0.250	0.500	0.750	0.5000	N3_3	0.2500	0.500	0.750	0.5000	N4_3	0.20
R1S2T1	0.500	1.000	1.500	1.0000	N3_4	0.0001	0.050	0.100	0.0530	N4_4	
R1S2T2	0.500	1.000	1.500	1.0000	N3_5	0.0001	0.050	0.100	0.0530	N4_5	
R1S2T3	0.500	1.000	1.500	1.0000	N3_6	0.0500	0.100	0.150	0.1000	N4_6	
R1S3T1	0.250	0.500	0.750	0.5000	N3_7	0.0001	0.050	0.100	0.0530	N4_7	
R1S3T2	0.0001	0.250	0.450	0.2560	N3_8	0.0001	0.050	0.100	0.0530	N4_8	
R1S3T3	0.0001	0.250	0.450	0.2560	N3_9	0.0001	0.250	0.500	0.2653	N4_9	
R2S1T1	0.250	0.500	0.750	0.5000	N3_10	0.0001	0.050	0.100	0.0530	N4_10	
R2S1T2	0.250	0.500	0.750	0.5000	N3_11	0.0001	0.050	0.100	0.0530	N4_11	
R2S1T3	0.250	0.500	0.750	0.5000	N3_12	0.0001	0.250	0.500	0.2653	N4_12	
R2S2T1	0.500	1.000	1.500	1.0000	N3_13	0.0001	0.050	0.100	0.0530	N4_13	
R2S2T2	0.500	1.000	1.500	1.0000	N3_14	0.0001	0.050	0.100	0.0530	N4_14	
R2S2T3	0.500	1.000	1.500	1.0000	N3_15	0.0001	0.100	0.200	0.1061	N4_15	
R2S3T1	0.500	1.000	1.500	1.0000	N3_16	0.0001	0.050	0.100	0.0530	N4_16	
R2S3T2	1.200	1.500	2.000	1.5368	N3_17	0.0001	0.050	0.100	0.0530	N4_17	
R2S3T3	1.000	1.500	2.000	1.5000	N3_18	0.0001	1.000	2.000	1.0612	N4_18	
R3S1T1	0.250	0.500	0.750	0.5000	N3_19	0.0001	0.050	0.100	0.0530	N4_19	
R3S1T2	0.250	0.500	0.750	0.5000	N3_20	0.0001	0.050	0.100	0.0530	N4_20	
R3S1T3	0.250	0.500	0.750	0.5000	N3_21	0.0001	0.500	0.750	0.4845	N4_21	
R3S2T1	0.500	1.000	1.500	1.0000	N3_22	0.0001	0.050	0.100	0.0530	N4_22	
R3S2T2	0.500	1.000	1.500	1.0000	N3_23	0.0001	0.050	0.100	0.0530	N4_23	
R3S2T3	0.500	1.000	1.500	1.0000	N3_24	0.0001	0.500	1.000	0.5306	N4_24	
R3S3T1	0.250	0.500	0.750	0.5000	N3_25	0.0001	0.050	0.100	0.0530	N4_25	
R3S3T2	0.0001	0.250	0.450	0.2560	N3_26	0.0001	0.050	0.100	0.0530	N4_26	
R3S3T3	0.0001	0.250	0.500	0.2653	N3_27	0.0001	0.025	0.050	0.0265	N4_27	
R4S1T1	0.250	0.500	0.750	0.5000	N3_28	0.0001	0.050	0.100	0.0530	N4_28	
R4S1T2	0.0001	0.250	0.450	0.2560	N3_29	0.0001	0.050	0.100	0.0530	N4_29	
R4S1T3	0.0001	0.250	0.500	0.2653	N3_30	0.0001	0.025	0.050	0.0265	N4_30	

Notes: Uncertainty quantiles are illustrative

R1 = RES1	S1 = SES1	T1 = 10ka
R2 = RES2	S2 = SES2	T2 = 100ka
R3 = RES3	S3 = SES3	T3 = 1000ka
R4 = RES4	S4 = SES4	

Cols E,J have cell names as per adjacent labels for ease of reference on nodes in main tree

Quantile values on this sheet are dummy placeholders, pending expert elicitation

Figure 7.2: Tabulated uncertainty quantiles for uplift and erosion rates, used to define probability density functions on the scenario tree for Monte Carlo analysis using *@Risk*.

Net exhumation and its associated probability is re-calculated 10,000 times over the whole tree by the Monte Carlo technique and the sampled evaluations stacked to provide statistical expression to the results.

Figure 7.3 illustrates the sort of exhumation exceedance probability curves that can be derived from a Monte Carlo analysis of this type.
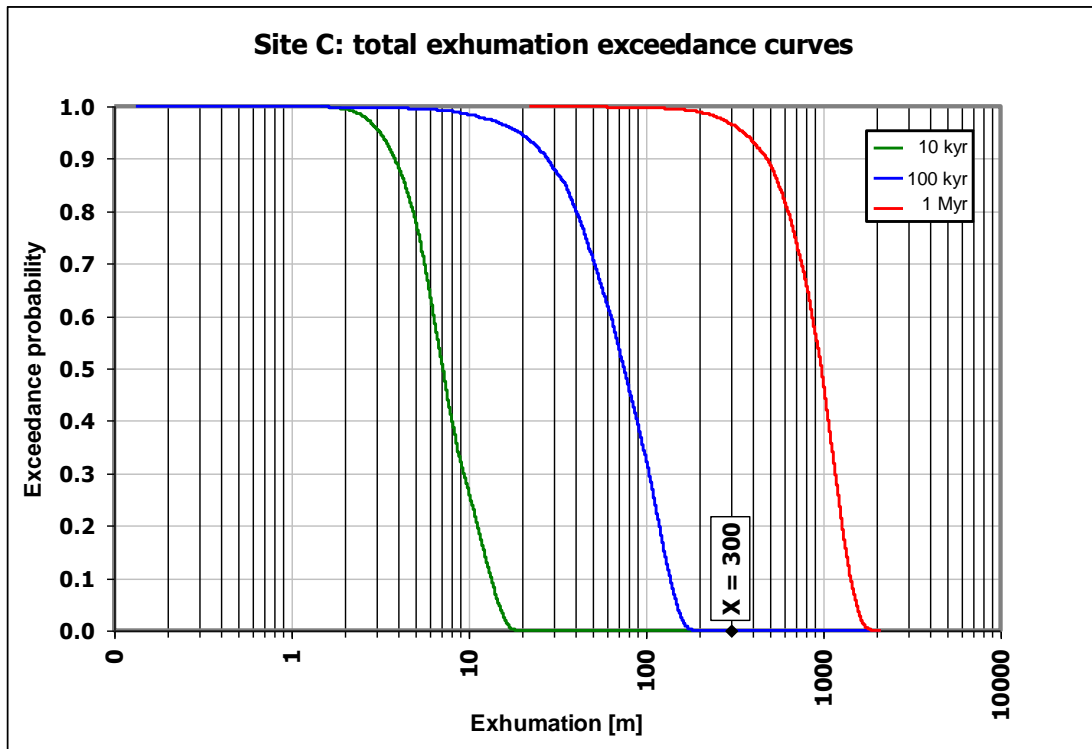
Figure 7.3: Example exhumation exceedance probability curves for three future periods (10 kyr; 100kyr; 1Myr).

To exemplify the risk indications that are provided by exceedance curves, such as those shown in Figure 7.3, the analysis suggests there is a probability < 0.0001 that exhumation at Site C will exceed 300m in 100 kyr. But, by contrast, the results also suggest that exhumation will exceed 300m a probability of 0.97, in 1Myr.

One of the strengths of the TOPAZ approach to site risk quantification - using uncertainty distributions on a scenario probability tree - is that the contributions of different scenarios, models or assumptions can be disaggregated and scrutinized. In Figure 7.4, for instance, the possible extent of exhumation over 100kyr is evaluated for two scenario combinations: RES1 & SES3, versus RES2 & SES3. The former has median 31m [90% range 8 – 53m], whereas the latter indicates 155 m median exhumation [90% range 123 – 208 m].

Such analysis capabilities can provide a reasoned stimulus for further investigation into contributory factors or other model aspects if results like these were considered critical or intolerable, or even just marginal.

The analysis based on the scenario tree, outlined above, need not stop there: having computed exhumation exceedance probabilities for three different periods into the future (e.g. Figure 7.3), those findings can be interpolated to determine, probabilistically, when any specific amount of exhumation may be experienced.

Thus, on Figure 7.5 the time to surface exhumation for three different repository burial depths can be quantified – conditional on the models incorporated on the scenario tree.

82
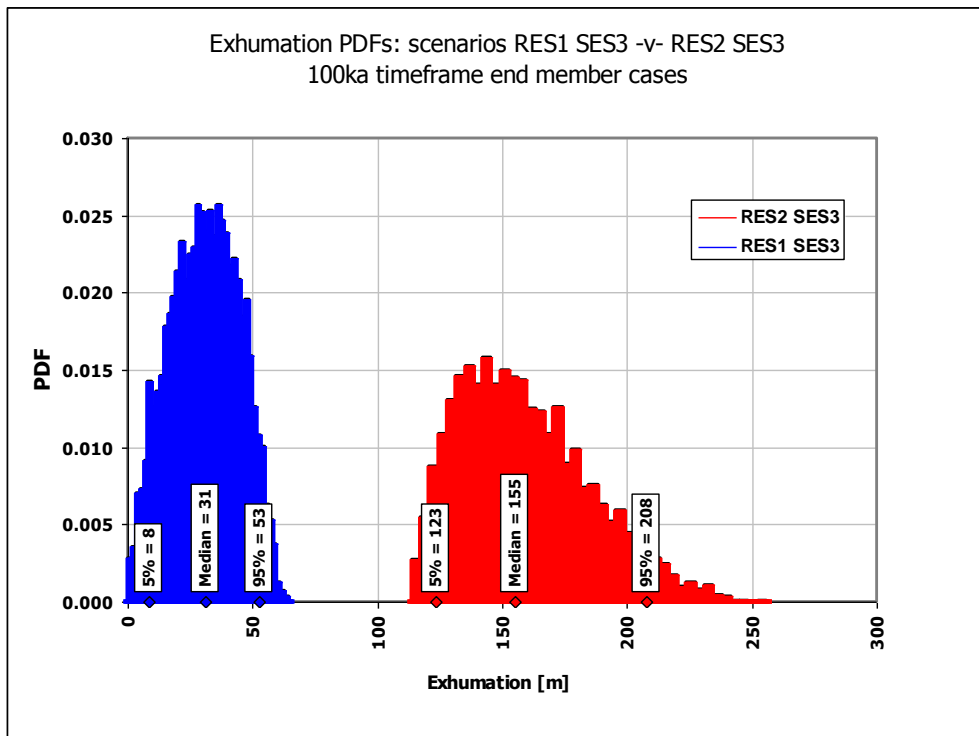
Figure 7.4: Example probability density function spreads for two end-member exhumation scenarios for 100 kyr timeframe.
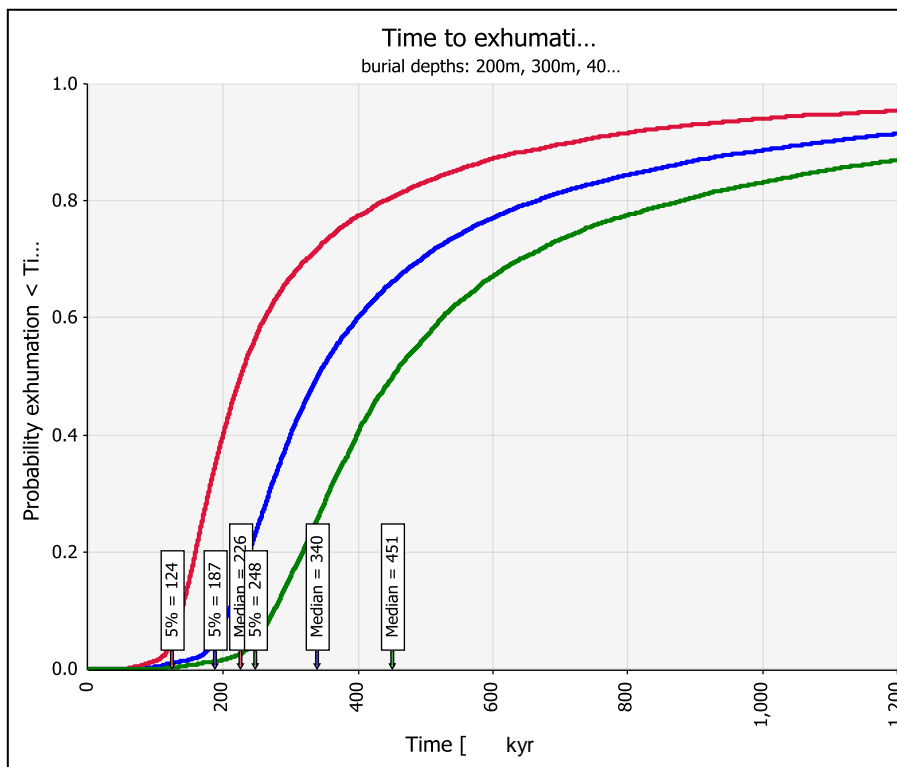
Figure 7.5: Illustrative curves for time to exhumation for three different burial depths [red=200m; blue=300m; green=400m].

Some implications of Figure 7.5 might be summarized as follows:

Time to exhumation for 200m burial (rounded values):

- Minimum* = 50 kyr
- 1 percentile = 90 kyr
- 5 percentile = 125 kyr
- Median = 225 kyr

Time to exhumation for 300m burial:

- Minimum* = 75 kyr
- 1 percentile = 120 kyr
- 5 percentile = 190 kyr
- Median = 340 kyr

Time to exhumation for 400m burial:

- Minimum* = 95 kyr
- 1 percentile = 170 kyr
- 5 percentile = 250 kyr
- Median = 450 kyr

* 'Minimum' is the shortest time from a Monte Carlo simulation with 10,000 iterations; i.e., here it approximates to 0.01% or 10^{-4} probability.

7.4   Summing up

The TOPAZ Project has developed a state-of-the-art probabilistic methodology for quantifying geological hazard risks for a geological repsoitory using conceptual hazard scenario trees that can represent plausible regional and site vicinity patterns of geological evolution, through time.

Separate trees can be configured to treat the different processes involved, for instance those that could engender future volcanic activity, tectonic strain and seismogenicity, or uplift and erosion (exhumation) at the site.

One important feature of this approach is that it incorporates capabilities for full treatment of model and parameter uncertainties, specifically including in exceedance calculations those that are obtained by structured expert elicitation, for which a formalized, and scientifically defensible, technique is identified.

The mode of implementation of this methodological approach is illustrated here by the example of a basic risk analysis for the exhumation, by tectonic uplift and erosion, of a buried facility. Application to a real site safety case, for this and other long-term geological processes, would almost certainly involve altogether more comprehensive and exhaustive models, and more detailed characterizations of associated uncertainties. This demonstration shows that such conceptual models can be developed, that elicitation protocols can be designed, and that software tools exist for executing the necessary probabilistic calculations.

The final step is to combine tectonic strain, seismicity, volcanic intrusion and uplift assessments into a single tectonic hazard map that evinces the overall susceptibility of a site to tectonic events over future time periods of interest. The methodology outlined in the present section allows the probabilities to ascribe to the different hazards and their maps to be determined in a tractable and auditable way, whence a joint hazard and risk evaluation case can be made.

8   Discussion for practical application

This chapter summarises points and issues in applying the ITM-TOPAZ methodology to the real site. It is, however, emphasised that how NUMO will actually apply this methodology requires further discussions in the future.

8.1   Practical application of the ITM-TOPAZ methodology

The ITM-TOPAZ methodology can produce quantitative information on the likelihood of specified tectonic events for a range of different timescales in the future: 1 ky, 10 kyr, 100 kyr and 1 Myr.

The user can specify the nature and magnitude of the events for which probability estimates are made. For development and demonstration purposes, a specific set of volcanic intrusion, fault movement and uplift/erosion events was identified, which provides a good general basis from which to assess project risk.

The overall aim of the methodology is to provide decision-makers with a scientifically based approach to evaluating geological stability that is based on managing and incorporating the inevitable uncertainties. The output of the methodology can be used by scientific/technical staff involved in site evaluation and performance assessment.

It is also intended to provide quantitative guides to management team on project risk – the risk to programme success of accepting a site for detailed study as a DIA, and can also be used as an effective communication tool.

The aim is to provide users with a tool that will assist with two important activities that will be carried out as part of the geological repository site selection programme:

> **Application 1:** Identify potentially suitable regions and sites with respect to their long-term tectonic hazards
>
> - this is done using regional hazard maps that show susceptibility to disruption by future volcanic events, rock deformation and uplift and erosion
>
> **Application 2:** Quantify the likelihood of specified tectonic impacts at any location over different timescales
>
> - this allows risks to be incorporated into safety case development and into quantitative safety assessment

Eventually, the methodology will be used to carry out increasingly detailed studies of tectonic hazards at a site during the later stages of PIA assessment and in the DIA stage, when detailed site investigation data become available. Application of the methodology in the run-up to site (PIA) selection will provide confidence in site choice from the perspective of geological stability. Application 2 might also have used to support preliminary PA studies of a site.

During the detailed surface investigations of a site, it will be possible to address uncertainties that have been identified by ITM-TOPAZ work. For example, uncertainties in age determinations of volcanic events in the region will affect the spatial mapping of future event probabilities and uncertainties in active fault histories in the region will affect the strain rate forecasts. These uncertainties can be overcome by gathering more data, not only within a PIA, but also locally and regionally. This type of fieldwork should plan to carry out, informed by ITM-TOPAZ regional evaluations, and making use of local geological knowledge.

With enhanced datasets, it will be possible to reapply the methodology to produce better-constrained probability values for risk estimation in later stages of safety assessment (e.g. for eventual licensing of construction of a repository). It is inevitable that the methodology will need to be reapplied several times over the whole period of PIA and DIA investigation, as improved safety assessments are carried out and as the safety case is being developed.

An important consideration in any of these applications concerns the time scales or relevance to assuring repository safety, as discussed in Section 1.4. Here, it is again emphasised that the critical period of concern to HLW disposal is the first thousand to 10 kyr. The ITM-TOPAZ methodology allows forecasting well beyond this period – out to 1 Myr – but decision-makers

need to be aware that not only does the methodology contain less uncertainty for these shorter times, but these times should also be at the forefront of their considerations and communications with the public. Factors that are of importance in different timeframes and the way in which ITM-TOPAZ provides support in each are shown in Table 8.1.

Table 8.1: Timescales in safety evaluation for a geological repository for high-level waste and how the ITM-TOPAZ methodology supports evaluation and decisions-making in these periods.

Period	What matters?	What is needed?	What does ITM-TOPAZ do?
0 – 1kyr	The waste is extremely hazardous and people must be isolated from any radionuclides released from it into the rock. The engineered containment in the repository will begin to degrade.	The waste and the engineered containment need to be protected from natural tectonic disruptive events. This must be done by **avoidance**: selecting a stable site where the probability of volcanic activity or penetration of the repository by faulting (e.g. from a hidden active fault deep beneath it) is extremely small over this period.	Provides quantitative probabilities of disruptive events of any specified magnitude, which must be so low that they can be discounted. Identifies areas and regions with a very high probability of providing stability over this period.
1kyr – 10kyr	Well within this period, the hazard from any releases from the waste has declined to levels of a natural ore body. The engineered containment has broken down and radionuclides are entering the deep groundwater system.	Because potential hazards from releases from the repository are still relatively significant, although likely within the ranges of global natural radiation exposures, it remains a central objective to protect the degrading repository from tectonic disruption over this period too. This is again achieved by siting in areas of low probability of such events – by continued **avoidance** of tectonic impacts. The isolation and containment functions of the repository are essentially fulfilled by the end of this stage.	This is arguably the principal period over which assurance of protection from tectonic events is required and when the ITM methodology is most valuable. Quantitatively assesses the probabilities of events and processes that might disrupt a repository over this timeframe. Allows siting decisions. Allows quantitative evaluations of dose and risk from disruptive tectonic scenarios
10kyr – 100kyr	The repository system is substantially degraded and remaining longer-lived radionuclides are dispersed though the deep geological environment in very low concentrations. Potential doses to people from these dispersed and dilute concentrations are extremely low and well below natural background radiation levels.	Over this timescale the longevity of safety functions can be qualitatively discussed to compare hazards to natural radiotoxic hazards and discuss the long-term fate of wastes as the repository degrades. Because there are still relatively high concentrations of some radionuclides immobilised in the wastes, scenarios where major tectonic events cause major disruption to the repository remain of interest in safety assessments, so quantitative estimates of probability are required.	Quantitatively assesses the probabilities of major tectonic events and processes that might disrupt a repository over this timeframe. Provide probability input to quantitative performance assessment to allow calculation of risks. This timeframe is the limit of forecasting with any reasonable level of certainty
100kyr – 1Myr	The waste materials are degraded, refractory residues with some radionuclides bound into newly formed minerals. The system has degraded almost completely and is releasing only small amounts of radioactivity, with potential doses to people being orders of magnitude below natural background.	The isolation and containment functions of the repository are complete. It is expected that tectonic processes and events will have significant impacts on the repository. Uplift and erosion may have brought the system closer to the surface. The probability that large magnitude volcanic events could disperse the remnants of the wastes into the environment are of interest to safety assessors, even though the relative hazard compared to that of such an event are trivial.	Although there are considerable uncertainties, semi-quantitative probabilistic forecasting is possible, to support major event and uplift-exhumation evaluations This is the timeframe considered by TOPAZ. Forecasts can be presented in the framework of alternative conceptual models characterising how the tectonic situation in a region might develop.

A specific use of the methodology in Application 1 is emphasised here: the use of hazard maps to assist decision makers by illustrating project risk. This is essentially a management tool, rather than a tool that is related directly to safety evaluation, in that it allows qualitative comparison of areas and sites, and highlights where problems might emerge as a project progresses. Complex hazard maps can be simplified to produce project management information by defining high, medium and low ranges of hazard. The implication of these terms is shown below.

High Project Risk	Sites located in these areas on the map would present considerable project management difficulties, such that it could be extremely difficult to make a credible safety case for a repository owing to tectonic hazards.
Medium Project Risk	Sites located in these areas on the map would present moderate project management difficulties. It would be possible to make a credible safety case for a repository that takes tectonic hazards into account, but difficulties may be encountered as more information is obtained about the site and its local area and more detailed modelling is undertaken.
Low Project Risk	There appear to be few tectonic hazards that would present a challenge to building a safety case, although detailed site characterisation and safety assessment modelling would be needed to confirm this.

Selecting the most appropriate numerical values of probability or hazard to define the boundaries between these categories will be a matter for users to discuss. It is also important to recognise that project risk will depend upon many more factors than just tectonic stability. For example, a site that carries low project risk from the viewpoint of tectonic stability might be unsuitable as a result of other bedrock features, such as deep groundwater flow properties.

Figure 8.1 (taken from Chapter 5) shows an example of a project risk map for Tohoku that combines volcanic hazard (using the probability of new volcanism) with uplift hazard (based on uplift rates) to show areas with high, medium and low risk with respect to these two factors. High project risk is shown in red. The boundaries used to distinguish, for example, high risk from medium risk (yellow) are a probability of volcanism of 10^{-7} per year and an uplift rate over 125,000 years of 0.5 mm/year.
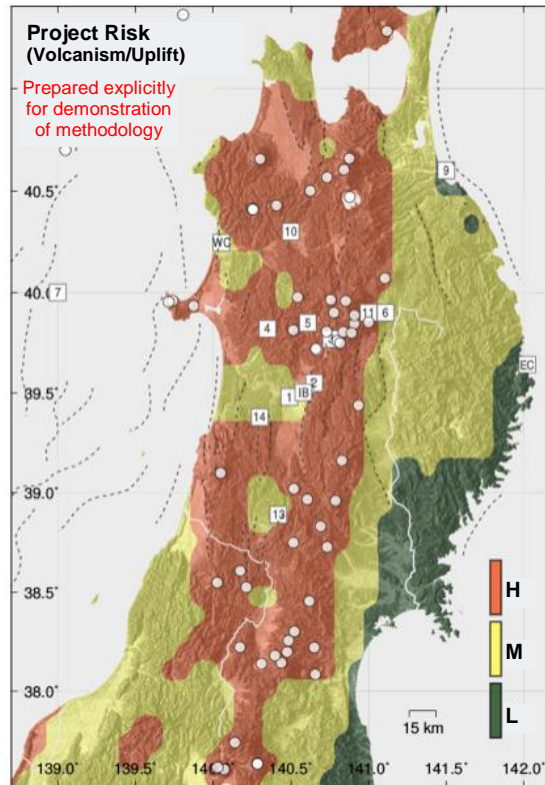
Figure 8.1 (re-presentation of Figure 5.21): The volcanism and uplift hazard maps are combined into a single project risk map for Tohoku. It is emphasised that this maps was developed for demonstrating the methodology for evaluation the potential project risk. Green zones on this map represent site areas that carries low risk with respect to volcano and uplift disruptive hazards, as probabilities of disruptive events are negligible for all scenarios analyzed. Yellow zones are characterized by one or more slightly higher probability – it is likely many of these sites carry moderate project risk. Red zones are areas in which one or more scenario indicates high project risk.

8.2   Uncertainty in the ITM hazard map

Uncertainty is a critical aspect of prognosis for natural hazards. In applying the ITM methodology (e.g. Chapman et al., 2009) for developing hazard maps, it is essential to characterise uncertainty in all its manifestations. Characterisation is much more than describing statistical errors in key parameters and includes deep understanding of epistemic and aleatory uncertainties as well recognition that some of the assessment will require formal expert judgement, particularly when it comes to weighting alternative conceptual models and forecasting hazards in deep time as is required for a geological disposal facility. Uncertainty assessment is not something that can be added on at the end of a hazard assessment and needs to be embedded and consciously done right from the outset. More detailed discussion of uncertainty in the context of hazards and risk assessment can be found in Rougier et al (2013).

Much of ITM hazard maps take place at a regional scale and it was originally developed to enable the relative hazards at different sites to be compared. Uncertainties grow greatly with time and there thus needs to be due regard how they change. When volunteer communities

emerge and the time comes to make real comparisons users need to recognise that the sources of the uncertainties are understood in terms of the nature of the evidence and understanding of the processes. We do not recommend using the results that are in this report once sites have been specified because knowledge and understanding in tectonics hazards of Japan will have advanced. Indeed a re-application of the methodology will give a sense of how stable the results of tectonic hazards assessment are and likely increase confidence in the method. We note that important components of tectonic hazards and uncertainty, for example random errors, will shift systematically at all sites if values change. So differences will not change even though absolute hazard changes. Other aspects of tectonic hazards may change as new knowledge or understanding is developed so that differences between sites may change.

Our case studies have shown that volcanic hazards vary by many orders of magnitude across Japan and so we are confident that ITM methodology allows a robust evidence-based approach to identify sites of very low or negligible volcanic hazard and to compare sites. Some of the output (e.g. Mahony et al. 2009) assesses spatial uncertainty in volcanic hazard and will enable the user to evaluate whether two or more sites have demonstrably different hazard. Seismic hazard can also be compared between sites, although the range of magnitude of hazard is typically less for earthquakes.

Users need to be much more circumspect in using hazard maps for a single site. Of course a single site can be compared with regional variations to establish that hazard is suitably low in a relative sense. Hazard assessment then needs to focus on a smaller scale and hazard maps should only be used in an indicative sense that the site shows promise. Much more detailed high-resolution site investigation is likely to change the hazard and the uncertainty in the hazard. There should be no assumption that more information, better understanding and high resolution study will reduce uncertainty.

References

AIST (2013): Active Fault Database of Japan, August 22, 2013 version, Research Information Database DB095, National Institute of Advanced Industrial Science and Technology, https://gbank.gsj.jp/activefault/index_e_gmap.html.

Chapman, N., Apted, M., Beavan, J., Berryman, K., Cloos, M., Connor, C., Connor, L., Jaquet, O., Litchfield, N., Mahony, S., Smith, W., Sparks, S., Stirling, M., Villamor, P. and Wallace, L (2008): Development of methodologies for the identification of volcanic and tectonic hazards to potential HLW repository sites in Japan: the Tohoku case study, NUMO-TR-08-03.

Chapman, N., Apted, M., Beavan, J., Berryman, K., Cloos, M., Connor, C., Connor, Ellis, S., Jaquet, O., Kiyosugi, K., Litchfield, N., Mahony, S., Smith, W., Sparks, S., Stirling, M., Villamor, P., Wallace, L., Goto, J., Miwa, T., Tsuchi, H. and Kitayama, K. (2009a): Development of methodologies for the identification of volcanic and tectonic hazards to potential HLW repository sites in Japan: Summary report, NUMO-TR-09-03.

Chapman, N., Apted, M., Beavan, J., Berryman, K., Cloos, M., Connor, C., Connor, Hasenaka, T., Jaquet, O., Kiyosugi, K., Litchfield, N., Mahony, S., Miyoshi, M., Smith, W., Sparks, S., Stirling, M., Villamor, P., Wallace, L., Goto, J., Miwa, T., Tsuchi, H. and Kitayama, K. (2009b): Development of methodologies for the identification of volcanic and tectonic hazards to potential HLW repository sites in Japan: the Kyushu case study, NUMO-TR-09-02.

Chapman N., Apted M., Aspinall W., Berryman, K., Cloos M., Connor C., Connor L., Jaquet O., Kiyosugi K., Scourse E., Sparks S., Stirling M., Wallace L. and Goto J. (2012): TOPAZ project – Long-term tectonic hazard to geological repositories, NUMO-TR-12-05.

Chapman, N.A. and Hooper, A. (2012): The disposal of radioactive wastes underground, proceedings of the Geologists' Association, 123, pp.46–63.

Chilès J.P. and Delfiner P. (1999): Geostatistics: modeling spatial uncertainty, Wiley Series in Probability and Mathematical Statistics, New York, Wiley.

Cooke, R.M. (1991): Experts in Uncertainty - Opinion and Subjective Probability in Science. Environmental Ethics and Science Policy Series. Oxford University Press.

Committee for the Catalogue of Quaternary Volcanoes in Japan (1999): Catalogue of Quaternary volcanoes in Japan, v 1.0 (CD-ROM), Volcanol. Soc. Japan.

Connor, C.B. and Hill, B.E. (1995): Three nonhomogeneous Poisson models for probability of basaltic volcanism: Application to the Yucca Mountain region, Nevada, J. of Geoph. Res., vol.100, No. B6, 10 107-10 125.

Connor, C., Connor, Jaquet, O., Wallace, L., Kiyosugi, K., Chapman N., Sparks, S. and Goto, J. (2013): Spatial and Temporal Distribution of Future Volcanism in the Chugoku Region: a partial application of NUMO's Topaz probabilistic tectonic assessment methodology, NUMO-TR-13-03.

Finn, C., Kimura, G. and Suyehiro, K. (1994): Introduction to the special section northeast Japan: A case history of subduction, Journal of Geophysical Research, 99, 22 137-22 145.

Fujiwara, O., Sanga, Y. and Ohmori, H. (1999): Regional distribution of erosion rates over the Japanese Islands, Japanese Nuclear Cycle Technical Review 5: 85-93 (In Japanese with an English abstract).

Fujiwara, H., Kawai, S., Aoi, S., Morikawa, N, Senna, S., Kobayashi, K., Ishii, T., Okumura, T., and Hayakawa, Y. (2006): National seismic hazard maps of Japan, Bulletin Earthquake Research Institute, University of Tokyo, v. 81, pp. 221-232.

Gutenberg, B., and Richter, C.F. (1944): Frequency of earthquakes in California, Bull. Seismol. Soc. Am. 34, pp.185–188.

Hall, R., Ali, J.R., Anderson, C.D. and Baker, S.J. (1995): Origin and motion history of the Philippine Sea plate, Tectonophysics, 251, pp.229–250, doi:10.1016/0040-1951(95)00038-0.

Hasegawa, A., Horiuchi, S. and Umino, N. (1994): Seismic structure of the northeast Japan convergent margin: A synthesis, J. Geophys. Res., 99(B11), 22 295-22 311.

Hasegawa, A., Yamamoto, A., Umino, N., Miura, S., Horiuchi, S., Zhao, D. and Sato, H. (2000): Seismic activity and the deformation process of the overriding plate in the northeastern Japan subduction zone, Tectonophysics, 319, pp.225-239.

Hasegawa, A. and Nakajima, J. (2004): Geophysical constraints on slab subduction and arc magmatism, in: Sparks, R. S. J. and Hawkesworth, C.J. (eds.): The state of the planet: Frontiers and challenges in geophysics, Geophysical Monograph Series 150, Washington DC, American Geophysical Union, pp.81–94.

Hasegawa, A., Nakajima, J., Umino, N. and Miura, S. (2005): Deep structure of the northeastern Japan arc and its implications for crustal deformation and shallow seismic activity, Tectonophysics, 403, pp.59–75.

Heki, K. (2004): Space geodetic observation of deep basal subduction erosion in northeastern Japan, Earth Planet. Sci. Lett., 219, pp.13-20.

Honda, S., Yoshida, T. and Aioke, K. (2007): Spatial and temporal evolution of arc volcanism in the northeast Honshu and Izu-Bonin Arcs: Evidence of small-scale convection under the island arc?, Island Arc, 16, pp.214-223.

Jaquet, O., Lantuéjoul, C. and Goto, J. (2009): Cox process models for the estimation of long-term volcanic hazard, in: Connor, C.B., Chapman, N.A. and Connor, L.J. (Eds.): Volcanic and tectonic hazard assessment for nuclear facilities, Cambridge University Press, pp. 369–384.

Jaquet, O., Lantuéjoul, C. and Goto, J. (2012): Probabilistic estimation of long-term volcanic hazard with assimilation of geophysics and tectonic data, Journal of Volcanology and Geothermal Research, 235–236, pp.29–36.

Jarvis, A., H.I. Reuter, A. Nelson, E. Guevara, 2008, Hole-filled SRTM for the globe Version 4, available from the CGIAR-CSI SRTM 90m Database (http://srtm.csi.cgiar.org).

Koike, K., Tamura, T., Chinzei, K. and Miyagi, T. (Eds) (2015): Geomorphology of Japan, 3, Tohoku, University of Tokyo Press.

Komazawa, M., Hiroshima, T., Joshima, M., Ishihara, T., Murata, Y., Yamazaki, T., Makino, M., Morijiri, R., Shichi, R., Kishimoto, K., Kikawa, E., Mishina, M. and Kawamura, M., (2004): Gravity CD-ROM of Japan, Geological Survey of Japan.

Kondo H. (2009): Regional-scale volcanology in support to site-specific investigations, in: Connor, C.B., Chapman, N.A., Connor, L.J. (Eds.): Volcanic and tectonic hazard assessment for nuclear facilities, Cambridge University Press, pp.307-325.

Kostrov, V. V. (1974): Seismic moment and energy of earthquakes, and seismic flow of rocks, Izv. Acad. Sci. USSR Phys. Solid Earth, 1, Eng. Transl., pp.23–44.

Lay, T., Fujii, Y., Geist, E., Koketsu, K., Rubinstein, J., Sagiya, T. and Simons, M. (2013): Introduction to the special issue on the 2011 Tohoku earthquake and tsunami: Seismological Society of America Bulletin, v.103, pp.1165-1170.

Mahony S.H., Sparks R.S.J., Connor L.J., Connor C.B. (2009): Exploring long-term hazards using a Quaternary volcano database, in: Connor, C.B., Chapman, N.A. and Connor, L.J. (Eds.): Volcanic and tectonic hazard assessment for nuclear facilities, Cambridge University Press, pp.326–345.

Matsu'ura, T., Furusawa, A., Saomoto, H. (2008): Late Quaternary uplift rate of the northeastern Japan arc. Geomorphology 95: pp.384-397.

Matsu'ura, T., Furusawa, A., Saomoto, H. (2009): Long-term and short-term vertical velocity profiles across the forearc in the NE Japan subduction zone, Quaternary Research 71, pp.227-238.

McCaffrey, R. (1992): Oblique plate convergence, slip vectors, and forearc deformation, Journal of Geophysical Research, 97(B6), pp.8905-8915.

McCaffrey, R., Zwick, P.C., Bock, Y., Prawirodirdjo, L., Genrich, J.F., Stevens, C.W., Puntodewo, S.S.O. and Subaraya, C. (2000): Strain partitioning during oblique plate convergence in northern Sumatra: Geodetic and seismologic constraints and numerical modeling, Journal of Geophysical Research, 105(B12), 28,363-28,376.

Minoura, K. and Nakaya, S. (1991): Traces of tsunami preserved in intertidal lacustrine and marsh deposits: Some examples from northeast Japan, Journal of Geology, v.99, pp.265-287.

Minoura, K., Imamura, F., Sugawara, D., Kono, Y. and Iwashita, T. (2001): The 869 Jogan tsunami deposit and recurrence interval of large-scale tsunami on the Pacific coast of northeast Japan, Journal of Natural Disaster Science, v.23, pp. 83-88.

Miura, S., Sato, T., Hasegawa, A. Suwa, Y., Tachibana, K. and Yui, S. (2004): Strain concentration zone along the volcanic front derived by GPS observations in the NE Japan arc, Earth Planets Space, 56, pp.1347-1355.

Miyauchi, T. (1988): Late Pleistocene marine terrace correlation and chronology in the northern northeast Japan, Geographical Reports of Tokyo Metropolitan University 23, pp.29-47.

Nature (2011): Rebuilding seismology, Nature Comment, v.473, pp.146-148.

Neri, A., Aspinall, W.P., Cioni, R., Bertagnini, A., Baxter, P.J., Zuccaro, G., Andronico, D., Barsotti, S., Cole, P.D., Esposti Ongaro, T., Hincks, T.K., Macedonio, G., Papale, P., Rosi M., Santacroce, R. and Woo, G. (2008): Developing an event tree for probabilistic hazard and risk assessment at Vesuvius, Journal of Volcanology & Geothermal Research, 178, pp.397-415, doi:10.1016/j.jvolgeores.2008.05.014.

Newhall, C. and Hoblitt, R. (2002): Constructing event trees for volcanic crises, Bull Volcanology, 64, pp.3 -20.

No, T. and Kodaira, S. (2013): Relationship between the seismogenic zone of the eastern margin of the Japan Sea and the crustal structure, Report of the Coordinating Committee for Earthquake Prediction, Japan, Vol.90, pp.521-524 (in Japanese).

NUMO (2004): Evaluating site suitability for a HLW repository, Scientific background and practical application of NUMO's siting factors, NUMO-TR-04-04.

NUMO (2013): Safety of the geological disposal project 2010, Safe geological disposal based on reliable technologies, English summary, NUMO-TR-12-05.

Okamura Y., Ishiyama T. and Yanagisawa Y. (2007): Fault-related folds above the source fault of the 2004 mid-Niigata Prefecture earthquake, in a fold-and-thrust belt caused by basin inversion along the eastern margin of the Japan Sea, Journal of Geophysical Research,112, B3, DOI: 10.1029/2006JB004320.

Ota, Y., Omura, A. (2009): Late Quaternary shorelines in the Japanese Islands, The Quaternary Research (daiyonki-kenkyu) 30, pp.175-186.

Ota, Y. (2010): Holocene marine terraces and coseismic coastal uplift in Japan, in: Progress in Quaternary studies in Japan (digital book), Japan Association for Quaternary Research, Tokyo.

Otsuki K. (1992): Oblique subduction, collision of microcontinents and subduction of oceanic ridges, their implications on the Cretaceous tectonics of Japan, Island Arc, 1, pp.51-63.

Regalla, C., Fisher, D.M., Kirby, E. and Furlong, K.P. (2013): Relationship between outer forearc subsidence and plate boundary kinematics along the Northeast Japan convergent margin, Geochem. Geophys. Geosyst., 14, pp.5227–5243, doi:10.1002/2013GC005008.

Rougier, J., Sparks, S. and Hill, L (2013): Risk and uncertainty assessment of natural hazards, Cambridge University Press.

Sato, H. (2013): Recent deep seismic profiling in the Niigata fold-and-thrust belt, central Japan, Report of the Coordinating Committee for Earthquake Prediction, Japan, Vol.90, pp.516-520 (in Japanese).

Sato, H., and K. Amano (1991): Relationship between volcanism, tectonism, sedimentation and basin development, late Cenozoic, central part of northern Honshu, Japan, Sedimentary Geology, 74, 1–4, pp.323-343.

Sawai, Y., Fujii, Y., Fujiwara, O., Kamataki, T., Komatsubara, J., Okamura, Y., Satake, K., and Shiskiura, M., (2008): Marine incursions of the past 1500 years and evidence of tsunamis at Suijin-numa, a coastal lake facing the Japan Trench, The Holocene, v.18, pp. 517-528.

Schellart, W.P. and Lister, G.S. (2004): Tectonic models for the formation of arc-shaped convergent zones and backarc basins, in Sussman, A.J. and Weil, A.B. (Eds): Orgenc curvature, Integrating paleomagnetic and structural analyses, Geological Society of America, Special Paper 383, pp.237-258.

Sdrolias, M., Roest, W.R. and Mueller, R.D. (2004): An expression of the Philippine Sea plate rotation: The Parece Vela and Shikoku Basins, Tectonophysics, 394, pp.69–86, doi:10.1016/j.tecto.2004.07.061.

Simon E. and Bertino L. (2009): Application of the Gaussian anamorphosis to assimilation in a 3-D coupled physical-ecosystem model of the North Atlantic with the EnKF, a twin experiment, Ocean Sci. Discuss., 6, pp.617–652.

Tajikara, M. and Ikeda, Y. (2005): Vertical crustal movement and development of basin and range topography in the middle part of the Japan arc estimated from fluvial/marine terrace data. Quaternary Research (daiyonki-kenkyu) 44: 229-245 (In Japanese with an English abstract).

Tamaki, K. and E. Honza (1985): Incipient subduction and obduction along the eastern margin of the Japan Sea, Tectonophysics, 119, pp.381-406.

Tamura Y., Tatsumi, Y., Zhao, D., Kido, Y. and Shukuno, H. (2002): Hot fingers in the mantle wedge, New insights into magma genesis in subduction zones, Earth and Planetary Sciences Letters, 197, pp.105-116.

Tamura Y., Nakajima J., Kodaira S. and Hasegawa A. (2009): Tectonic settings of volcanic centres in subduction zones: three dimensional structure of mantle wedge and arc crust, in: Connor, C.B., Chapman, N.A. and Connor, L.J. (Eds.): Volcanic and Tectonic Hazard Assessment for Nuclear Facilities. Cambridge University Press, pp. 176–194.

Tamura, Y., Ishizuka, O., Aoike, K., Kawate, S., Kawabata, H., Chang, Q., Saito, S., Tatsumi, Y., Arima, M., Takahashi, M., Kanamaru, T., Kodaira, S. and Fiske, R.S. (2010): Missing Oligocene crust of the Izu-Bonin arc: Consumed or rejuvenated during collision?, J. Petrology, 51(4), pp.823-846.

Umeda, K., Hayashi, S., Ban, M., Sasaki, M., Oba, T. and Akashi, K. (1999): Sequence of the Volcanism and Tectonics during the Last 2.0 Million Years along the Volcanic Front in Tohoku District, NE Japan,Volc. Soc. J., 44(5), pp.233-249.

Walcott, R. I. (1987): Geodetic strain and the deformational history of the North Island of New Zealand during the late Cainozoic, Philos. Trans. R. Soc. London, Ser. A, 321, pp.163–181.

Wallace, L.M., Beavan, J., Miura, S., McCaffrey, R. (2009): Using Global Positioning System data to assess tectonic hazards, in: Connor, C.B., Chapman, N.A. and Connor, L.J. (Eds.): Volcanic and tectonic hazard assessment for nuclear facilities, Cambridge University Press, pp.156-175.

Wessel, P. and Kroenke, L.W. (2000): Ontong Java plateau and late Neogene changes in Pacific Plate motion, J. Geophys. Res., 105(B12), 28 255–28 278.

Wessel, P., and Kroenke, L.W. (2007): Reconciling late Neogene Pacific absolute and relative plate motion changes, Geochemistry, Geophysics, Geosystems, Volume 8, Number 8.

Yoshiyama, A. and Yanagida, M. (1995): Uplift rates estimated from relative heights of fluvial terrace surfaces and valley bottoms, Chigaku Zasshi (Journal of Geography), 104, pp.809-826.

Zhao D., Hasegawa A. and Horiuchi S. (1992): Tomographic imaging of P and S wave velocity structure beneath northeastern Japan, Journal of Geophysical Research, 97, 19 909–19 928.

Zhao D., Hasegawa A. and Kanamori H. (1994): Deep structure of Japan subduction zone as derived from local, regional and teleseismic events, Journal of Geophysical Research, 99, 22 313–22 329.

Zhao D., Ochi F., Hasegawa A. and Yamamoto A. (2000): Evidence for the location and cause of large crustal earthquakes in Japan, Journal of Geophysical Research, 105, 13 579–13 594.

（　　　　　）
Nuclear Waste Management Organization of Japan(NUMO)